

Photo-protective Function of Carotenoids in Photosynthesis

DISSERTATION
zur Erlangung des Doktorgrades
der Naturwissenschaften

vorgelegt beim Fachbereich
Biochemie, Chemie und Pharmazie
der Johann Wolfgang Goethe-Universität
in Frankfurt am Main

von
Sergiu Amarie
aus Dorohoi

Frankfurt am Main, 2008

vom Fachbereich Biochemie, Chemie und Pharmazie der
Johann Wolfgang Goethe-Universität als Dissertation angenommen.

Dekan: Prof. Dr. Dieter Steinhilber
1. Gutachter: Prof. Dr. Josef Wachtveitl
2. Gutachter: PD Dr. Andreas Dreuw

Datum der Disputation: 17.03.2009

Contents

1	Introduction.....	1
	1.1 Photosynthesis.....	2
	1.2 Non-photochemical Quenching.....	3
	1.3 Pigments.....	5
1	1.3.1 (Bacterio)Chlorophylls.....	5
2	1.3.2 Carotenoids.....	8
	1.4 Plant Light-Harvesting Complexes.....	12
3	1.4.1 Light-Harvesting Complex II (LHC II).....	13
4	1.4.2 Minor Peripheral Antenna Complexes (CP24, CP26 and CP29).....	16
	1.5 Bacterial Light Harvesting Complex 1 (LH1).....	17
2	Experimental Methods.....	19
	2.1 The Femtosecond Laser System.....	20
5	2.1.1 Non-collinear Optical Parametric Amplifier (NOPA).....	21
6	2.1.2 Pulse Compressor.....	22
7	2.1.3 White Light Generation.....	23
8	2.1.4 Detector and Choppers.....	23
	2.2 General Description of the Pump-probe Method.....	25
	2.3 Data Analysis.....	27
3	Excited State Dynamics of <i>Rhodospirillum rubrum</i> Reaction Center Mutants.....	28
	3.1 Introduction.....	28
	3.2 Materials and Methods.....	31
	3.3 Results.....	32
9	3.3.1 Steady-state Absorption Spectroscopy.....	32
10	3.3.2 Excited State Dynamics of Wild Type, SPUHK1 and SKΔLM Mutants of <i>Rhodospirillum rubrum</i> PSU Following Excitation of the Spx S ₂ State.....	33
11	3.3.3 Photoprotection via Triplet Energy Transfer from ³ BChl to ³ Car.....	39
	3.4 Discussion.....	43
4	Carotenoid Radical Cation as a Probe for Non-photochemical Quenching.....	45
	4.1 Introduction.....	45
	4.2 Sample Preparation.....	47
	4.3 Chlorophyll Excited-State Dynamics in LHC Proteins.....	48
12	4.3.1 Excitation Energy Transfer.....	48
13	4.3.2 Electron Transfer.....	51
	4.4 Generation of Carotenoid Radical Cations in Solution.....	53
	4.5 Carotenoid Radical Cation Detection in LHC II.....	58
	4.6 Discussion.....	60
14	4.6.1 Location and Mechanism of qE.....	62
5	Carotenoid Radical Cation Proprieties.....	64

5.1	Introduction.....	64
5.2	Materials and Methods.....	66
5.3	Results and Discussion	67
15	5.3.1 Optical Properties of Lutein and β -Carotene Radical Cations	67
16	5.3.2 Excited State Dynamics of Carotenoid Radical Cations	69
17	5.3.3 Nature of the Low Lying Excited States of Carotenoid Radical Cations	73
18	5.3.4 Chlorophyll Excited State Quenching by Carotenoid Radical Cations - Implications for NPQ.....	75
6	Excited State Dynamics of Astaxanthin Radical Cation	79
6.1	Introduction.....	79
6.2	Materials and Methods.....	81
6.3	Results.....	82
19	6.3.1 Excited State Dynamics of Astaxanthin in Chloroform	82
20	6.3.2 Optical Properties of the Astaxanthin Radical Cation.....	85
21	6.3.3 Excited State Dynamics of the Astaxanthin Radical Cation	87
6.4	Discussion	91
7	Summary and Outlook	94
References		100
Acknowledgements		
Publications		
Curriculum Vitae		

List of Figures

- 1.1. Detailed model of the protein complexes involved in electron and proton transport within the thylakoid membrane of green plants 2
- 1.2. Light conditions of field plants during one representative day 3
- 1.3. Possible fates of excited Chl embedded in the light harvesting complexes of plants4
- 1.4. Structure of BChl *a* (left), Chl *a* and Chl *b* (right). R represents the phytyl chain, R₁: CH₃ for Chl *a* and CHO for Chl *b*. The arrow indicates the direction of the Q_y transition dipole moment6
- 1.5. Absorption spectra of chlorophyll *a* and *b* solubilized in methanol 6
- 1.6. Molecular structures of plant photosystem carotenoids, conjugation length is denoted in parentheses .8
- 1.7. Room temperature absorption spectra of the neutral form of violaxanthin, lutein, zeaxanthin and β-carotene 9
- 1.8. Transient absorption spectra of spinach thylakoids recorded upon excitation at 664 nm and probed at 1000 nm (left). Reconstructed quenched minus unquenched difference spectrum (solid line with circles) at a time delay of 20 ps, together with the spectrum of β-Car⁺ (dashed line) (right) 11
- 1.9. Scheme of the qE quenching mechanism, showing generation of Zea⁺ after selective excitation of the Chl Q_y band at 664 nm 11
- 1.10. PS II supercomplex, electron micrograph image 12
- 1.11. Top view of the LHC II trimer. Grey-polypeptide; cyan-Chl *a*; green-Chl *b*, orange-carotenoids, pink-lipids 13
- 1.12. Scheme of energy levels and energy-transfer pathways between carotenoids and Chl molecules in the LHC II complex 14
- 1.13. Absorption spectrum of the LHC II complex with contributions of different molecular species to the particular spectral region denoted by horizontal bars. Carotenoids (orange), Chl *a* (light green), and Chl *b* (dark green). 15
- 1.14. Absorption spectrum of the LH1 complex from *R. rubrum* 17
- 1.15. Pigment model of the ring structure of the LH1 complex, enclosing the reaction center 18

- 2.1. Experimental setup of the pump-probe experiment 20
- 2.2. Schematic representation of a non-collinear optical parametric amplifier (NOPA) 21
- 2.3. Double-pass prism-pair compressor 22
- 2.4. Schematic representation of the pulse pattern caused by the chopper 24
- 2.5. Concept of the pump-probe transient absorption experiments showing various signal components during excited state evolution: ground state bleach, stimulated emission (SE) and excites state absorption (ESA). 26

- 3.1. Molecular models of the intact PSU (LH1+RC) and the putative PSUs of SKΔLM and SPUHK1 mutants, as viewed from the periplasmic surface. The RC subunits L, M and H are indicated 29

- 3.2.** Absorption spectrum of the chromatophore membranes from the WT (solid line) SPUHK1 and SKΔLM mutants. The peaks at 760 and 802 nm correspond to BPhe and the RC-accessory BChl (absent in the SPUHK1 and SKΔLM). 33
- 3.3.** Schematic representation of energy levels and energy-transfer pathways between carotenoids and BChl *a* in the LH1 complex (left). Transient absorption data of LH1, upon carotenoid excitation at 546 nm (right) 34
- 3.4.** Left: amplitude spectra (decay associated spectra) of the multi-exponential global fit analysis for wild-type (continuous line) and SPUHK1 mutant (dotted line). Right: transient spectra at 1.5 ns 35
- 3.5.** Transmission difference spectra for wild-type sample at different time delays after photoexcitation at 546 nm 36
- 3.6.** Kinetic traces of the PSU of *R. rubrum* wild-type (black) and SPUHK1 mutant (red) measured after the excitation at 546 nm. Probing wavelengths are indicated for each curve. Solid lines represent the best fits obtained from multiexponential global fitting procedure 37
- 3.7.** Fit amplitudes characterizing the spectral evolution of the transient absorption for WT (left) and SPUHK1 (right) in the near-IR region after excitation at 546 nm 38
- 3.8.** Transient absorption difference spectra taken at 1.5 ns for WT (solid line), SPUHK1 (dotted line) and SKΔLM (dot-dashed line) chromatophores of *R. rubrum* 39
- 3.9.** Amplitude spectra (decay associated spectra) of the multiexponential global fit analysis upon excitation at 880 nm 40
- 3.10.** Kinetic trace of the *R. rubrum* SPUHK1 mutant measured after excitation at 546 nm (carotenoid moiety) and 880 nm (Bchl Q_Y transition). The probing wavelength was centred around 575 nm 41
- 3.11.** Transient triplet state absorption spectra of SPUHK1-sample detected at 1.5 ns upon excitation of carotenoid (blue curve), and BChl (green curve) 42
- 3.12.** Kinetics traces for SPUHK1 upon excitation at 546 nm (blue) and 880 nm (green), while the probing wavelength was centred at 575 nm. Solid lines are fit curves 42
- 3.13.** Carotenoid S₁ signature probed at 1000 nm upon carotenoid excitation at 546 nm (blue curve) or BChl excitation at 880 nm (green curve) 43
- 4.1.** Schematic representation of the gear-shift model 50
- 4.2.** Carotenoid composition in native and Zea-enriched preparations of LHC II (left). TA data for LHC II-Vio (blue) and LHC II-Zea (red) detected at 904 nm upon excitation at 660 nm. The solid lines correspond to the fit curve obtained by a global fitting routine (right) 51
- 4.3.** TA data detected at 904 nm upon excitation at 660 nm (left) and HPLC analysis (right) for native (blue) and Zea enriched (red) CP26, CP26 and CP29. The solid lines correspond to fit curves obtained by a global fitting routine 52
- 4.4.** Near-IR spectrum of native (blue) and Zea enriched LHCs (red) recorded 20 ps upon excitation of Chl bulk at 660 nm 54
- 4.5.** Schematic diagram of the resonant two-photon two-color ionization (R2P2CI) experiment on carotenoids 55
- 4.6.** Temporal evolution of β-Car^{•+} upon generation by R2P2CI 56
- 4.7.** Absorption spectra of Lut^{•+} in ethanol for different time delays (τ₁) 56

- 4.8. Absorption spectra of $\text{Vio}^{\bullet+}$ in ethanol for different time delays (τ_2) after cation generation 57
- 4.9. Bandwidth at FWHM vs. time delay of $\text{Vio}^{\bullet+}$ 57
- 4.10. Transient absorption spectra of the investigated $\text{Car}^{\bullet+}$ in the near-IR region in ethanol, taken 40 ps after generation. From left to right: violaxanthin, lutein, zeaxanthin, and β -carotene 58
- 4.11. Transient absorption spectra of $\beta\text{-Car}^{\bullet+}$ in acetonitrile, ethanol, acetone, dichloromethane, chloroform and CS_2 59
- 4.12. Difference transient absorption spectra between R2P2CI and PP revealing all $\text{Car}^{\bullet+}$ in LHC II-Vio (circles) and LHC II-Zea (triangles). The solid line corresponds to Gaussian fits of the data points. The difference between Zea and Vio LHC II (black triangles) and the respective Gaussian fits with extrema at 909 and 983 nm reflects the decrease in $\text{Vio}^{\bullet+}$ and the increase in $\text{Zea}^{\bullet+}$ 60
- 4.13. Location of violaxanthin at the interface between two monomers of the trimeric LHC II protein 65
- 5.1. **Optical absorption of the neutral β -carotene (blue line) and β -carotene radical cation (red line) recorded upon addition of 0.5 M equivalent of FeCl_3 in chloroform 70**
- 5.2. Optical absorption of β -carotene radical cation in different solutions: acetonitrile, chloroform and CS_2 71
- 5.3. Optical absorption of lutein (blue line) and β -carotene (red line) radical cations recorded upon addition of 0.5 M equivalent of FeCl_3 in chloroform 72
- 5.4. 2D plot of the transient absorption data of lutein and β -carotene radical cations upon excitation at 935 nm 73
- 5.5. Transient absorption kinetic traces of lutein (circles) and β -carotene (triangles) radical cations probed at the $\text{D}_2 \rightarrow \text{D}_M$ ESA maxima (top panel), at the ground state bleach minima (middle panel), and at the $\text{D}_1 \rightarrow \text{D}_N$ ESA maxima (bottom panel) after excitation to 935 nm 74
- 5.6. Amplitude spectra represented by the global fit amplitude of β -carotene (top panel) and lutein (bottom panel) radical cations upon 935 nm excitation 75
- 5.7. Energy level diagram depicting relaxation processes that occur after photoexcitation of lutein/ β -carotene radical cations. Double arrow represents excitation of the D_3 state, dotted arrows corresponds to excited state transitions of $\text{D}_1 \rightarrow \text{D}_M$ (ESA_1) and $\text{D}_2 \rightarrow \text{D}_N$ (ESA_2), while wavy arrows denote intramolecular relaxation processes. The processes described in this study are labeled by their corresponding time constant. Excitation of chlorophylls into the first excited state (Q_y transition) leads to efficient excitation energy transfer (EET) to D_3 excited state. See the text for details 77
- 5.8. Experimental approach for chlorophyll excited state quenching by carotenoid radical cations. First two pulses of 490 and 775 nm, separated by $\tau_1=50$ fs, leads to generation of carotenoid radical cations. The pump-probe experiment is performed upon chlorophyll excitation of 388 nm at $\tau_2=40$ ps, and probing the chlorophyll excited state dynamics by varying τ_3 79
- 5.9. Difference transient absorption spectra between R2P2CI and PP revealing all $\text{Car}^{\bullet+}$ in LHC minors, detected 40 ps upon generation. The solid line corresponds to Gaussian fits of the data points 79

5.10. TA kinetic traces for LHC minors in the presence (triangles) or absence (squares) of carotenoid radical cations, detected at 900 nm upon excitation into Chl solet band at 388 nm. The solid lines correspond to the fit curve obtained by a global fitting routine 80

- 6.1.** Molecular structure of astaxanthin 83
- 6.2.** Absorption spectrum of astaxanthin in chloroform 86
- 6.3.** Transient absorption spectra of astaxanthin in chloroform. 3D plot (left) and kinetic traces selected at the ground state bleach minimum (right top), and excited state absorption maximum (right bottom) 87
- 6.4.** Amplitude spectra represented by the global fit amplitude of astaxanthin upon 500 nm excitation 88
 - 6.5.** Energy level diagram depicting relaxation processes that occur after photoexcitation of astaxanthin 88
 - 6.6.** Absorption spectra of the astaxanthin radical cation in different solvents: acetone, chloroform, dichloromethane and CS₂ 89
 - 6.7.** Transient absorption spectra of astaxanthin radical cation recorded 55 ps after generation in acetone, dichloromethane, chloroform and CS₂ 90
- 6.8.** 2D plot of transient absorption data for astaxanthin radical cation upon excitation at 890 nm 91
 - 6.9.** Transient absorption kinetic traces of astaxanthin radical cation probed at the excited state absorption (ESA) maxima ESA₁, ESA₂, ESA₃, ESA₅ and at the ground state bleach (GSB) minimum after excitation at 890 nm 92
 - 6.10.** Amplitude spectra represented by the global fit amplitude of astaxanthin radical cation upon 890 nm excitation 93
 - 6.11.** Energy level diagram depicting relaxation processes that occur after photoexcitation of astaxanthin radical cations. The red double arrow represents excitation of the D₃ state, colored arrows correspond to excited state transitions of D₂→D_N (ESA₁), D₃→D_N (ESA₂), D₁→D_M (ESA₃), D₂→D_M (ESA₄) and D₃→D_M (ESA₅), while wavy arrows denote intramolecular relaxation processes. The processes described in this study are labeled by their corresponding time constant (see the text for details). 96

List of Tables

- 1.1.** Pigment composition of PS II complexes 14
- 6.1.** Absorption maxima of the D_3 bands obtained by chemical oxidation or resonant two-photon two-color ionization (R2P2CI) 89

Zusammenfassung

In der vorliegenden Arbeit wurden die Photoschutzmechanismen in Pflanzen und Purpurbakterien auf molekularer Ebene experimentell untersucht. Zu diesem Zweck kamen verschiedene spektroskopische Methoden zur Aufklärung der Funktion der dabei vor allem beteiligten Carotinoide zur Anwendung. Die Experimente konzentrierten sich auf die Quenching-Mechanismen von Singulett- und Triplett-Zuständen der elektronisch angeregten (Bacterio-) Chlorophylle. Diese photosynthetischen Reaktionen treten auf ultraschnellen Zeitskalen im Bereich vom Femtosekunden bis Nanosekunden auf, sodass sich Femtosekunden zeitaufgelöste Absorptionsspektroskopie als geeignete Methode erweist die molekulare Dynamik in Echtzeit zu verfolgen.

Sowohl mittels herkoemlicher Anreg-Abtast-Spektroskopie als auch mit im Rahmen dieser Arbeit weiter entwickelter resonanter Zwei-Photonen Zwei-Farben Ionisation (R2P2CI), wurden eine Reihe von photosynthetischen Antennensystemen untersucht: Aus photosynthetischen Purpurbakterien wurden der Lichtsammelkomplex 1 (LH1) sowie der Lichtsammelkomplex II (LHC II) und die chlorophyllgebunden Proteine CP24, CP26 und CP29 höherer Pflanzen charakterisiert. Darüber hinaus wurden eine Reihe von Carotinoiden und ihre Radikalkationen als wesentlicher Bestandteil der photoinduzierten Reaktionskanäle in Lösung untersucht. Diese Experimente erlauben die Auswirkung der Lösungsmittelpolarität auf die Eigenschaften der Carotinoide (energetische Lage und die Dynamik der angeregten Zustände, Wechselwirkung mit benachbarten photosynthetischen Pigmenten) zu untersuchen.

Bakterielle Photosynthese

Das bakterielle LHC1 von *Rhodospirillum rubrum* bildet im Gegensatz zu pflanzlichen Lichtsammelkomplexen einen hochsymmetrischen makromolekularen Komplex enthält jedoch nur zwei Pigmente: ein Spirilloxanthin (Spx) (Carotinoid-Molekül) und ein Bacteriochlorophyll (BChl) Dimer. Aus diesem Grunde kann die photoinduzierte Dynamik mittels transienter Absorptionsspektroskopie verfolgt werden. Die photosynthetische Einheit von Purpurbakterien besteht aus einem Reaktionszentrum (RC) umgeben von einem Lichtsammelkomplex. Die in dieser Arbeit verwendeten *R. rubrum* Bakterien besitzen ein heterotrimeres Reaktionszentrum aus den membrangebundenen Untereinheiten L, M und H. Bisher ist jedoch noch unklar, ob der LH1-Ring kreissymmetrisch ist. Da sich eine signifikante Verzerrung der LH1-Symmetrie u.a. auch auf die Energietransferraten zwischen enthaltenen BChl und Spx-Molekülen auswirken sollte wurden verschiedene Mutanten mittels Kurzzeitspektroskopie untersucht. Im Zentrum der Betrachtung stand dabei der Energietransfer in Chromatophoren aus Wildtyp (WT) *R. rubrum* und Deletionsmutanten ohne das gesamte Reaktionszentrum (Mutante SPUHK1) bzw. ohne die L- und M-Untereinheiten (Mutante SK Δ LM). Messungen der Energietransferprozesse beider Mutanten wurden mit den Daten des inzwischen gut charakterisierten Wildtyp-Systems verglichen. Die Untersuchung zeigt, dass die Entfernung der H-Untereinheit die Bildung des RCs hemmt, insbesondere wurden keine spektralen Charakteristiken der L und M Untereinheiten des Reaktionszentrums beobachtet.

Die Anregung in der Hauptabsorptionsbande des Spx bei 550 nm in den SPUHK1 und SKΔLM Proben initiiert im Carotinoid-Bereich eine spektralen Entwicklung, die der WT-Probe sehr ähnlich ist. Der Anregung des S₂ Zustandes folgt die gleichzeitige Bevölkung der unteren angeregten Singulett Zustände S₁ und S*, die mit Zeitkonstanten von 1,4 und 5 ps (jeweils für beide Mutanten, 1,4 und 4 ps für den WT) depopuliert werden. Dies deutet darauf hin, dass die Dynamik der niedrig liegenden angeregten Spx Zustände sich in diesen Komplexen nicht erheblich ändert. Im Vergleich zum WT wurde jedoch eine längere Lebensdauer des angeregten BChl Zustandes in der SPUHK1-Mutante beobachtet, was im Einklang mit dem Auftreten eines photochemischen Quenchenkanals des Reaktionszentrums ist. Die Lokalisierung der Anregungs-Energie am RC wurde mit 46 ps bestimmt. Zu langen Verzögerungszeiten zeigt der WT, nicht aber die Mutanten, aufgrund von Photobleichen dimeren BChl *a special pairs* im RC und der elektrochromen Blauverschiebung des monomeren BChl *a* ein negatives Signal. Die Absorption des ersten angeregten Triplett-Zustands von Spx bei 575 nm zeigt den Prozess der ³BChl-³Spx Energieübertragung, die mit einer Zeitkonstante von 1,2 ns stattfindet. Bemerkenswert ist, dass dies die erste direkte Beobachtung eines Triplet-Triplett Energietransfers gemessen auf einer ultraschnellen Zeitskala in einer photosynthetischen Antenne ist. Die Ähnlichkeit der Zerfallsprozesse der angeregten Zustände aller Stämme deutet darauf hin, dass das Fehlen des RC im modifizierten Membranen keinen Einfluss auf die Pigmentgeometrie des LH1 hat.

Pflanzliche Photosynthese (NPQ)

Nicht-photochemisches Quenchen (NPQ) ist ein grundlegender Mechanismus der Photosynthese in Pflanzen, schützt die Pflanzen gegen übermäßige Anregungsenergie, und ist von entscheidender Bedeutung für das Überleben und die Fitness der Pflanzen. Energieabhängiges Quenchen (qE) beinhaltet die Deaktivierung des angeregten Singulett-Zustands von Chlorophyll in der Antenne des Photosystem II, bei der die schädliche Wirkung von Licht über thermische Dissipation der Überschussenergie minimiert wird. Während die physiologische Bedeutung von qE seit vielen Jahren anerkannt ist, fehlt eine Beschreibung der physikalischen Mechanismen nach wie vor.

Im Rahmen dieser Arbeit sollte geklärt werden, inwieweit ein neueres Modell anwendbar ist, in welchem der Austausch von Violaxanthin (Vio) (Carotinoid mit 9 konjugierten C=C Doppelbindungen) durch Zeaxanthin (Zea) (11 C=C) in der Vio-Bindungstasche des LHC II im Prinzip zu qE durch den so genannten "Gear-shift" Mechanismus führen kann. Eine Notwendigkeit hierfür ist, dass der erste angeregte Vio Zustand (S₁) eine höhere Energie als der erste angeregte Zustand von Chl(Q_y) hat und der S₁ Zustand von Zea wiederum energetisch niedriger als Q_y liegt. Um das vorgeschlagene Modell zu bestätigen, wurden in der vorliegenden Arbeit ultraschnelle Pump-Probe-Messungen an nativem LHC II und an LHC II-Proben, in denen Vio biochemisch in Zea umgewandelt wurde, durchgeführt. Der experimentelle Ansatz besteht aus der Anregung der LHC II Chlorophylle in den ersten angeregten Zustand, wobei Vio oder Zea an diese Komplexe gebunden sind. Die Lebensdauer des angeregten Zustands wurde durch Messung der Kinetik des ESA-Signals untersucht. In dieser Arbeit wird zweifelsfrei gezeigt, dass der Austausch von Vio und Zea im isolierten LHC II keinen Einfluss auf Lebensdauer des angeregten Chl-Zustandes hat. Zudem wurde der gleiche experimentelle Ansatz auf rekonstituierte Lichtsammelkomplexe (CP29, CP26 und CP24), die im nativen System eine Zwischenstellung zwischen den peripheren LHC II und dem Reaktionszentrum besetzen,

angewandt. Diese Messungen unterstützen die Schlussfolgerung, dass die Anwesenheit von Zea nicht dazu führt, dass die Chlorophylle gequench sind. Das Fehlen der Anregungsenergie-Übertragung vom niedrigsten angeregten Chl Zustand auf den niedrigsten angeregten Zustand von Zea lässt sich durch die schwache Kopplung von diesen zwei angeregten Zuständen, aufgrund des kleinen Übergangdipolmoments des Carotinoid-S₁ Zustands, erklären.

In einem anderen NPQ-Modell wird angenommen, dass Zea eine indirekte Rolle beim Quenchen der Anregungsenergie spielt: während der qE-Induktion bildet sich zwischen Chl *a* und Zea ein Quenching-Komplex. Dabei fungiert Zea über einen Elektrontransfer als terminaler Quencher, was zur Bildung eines Carotinoid-Radikalkations führt. Theoretische Vorhersagen zeigen, dass für eine geeignete Geometrie des Chl-Zea-Heterodimers das Quenchen mittels eines Ladungstransfers möglich ist. Das entspricht einem strahlungslosen Zerfall in einen entsprechend energetisch tiefer liegenden Ladungstransferzustand. Das zugehörige Experiment wurde mit intakten Thylakoidmembranen isoliert aus Spinat durchgeführt. Dabei wurde nach Anregung bei einer Wellenlänge von 664 nm im nahen IR-Bereich unter gequenchten und ungequenchten Bedingungen gemessen. Die spektralen Unterschiede, die sich aus den gequenchten und ungequenchten Zuständen ergaben, wurden der Bildung des Zea-Radikalkations zugeschrieben. Die hier vorgestellten Experimente wurden mit isolierten Lichtsammelkomplexen (LHC II, CP24, CP26 und CP29) durchgeführt, wobei der gequenchte bzw. ungequenchte Zustand durch LHCs simuliert wurde, in welchen das Zea angereichert war bzw. fehlte. Die Bildung des Zea-Radikalkations konnte durch den Vergleich der transienten Differenzspektren dieser zwei Komplexe identifiziert werden. Die Spektren der untersuchten LHCs gleichen sich im untersuchten Spektralbereich bis auf kleinere Unterschiede, die im Bereich des experimentellen Fehlers des Experiments liegen. Außer bei CP26, in welchem mehr Zea angereichert wurde und für welches ein kleines Radikalkation-Signal aufgenommen werden konnte, zeigen keine der Differenzspektren Signaturen, die man für ein Zea-Radikalkation erwarten würde. Dies steht im Gegensatz zu aktuellen Studien, in welchen das Signal des Radikalkations verwendet wurde um auf qE zu schlüssen. Dies deutet darauf hin, dass alle LHC-Minoren (CP24, CP26 und CP29) mögliche quenching-Zentren sind. Dennoch ist das Signal, das man von den LHC-Minoren erhält, etwa 50 mal kleiner und um 20 nm rot-verschoben im Vergleich zu demjenigen, das man von den intakten Thylakoidmembranen erhält. Das lässt vermuten, dass das Zea-Radikalkation an den Grenzflächen der LHCs gebildet wird. Daher ist es nach wie vor notwendig zu zeigen, wo genau und in welchem Pigment-Protein-Komplex des Photosyntheseapparates qE tatsächlich stattfindet. Dies ist ein weiterer entscheidender Schritt für das Verständnis des qE-Schutzmechanismus in höheren Pflanzen. Daher wurde in dieser Arbeit Multiphotonenspektroskopie eingesetzt, um die ultraschnelle Dynamik der Bildung der Carotinoid-Radikalkationen zu untersuchen und die spektroskopischen Signaturen in Zea-angereicherten Komplexen zu ermitteln. In Ergänzung zur bisher vorgestellten Anregungs-Abtast-Spektroskopie kam zur Erzeugung der Carotinoid-Radikalkationen und Charakterisierung des Systems die resonante Zwei-Photonen-Zwei-Farben Ionisations-Spektroskopie (R2P2CI) zum Einsatz.

Die ultraschnelle Dynamik der Bildung des Carotinoid Radikalkations wurde sowohl in Lösungen der isolierten Chromophoren untersucht, als auch in vollständigen LHC II, das aus Pflanzen-Thylakoiden gewonnen wurde. Die Drei-Puls-Technik umfasst Beiträge aus zwei Pulsen mit hoher Intensität zur Einleitung einer resonanten Zwei-Photonen-Zwei-

Farben-Ionisation und einem Puls geringer Intensität mit großer Bandbreite, dem so genannten Abtast-Puls. Die R2P2CI-Messungen lassen die spektroskopischen Eigenschaften von Car^{++} und die spektralen Eigenschaften der Zea und Vio Radikalkationen in LHC II erkennen. In Ethanol haben die Car^{++} -Banden Maxima bei 830 nm (Vio), 880 nm (Lutein), 900 nm (Zea) und 920 nm (β -Carotin). Die Position dieser Maxima hängt stark von dem eingesetzten Lösungsmittel, der Zahl der konjugierten C=C-Bindungen und der molekularen Struktur ab. Außerdem zeigen die R2P2CI-Messungen an LHC II-Proben sowohl mit als auch ohne Zea Radikalkation-Banden von Vio und Zea bei 909 nm bzw. 983 nm, wobei die Bande um etwa 20 nm blauverschoben ist im Vergleich zu Carotinoid Radikalkationen, die zuvor während qE in intakten Thylakoiden identifiziert werden konnten. Außerdem zeigen die transienten Absorptionsmessungen, dass sich Zea angereicherte LHC II-Komplexe nicht im gequenchten Zustand befinden. Frühere biochemische Studien legen nahe, dass nach qE-Induktion das Protein PsbS (Proteinuntereinheit, der eine zentrale Funktion bei qE zugeschrieben wird) monomerisiert und sich an die LHC II-Antennen assoziiert. Wenn Zea tatsächlich an der gleichen Stelle im LHC II wie Vio bindet, dann wäre eine OH-Gruppe des Zea verdeckt, während die andere dem hydrophoben Bereich der Membran zugewandt wäre. Will man das vorgeschlagene Modell beibehalten, in welchem Zea als quencher an LHC II gebunden ist, so wäre ein PsbS/LHC II-Superkomplex ein mögliches Szenario. Dieser Komplex schafft eine hochpolare Umwelt, die die photophysikalischen Eigenschaften von Zea während der qE-Induktion stark beeinflusst. Als Ergebnis kann die Chl-Anregungsenergie gequenchet werden. Wie Carotinoid Radikalkationen die Chl-Anregungsenergie quenchen könnten, wird in dieser Arbeit diskutiert und ein möglicher Quenching-Mechanismus vorgeschlagen.

Photodynamik von Carotinoidradialen

Es wurde gezeigt, dass Carotinoide die entscheidenden Pigmente im Photoschutzmechanismus sind und auch als Radikalfänger in lebenden Zellen agieren können. Die zugrunde liegenden chemischen Prozesse sind der Ladungstransfer und die Reaktionen freier Radikale. Beide führen zur Bildung von Carotinoid Radikalkationen. Trotz ihrer fundamentalen Bedeutung beim nicht photochemischen Quenchen in Grünpflanzen ist nur wenig bekannt über die Lage der angeregten Zustände von Car^{++} , ihre Wechselwirkung mit benachbarten photosynthetischen Pigmenten oder auch über ihre optischen Eigenschaften. Ein detailliertes Verständnis ist nicht nur bezüglich der Beschreibung natürlicher photosynthetischer Prozesse sondern auch beim Studium und Design künstlicher photosynthetischer Systeme notwendig. Carotinoide sind aufgrund ihres niedrigen Ionisierungspotentials exzellente Elektronen-Donoren, was sie zu ausgezeichneten Kandidaten für das Design derartiger Systeme macht.

Generell werden Erzeugung und Analyse von Car^{++} mit mehreren optischen Methoden durchgeführt: in Lösung sowie auch direkt im Protein. Die Zwei-Photonen Zwei-Farben Technik die hier diskutiert wurde, hat den großen Vorteil, dass Experimente in der natürlichen biologischen Umgebung ohne große Störung der natürlichen Situation durchgeführt werden können. Jedoch führt diese Methode nur zu kurzlebigen Populationen von Car^{++} , die innerhalb von Mikrosekunden durch Ladungsrekombination zerfallen. Im Gegensatz dazu ist die chemische Oxidation eine attraktive und einfache Methode zur Erzeugung langlebiger Car^{++} Moleküle, welche für Stunden stabil sind und im Wesentlichen nur durch die Reaktion mit O_2 zerfallen. Anschließend kann die Pump-Probe Spektroskopie

für die Untersuchung der Dynamik der angeregten Zustände durchgeführt werden. Das Oxidationsmittel, das in dieser Arbeit benutzt wurde, ist Eisenchlorid (FeCl_3), welches mit dem neutralen Carotinoid reagiert und zur Bildung von $\text{Car}^{\bullet+}$ führt.

Die experimentellen Untersuchungen zeigen die Existenz eines zweiten niedrig gelegenen $\pi\pi^*$ angeregte Zustand (D_2) Zwischen dem stark erlaubten angeregten D_3 Zustand und dem schwach erlaubter angeregte D_1 Zustand. Die Entdeckung eines niedrig liegenden angeregten Zustandes hat auch Folgen für das NPQ in grünen Pflanzen, da direktes Quenchen angeregter Zuständen durch den Förster Energie-Transfer möglich und effizient ist. Und in der Tat, in einem 4 Puls Experiment konnte gezeigt werden, dass wenn $\text{Car}^{\bullet+}$ durch R2P2CI in Lichtsammelkomplexen von Pflanzen induziert werden, sich die Lebensdauer angeregten Zustände des Chl verringert.

Die Ergebnisse zeigen weiterhin, dass die Wellenlänge der $\text{Car}^{\bullet+}$ Absorptionsbande abhängig von der Polarisierbarkeit des Lösungsmittels und der Zahl der konjugierten Doppelbindungen der Carotinoide ist. Diese Erkenntnis kann in der Praxis genutzt werden, um die Polarität der Mikroumgebung der Carotinoide festzustellen. Wenn die Konjugationslänge eines Carotinoids bekannt ist, kann es als Sensor für die Polarisierbarkeit der Umwelt dienen.

Astaxanthin, mit 11 konjugierten C=C Bindungen, ist ein zehnfach stärkeres Antioxidans als jedes andere Carotinoid. Das Astaxanthin-Molekül ähnelt dem bekannteren β -Carotin besitzt aber die kleineren Unterschiede in der Struktur, wie die zwei zusätzlichen funktionellen Gruppen (Keto und Hydroxy) an jedem Ende. Diese führen zu großen Unterschieden in den chemischen und biologischen Eigenschaften der beiden Moleküle. Im Gegensatz zu β -Carotin, zeigt Astaxanthin eine breitere Absorptionsbande als Folge des Verlustes der Vibrations-Struktur. Photoanregung von Astaxanthin wird gefolgt von intramolekularer Relaxation über strahlungslose Wege des angeregten S_2 und S_1 Zustandes. Die Ergebnisse dieser Arbeit stimmen gut mit früheren Untersuchungen von Astaxanthin in Methanol und Acetonitril überein. In dieser Arbeit habe ich eine globale Fitanalyse benutzt, um die zeitaufgelösten Daten von Astaxanthin in Chloroform zu untersuchen. Zwei kinetische Komponenten mit Zeitkonstanten von 130 fs (Zerfall des angeregten S_2 Zustand) und 5,2 ps (Zerfall des angeregten S_1 Zustand) waren ausreichend zur Beschreibung des kinetischen Verhaltens.

Andererseits unterscheidet sich das Absorptionsspektrum des Astaxanthin-Radikalkations in Chloroform erheblich von dem seiner neutralen Form. Es zeigt eine starke Bande bei 880 nm ($D_0 \rightarrow D_3$ Übergang) und eine schwache Bande bei 1320 nm ($D_0 \rightarrow D_1$ Übergang). Darüber hinaus ist der angeregte D_3 Zustand sehr empfindlich bezüglich der Polarität des Lösungsmittels. Die Änderungen in der Absorptionsbande resultieren aus Wechselwirkungen zwischen dem Lösungsmittel und dem gelösten Stoff, die die Energiedifferenz zwischen dem Grundzustand und dem angeregten Zustand des solvatisierten Astaxanthin-Radikalkations verändert. Astaxanthin-Radikalkationen ($\text{Axt}^{\bullet+}$) werden mittels R2P2CI auf einer Femtosekunden-Zeitskala durch die direkte Abgabe eines Elektrons an das Lösungsmittel erzeugt. Die beobachteten Unterschiede in den Absorptionsspektren von R2P2CI und chemischer Oxidation lassen sich durch dieses freie Elektron erklären. Das Elektron erzeugt eine starke Veränderung der Umgebung, die die optischen Eigenschaften der Carotinoid-Radikalkationen beeinflusst.

Die globale Fitanalyse zeigt die Beteiligung von drei angeregten Zuständen an der beobachteten Dynamik des angeregten Zustands des Astaxanthin-Radikalkation. Der

zunächst angeregte D_3 Zustand zerfällt schnell mit einer Zeitkonstanten von etwa 100 fs in den tiefer liegenden D_2 Zustand. Der angeregte D_2 Zustand zerfällt innerhalb von 0,9 ps durch Übergang in den Grundzustand D_0 und/oder in einen zweiten tiefliegenden angeregten Zustand D_1 . Die Rückkehr aus dem D_1 Zustand in den Grundzustand findet schließlich mit einer Zeitkonstanten von etwa 4,9 ps statt. Im Gegensatz zum neutralen Astaxanthin zeigt sein Radikalkation zwei tiefliegende angeregte Zustände energetisch unterhalb des stark erlaubten angeregten Zustands, der für die intensive Absorption im nahen IR-Bereich verantwortlich sind.

Diese Arbeit ermöglicht jetzt, die grundlegenden Methoden zu verbessern und die Anwendungen auf mehrere Systeme zu erweitern. Zum Beispiel kann die hier entwickelte Zwei-Photonen-Zwei-Farben-Technik angewandt werden, um das vorgeschlagene kinetische Modell der Carotinoid-Radikal-Bildung in LH2-Komplexen experimentell zu bestätigen. In diesem theoretischen Modell wird der angeregte S_1 Zustand der Carotinoide als Vorläufer für den Ladungstransfer-Zustand vorgeschlagen. Im experimentellen Ansatz wird zunächst der S_2 Zustand des Carotinoids angeregt. Nach einer gewissen Verzögerungszeit kann der S_1 Zustand durch einen zweiten Laserpuls depopuliert werden. Gleichzeitig wird die Signatur des Radikalkations abgetastet. Ist der vorgeschlagene Mechanismus korrekt, so wird das Signal des Radikalkations verringert, wenn der S_1 Zustand entvölkert ist.

1 Introduction

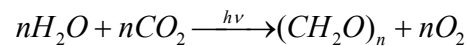
Throughout the industrial world it becomes increasingly clear that mankind urgently needs to find new ways to produce clean and renewable sources of energy that do not produce green house gases. The amount of solar energy hitting the Earth every hour is greater than the total amount of energy that the world's population consumes in a whole year. This fact makes the activities to convert solar energy into electrical power an important issue for future energy production. Nature has overcome this issue by photosynthesis. Consequently there is, currently, enormous interest to obtain detailed information on the molecular mechanisms of photosynthetic solar energy conversion. The various natural light-harvesting systems in photosynthesis can serve as blueprints for the construction of novel solar cells based on organic matter.

Light harvesting is the primary process in photosynthesis. However, all photosynthetic organisms have an ambivalent relationship with light. They require light for life, but on the other hand, too much light leads to chlorophyll triplets and reactive oxygen species, photoproducts which trigger photodamage. Fortunately, carotenoids are membrane bound antioxidants that can quench both singlet and triplet chlorophyll; nevertheless the detailed mechanisms at the molecular level are far from being well understood. The aim of this thesis is to deal with excited state dynamics of carotenoids and carotenoid radical cations in solution as well as in protein complexes, to further understand the photo-protection mechanisms at a molecular level.

1.1 Photosynthesis

Life on earth is almost entirely solar powered.

All organisms require energy for their chemical reactions. These reactions may be involved with reproduction, growth, or other activities. Photosynthetic organisms use light energy to produce carbohydrate, which can be used at a later time to supply the energy needs of the cell. Photosynthesis is therefore the most important biological process on earth, in which sunlight is converted into chemical energy. In most general form, this photochemical process can be described by the equation:



which represents the light-induced cleavage of water and fixation of carbon by formation of a carbohydrate $(CH_2O)_n$ and free oxygen O_2 .

In more details, during photosynthesis, photons are absorbed by light harvesting antenna, membrane proteins which bind chlorophylls and carotenoids. Afterwards, the excitation energy is transferred from the site of absorption to the reaction centers (RCs) (1). Here, excitation is converted into charge separation, which drives the electron flow between photosystem II (PS II) and photosystem I (PS I) through the cytochrome b_6/f complex. The net result of this process is the oxidation of water molecules, the production of molecular oxygen, the reduction of $NADP^+$ and the generation of a proton gradient (ΔpH). The energy stored as ΔpH is exploited for ATP synthesis (Fig. 1.1).

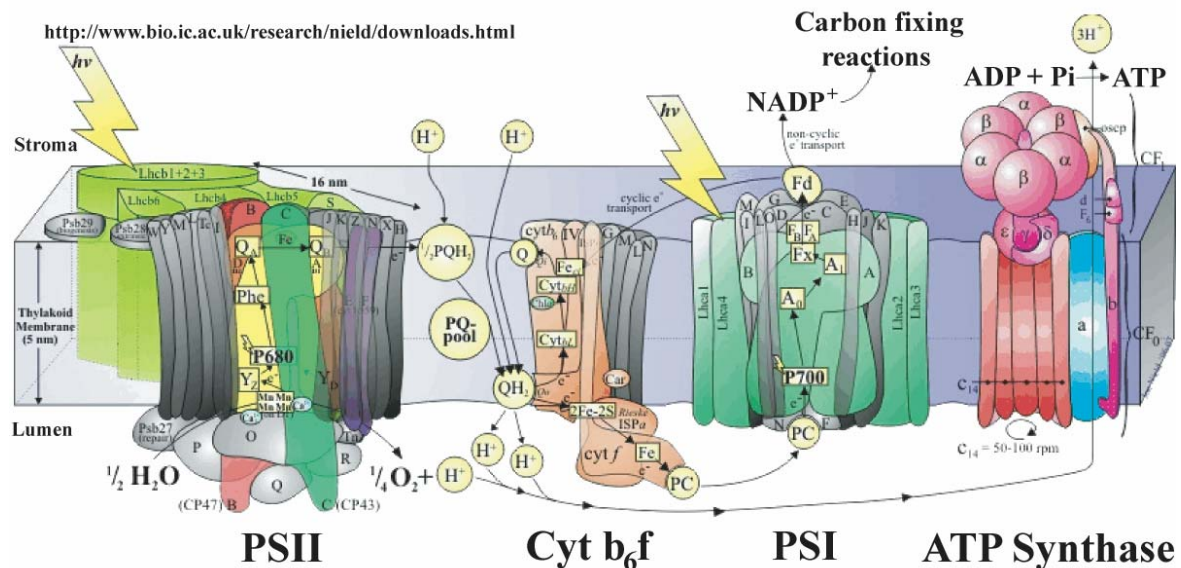


Fig. 1.1. Detailed model of the protein complexes involved in electron and proton transport within the thylakoid membrane of green plants.

1.2 Non-photochemical Quenching

Plants are exposed to sun light intensities that vary rapidly over several orders of magnitude during a typical day (Fig. 1.2), thus the green plants' ability to dissipate energy is, as fundamentally important to its survival as its ability to harvest energy.

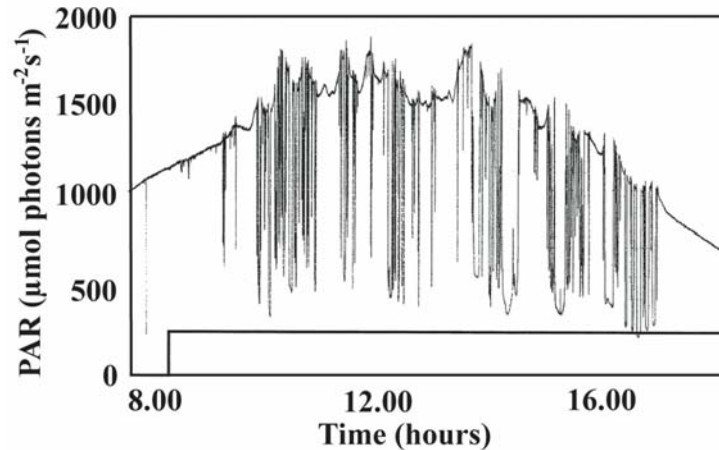


Fig. 1.2. Light conditions of field plants during one representative day (2). PAR: photosynthetically active radiation.

Photoprotective energy quenching limits the production of harmful oxygen species that accumulate under conditions in which the input light intensity exceeds a plants capacity for carbon fixation, a daily stress experienced by a variety of organisms (2). These species destroy vital proteins, such as the PS II D1 reaction center subunit, as well as lipid bilayers, and pigments (3, 4). The effects of such damage range from temporary decreases in photosynthetic efficiency to, in the worst case, death of the organism. Lessons learned from how plants carefully, and very successfully, balance photosynthesis and photo-protection may provide invaluable information about how to engineer and select plants that will be suited to specific environmental conditions. The most common physical observable used to assess photosynthetic function and its subsequent down-regulation in excess-light conditions is chlorophyll (Chl) fluorescence, because it is sensitive to a wide range of changes in the overall apparatus. Processes that decrease the overall Chl fluorescence quantum yield are generally divided into two categories, photochemical quenching (qP), which is exclusively associated with photochemical charge separation in the PS II reaction center (RC), and non-photochemical quenching (NPQ). The latter process is broadly defined as all fluorescence quenching that is not directly related to charge separation. NPQ can be subdivided into three components: feedback de-excitation quenching or high-energy state quenching (qE), photoinhibition (qI), and state transitions (qT), each of which has characteristic induction and relaxation kinetics (5). qE is the only NPQ component that is correlated with changes induced by rapid fluctuations, on the order of seconds to minutes, in input light intensity (6).

When Chl absorbs light it is excited from its ground state to its singlet excited state, $^1\text{Chl}^*$. From there several relaxation pathways lead back to the ground state (Fig. 1.3).

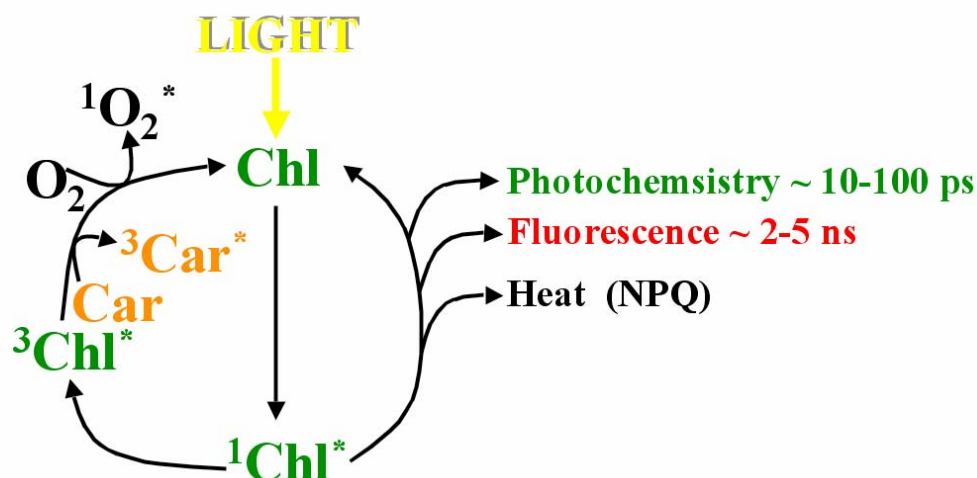


Fig. 1.3. Possible fates of excited Chl embedded in the light harvesting complexes of plants (6).

It can relax by emitting light, seen as fluorescence. Its excitation can be used to fuel photosynthetic reactions, or it can de-excite by dissipating heat; both of these mechanisms reduce the amount of fluorescence. They are therefore referred to as qP (photochemical quenching) and NPQ (non-photochemical quenching) of Chl fluorescence. Finally, $^1\text{Chl}^*$ can, by intersystem crossing, produce $^3\text{Chl}^*$, which in turn is able to produce $^1\text{O}_2^*$, a very reactive oxygen species. To prevent formation of singlet oxygen ($^1\text{O}_2^*$), photosynthetic organisms use carotenoids (Car), which can quench both chlorophyll triplet ($^3\text{Chl}^*$), and singlet ($^1\text{Chl}^*$) excited states.

This thesis is focused on understanding the photo-protection mechanisms in plants and purple bacteria. For this purpose, several spectroscopic methods, were combined and applied to elucidate the function of carotenoids in photo-protection. The experiments presented in chapters 3-6 were focused on the mechanisms involved in quenching of singlet and triplet state of the electronically excited (bacterio)chlorophylls.

Next section of this chapter deals with the pigments involved in photo-protection, while the ultrafast transient absorption method used to investigate the excited state dynamics of these molecules is described in chapter 2.

1.3 Pigments

Pigments are largely responsible for generating skin and eye color in humans and are also responsible for the green color in plants. In plants and bacteria the pigments of antenna systems are designed to serve several functions: i) absorption of light with high efficiency, ii) transfer of excitation energy with minimum losses to the reaction centers, iii) stabilization of the photosynthesis apparatus and iv) dissipation of excess energy through heat. The main pigments, which fulfill these functions, are chlorophylls, bacteriochlorophylls and carotenoids.

1.3.1 (Bacterio)Chlorophylls

Chlorophylls are probably the most abundant and certainly the most obvious biological pigments. Structurally, they are characterized by a porphyrin ring possessing a central metal, usually Mg, and a long phytol chain. Chemically, they are unstable to both acids and bases, to oxidation and light, and have a pronounced tendency for aggregation. Physically, they are characterized by long-lived excited states and by intense absorption covering the spectral range between 330 and 800 nm. Most of chlorophylls and bacteriochlorophylls are bound to proteins, where they contribute to the folding and stabilization of the polypeptide chain. In LHC II, the major peripheral light harvesting pigment–protein complex of photosystem II in higher plants, for example, 14 Chls plus 4 carotenoids are bound to only 250 amino acids. This close packing of pigments ensures not only a high light absorption per unit volume, but also increases the photo-protection level through quenching channels. This quenching can be imagined as a statistical process: There is a certain chance that in the photoprotective act a quencher molecule is formed, whose excited state is short-lived and relaxes by rapid internal conversion to the ground state. If this quencher is isolated, the effect is negligible but when this quencher is tightly coupled to the other pigment molecules, it will act as a sink and convert any excitation of the entire coupled unit to heat.

Some common chlorophyll characteristics can be seen in Figure 1.4, where the three kinds of chlorophyll investigated in this thesis are shown.

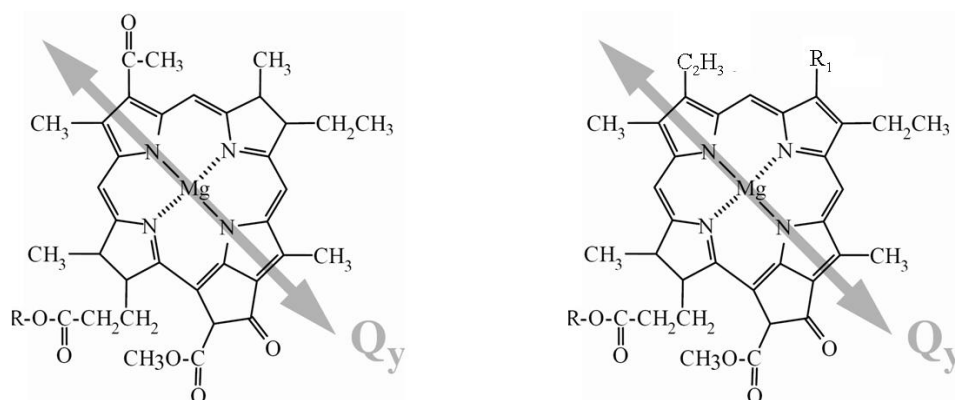


Fig. 1.4. Structure of BChl *a* (left), Chl *a* and Chl *b* (right). R represents the phytyl chain, R₁: CH₃ for Chl *a* and CHO for Chl *b*. The arrow indicates the direction of the Q_y transition dipole moment.

Chlorophylls are almost flat molecules built up of 5 carbon rings. The four most central rings contain nitrogen at their innermost position, and together, the four nitrogen atoms coordinate a magnesium ion located in the central cavity of the molecule. To one of the rings, a long chain of about 20 carbon atoms is attached, the phytyl chain, which often serves as an anchor for fixing the chlorophyll in the protein. Depending on the particular chlorophyll, various smaller side groups are attached to several carbons in the rings, as is illustrated in Fig. 1.4.

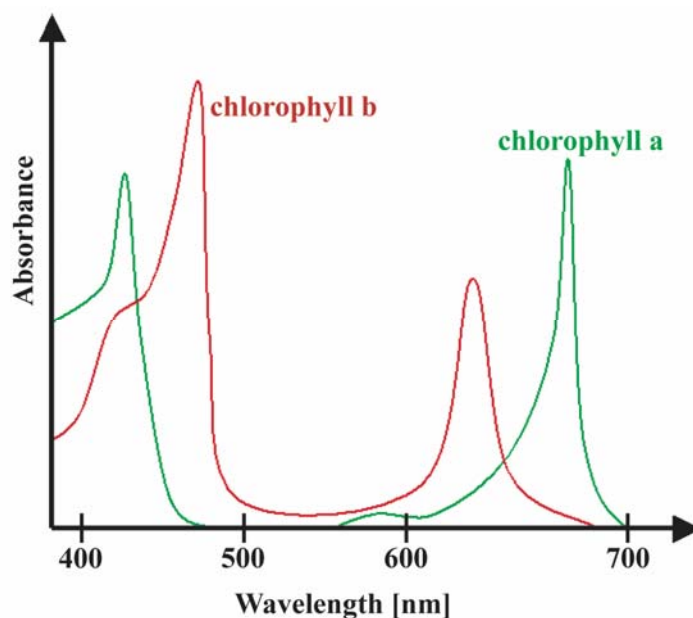


Fig. 1.5. Absorption spectra of chlorophyll *a* and *b* solubilized in methanol.

The absorption spectra of free chlorophyll *a* (green) and *b* (red) in methanol are shown in Figure 1.5. The direction of the transition dipole moment of the red most transition, Q_y lies roughly in the direction of the $N_{II} - N_{IV}$ axis. Counting of N atoms is clockwise starting with N_I at the phytol chain. The Q_x transition has a dipole moment along the $N_I - N_{III}$ axis, perpendicular to the Q_y dipole. Because of the symmetry breaking character by the 5th ring and the side groups, the Q_x has a higher energy and lower oscillator strength than the Q_y . At even higher energy, the strongest transition in the visible, the Soret band, is found. Both Q_x and the Soret states are very short-lived, with internal conversion to the Q_y state taking place in less than 100 fs. Q_y , on the other hand, lives for several nanoseconds, and almost all excitation transfer between chlorophylls takes place via interaction between Q_y transition dipoles.

Apart from Chl *a* and Chl *b*, I investigated the purple bacterial pigment bacteriochlorophyll *a* (Bchl *a*). Compared to chlorophylls, bacteriochlorophylls lack one double bond in one of the pyrrole rings, ring II, and extra side groups are attached to both carbon atoms involved in that bond (Fig. 1.4). This difference causes a huge shift in excited-state energy: in a typical solvent like methanol, the Q_y band of Bchl *a* absorbs at 777 nm, and the Chl *a* and Chl *b* Q_y at 665 nm and 645 nm, respectively. The higher transitions Q_x and Soret, on the other hand, are found at similar wavelengths as in Chl 550 – 600 nm and 400–480 nm, respectively. *In vivo*, the difference between the Q_y energies is further enhanced. For both Chl and Bchl, the interaction with the protein will lead to a red-shift, but the size of this shift is different. Almost all Chl in protein will absorb at wavelengths shorter than 680 nm. The bacterial light-harvesting complexes on the other hand, use BChs and absorb light at wavelength shorter than 880 nm. The red-shift compared to the free Bchl transition can be as large as 100 nm. These huge shifts arise both from the interaction between Bchl and protein, especially in the form of hydrogen bonds, and from the interaction between the pigments themselves. This interaction is relatively strong in purple bacterial antenna because they consist of well-ordered, tightly packed pigment assemblies. Such aggregates enable the bacteria to absorb a relatively large fraction of the incident light and to transfer energy very rapidly. Moreover, the large red-shift is not only a byproduct of the tight packing, but it also provides the bacteria with a niche that is not taken up by plants or algae.

The above mentioned excited states Q_x , Q_y , and Soret are all singlet states, accessible from the singlet ground state via dipole-allowed singlet-singlet transitions. Next to the system of singlet states, Chls also have a triplet system, of which the lowest state lies well below Q_y . A Chl in the Q_y state can convert to the triplet state via intersystem crossing. The triplet state decays much more slowly than the Q_y , on a millisecond timescale, which results in a loss of ground state (B)Chl. Even more problematic is the ability of triplet Chl to interact with oxygen molecules, which results in the conversion of the ground-state triplet O_2 to an excited-state singlet O_2 . Singlet oxygen converts in turn to an oxygen radical which can damage organic material very effectively. It is one of the main functions of the second major class of photosynthetic pigment, carotenoid, to prevent photodamage by quenching both singlet and triplet states of the photosynthetic apparatus.

1.3.2 Carotenoids

Carotenoids, the other class of pigments in photosynthetic organisms, fulfill important functions in light harvesting and photo-protection. As light-harvesting pigments carotenoids complement the absorption spectrum by covering the blue and green spectral region not accessible by chlorophylls and bacteriochlorophylls. In addition, they scavenge dangerous singlet oxygen molecules and quench both singlet and triplet states of the photosynthetic apparatus. Outside photosynthesis, they are known as efficient quenchers of various reactive radicals by intercepting the chain of oxidative reactions. There is accumulating evidence that this antioxidative function is a key mechanism of protection against various diseases including cancer, atherosclerosis, and macular degeneration in humans (7, 8). Yet, knowledge of the detailed molecular mechanism of such actions is so far very limited.

Carotenoids are almost linear rod-like stretched molecules which consist of a polyene chain with small end-groups at both sides. The basic building block of a carotenoid molecule is the isoprenoid unit and the number of double bonds in the linear chain, which is the essential factor in determining its optical properties. All carotenoids which occur in photosynthetic systems have a polyene chain consisting of 9 to 13 double conjugated C=C bonds. The structures of carotenoids studied in this thesis are shown in Figure 1.6, i.e. violaxanthin, lutein and zeaxanthin, which are bound to the peripheral antenna complexes of PSII, β -carotene bound to the reaction center, astaxanthin, and spirilloxanthin, which is bound to the core antenna of the purple bacterium *Rhodospirillum rubrum*.

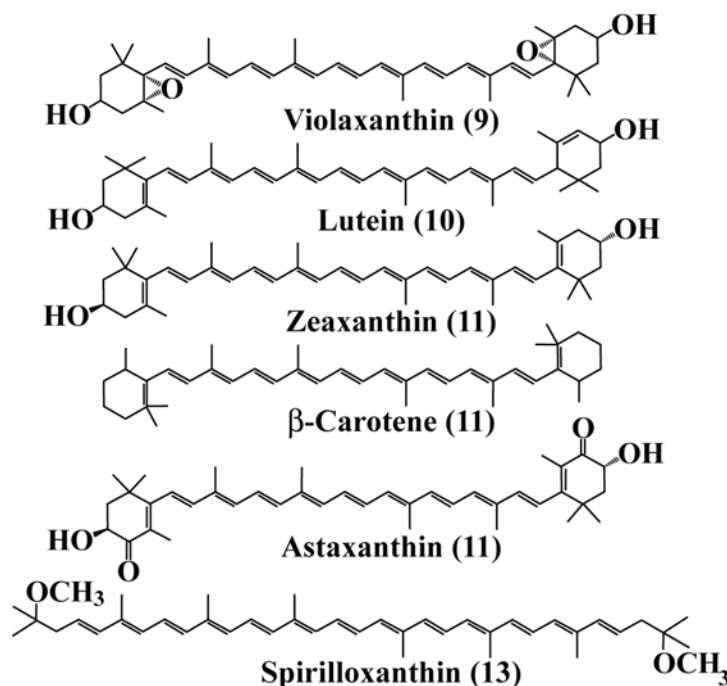


Fig. 1.6. Molecular structures of plant photosystem carotenoids, conjugation length is denoted in parentheses.

The carotenoid excited states are similar to those of polyenes, which belong to the C_{2h} point symmetry group. Carotenoids exhibit intense absorption in the spectral region 400–600 nm (Fig. 1.7), which originates from a strongly allowed transition from the 1^1A_g (S_0) ground state to the second excited state 1^1B_u (S_2), according to the idealized C_{2h} point group of the linear polyene.

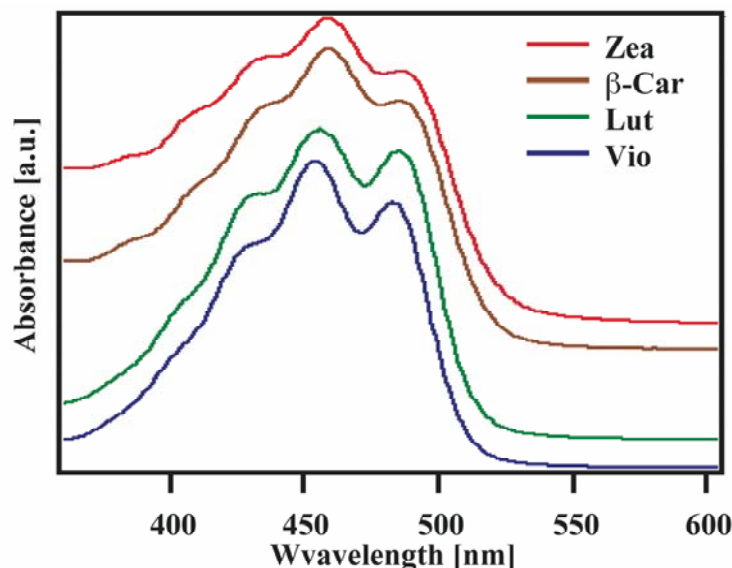


Fig. 1.7. Room temperature absorption spectra of the neutral form of violaxanthin, lutein, zeaxanthin and β -carotene.

The lowest singlet excited state, S_1 (2^1A_g), has the same inversion symmetry as S_0 , and thus it is inaccessible from the ground state S_0 by one-photon excitation. However, the S_1 state has been directly investigated by two-photon excitation experiments (9–11). In carotenoids, this symmetry is always slightly disturbed by the head groups and sometimes by side groups, or by a twisting of the carbon chain when the molecule is bound to a protein. In carotenoids, $S_0 \rightarrow S_1$ is not entirely forbidden, but the transition dipole moment is exceedingly weak. This has made it difficult to determine the transition energy, but several fluorescence and two-photon excitation studies indicate that, for most carotenoids, S_1 lies slightly above the Q_y of chlorophyll, at around 600–630 nm. The second excited state S_2 has different symmetry, so the transition $S_0 \rightarrow S_2$ is strongly allowed and lies at around 500 nm.

The vibronic features in the S_2 band are dominated by C=C and C–C stretching modes, with frequencies of $\sim 1500\text{ cm}^{-1}$ and $\sim 1150\text{ cm}^{-1}$, respectively. Due to its large associated dipole (~ 15 Debye), the $S_0 \rightarrow S_2$ transition is strongly affected by the solvent polarizability through dispersion interaction. In contrast, the S_1 energy level is hardly affected by the environment because of its near-zero transition dipole.

Excited state dynamics of carotenoids is described in terms of downhill internal conversion between S_2 , S_1 , and S_0 states. Absorption of light promotes carotenoids to the S_2 state, whose population rapidly relaxes to the lower S_1 state on a time scale of 50–300 fs. Subsequently, the S_1 state decays by internal conversion to the ground state on the picosecond time scale. For carotenoids to be efficient light-harvesters, these fast decay

channels need to be counteracted by equally fast energy transfer to nearby (B)Chl molecules, and, indeed, the efficiency of this ET process can be as high as 90-95 %.

All the carotenoid excited states live much shorter than the Chl Q_y state and the Cars should quickly transfer the absorbed energy to Chls in their vicinity. Depending on the particular light-harvesting complex, this transfer proceeds via the route $S_2(\text{Car}) \rightarrow Q_x(\text{Chl}) \rightarrow Q_y(\text{Chl})$, and/or via $S_2(\text{Car}) \rightarrow S_1(\text{Car}) \rightarrow Q_y(\text{Chl})$. Either way, transfer from Car to Chl asks for close contact between the molecules

A second function of carotenoids is the protection against singlet oxygen formation mentioned above. This mechanism also operates only at small distances and is based on triplet (Chl) to triplet (Car) transfer via electron exchange. Whereas the Chl triplet lies above the oxygen singlet state in energy, the carotenoid triplet state lies below it and thus cannot excite oxygen. Another advantage of the carotenoid triplet state vs. that of Chl is its shorter lifetime, which is in the microsecond rather than millisecond range. Therefore, less molecules will be in this photosynthetically inactive state at any time.

When the flux of incident light is too high, another protective role of Cars becomes important, the non-photochemical quenching of excitations. Most carotenoids also have a third role as a structural building block, weaving themselves in between the protein polypeptide chains. This is certainly true for the two xanthophylls in the centre of LHC II, without which the complex does not form. In some purple bacterial antennae the structural and photo-protection function appears to be the main role as the energy transfer efficiency of carotenoid to bacteriochlorophyll is only 40%.

Carotenoids can serve as accessory light harvesting pigments, whereas their functions in the photo-protection and non-radiative dissipation of excess excitation energy are more important for plants (12). It is thought that zeaxanthin may have a direct role in quenching the excitation energy (13-15), forming a quenching complex between Chl *a* and zeaxanthin during the induction time of qE , in which case zeaxanthin acts as the terminal quencher. This hypothesis was predicted by theory and indeed it has been confirmed experimentally that carotenoid radical cations are formed during qE . The experiment was performed on spinach thylakoid membranes upon excitation at 664 nm under quenched and unquenched conditions. The spectral difference observed between the quenched and the unquenched state was ascribed to the formation of a zeaxanthin radical cation (Fig. 1.8) (15).

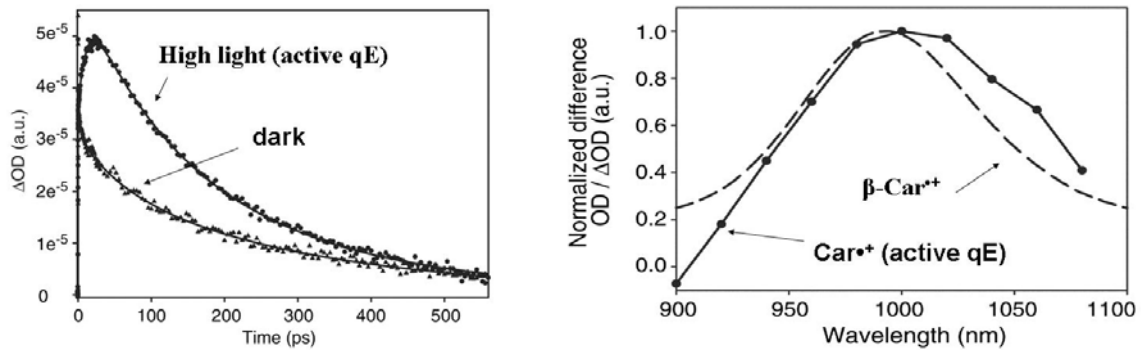


Fig. 1.8. Transient absorption spectra of spinach thylakoids recorded upon excitation at 664 nm and probed at 1000 nm (left). Reconstructed quenched minus unquenched difference spectrum (solid line with circles) at a time delay of 20 ps, together with the spectrum of $\beta\text{-Car}^{++}$ (dashed line) (right) (16).

The sketch of the proposed quenching model is shown in Fig. 1.9 below.

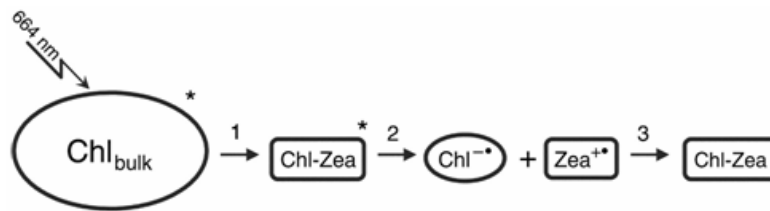


Fig. 1.9. Scheme of the qE quenching mechanism, showing generation of Zea^{++} after selective excitation of the Chl Q_y band at 664 nm.

This model involves three species: a bulk Chl pool (Chl_{bulk}), a Chl-Zea heterodimer that quenches excited Chl_{bulk} molecules, and a charge-separated ground state consisting of Chl^{\bullet} and Zea^{++} (Fig. 1.9). The charge transfer state is formed from relaxation of the Chl-Zea excited state, $(\text{Chl-Zea})^*$ (17). Transient generation of Zea^{++} in ~ 11 ps was observed. This component corresponds to the net dynamics of the Chl_{bulk} molecules that transfer the excitation to the Chl-Zea heterodimer (step 1), followed by an ultrafast charge separation leading to a Chl^{\bullet} and a Zea^{++} (step 2). The charge separated Zea^{++} can be detected as a transient absorption signal in the spectral region specific for carotenoid radical cations. In a third step the Zea^{++} signal decays on a timescale of 150 ps, which corresponds to charge recombination between Chl^{\bullet} and Zea^{++} .

1.4 Plant Light-Harvesting Complexes

Higher plants have two different reaction centers, PS I and PS II, both contained in the thylakoid membrane. Within this membrane, these RCs occupy different locations. As can be seen in Figure 1.1, the LHC II antenna is usually associated with PS II, but it can also migrate in the membrane in order to harvest light for PS I. Figure 1.10 shows an electron micrograph image of a large membrane fragment, a so-called PSII supercomplex, consisting of a PS II RC dimer and its surrounding LHCs (18).

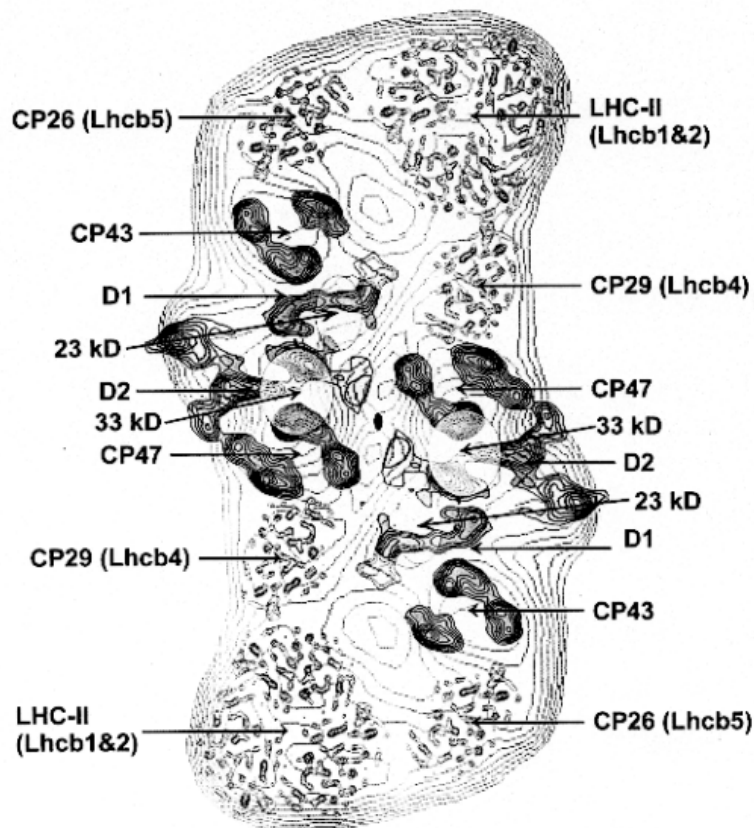


Fig. 1.10. PS II supercomplex, electron micrograph image.

The central part of the supercomplex is formed by a dimer of PS II reaction centers, surrounded by the core antennae CP43 (Chlorophyll Protein, weight 43 KiloDalton (kDa)) and CP47. Next to the RC-core complex dimer, the monomers CP29, CP26 and CP24, the so-called “minor antennae”, are found. The LHC II antennae are located at the edge of the supercomplex, the farthest from the RC. Within the PS II supercomplex, two types of chlorophylls are found: Chl *a* and Chl *b*. The RC-core complex binds only Chl *a*, the Chl *a*:Chl *b* ratio in the three minors is about 3:1, and LHC II binds nearly as much Chl *b* as Chl *a* (in an *a*:*b* ratio of 7:5 to 8:6). This gradient in Chl *b* content is consistent with excitation energy flow toward the RC.

1.4.1 Light-Harvesting Complex II (LHC II)

The major light-harvesting complex of photosystem II (LHC II) serves as the principal solar energy collector in the photosynthesis of green plants and presumably also functions in photo-protection under high-light conditions. It is by far the most abundant light-harvesting complex, with an average ratio of four LHC II trimers per RC monomer; altogether, LHC II binds about 50% of all chlorophyll. It accounts for roughly 30% of the total protein in the chloroplast membrane (Table 1.1), which makes it the most abundant membrane protein on earth.

The 2.5 Å structure of pea LHC II determined by X-ray crystallography reveals the mutual arrangement of 42 chlorophylls *a* and *b*, 12 carotenoids and six lipids in the LHC II trimer (Fig. 1.11).

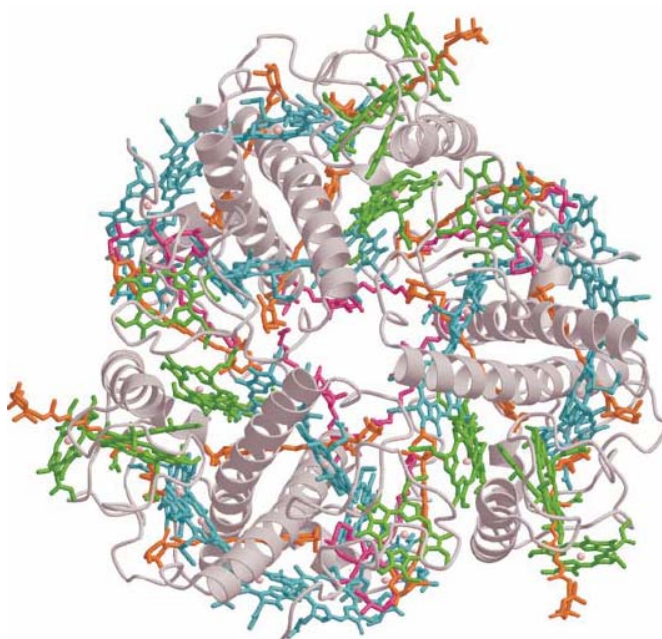


Fig. 1.11. Top view of the LHC II trimer. Grey-polypeptide; cyan-Chl *a*; green-Chl *b*, orange-carotenoids, pink-lipids.

LHC II from dark adapted plants contains lutein, neoxanthin and violaxanthin in a ratio of about 2:1:1. However, LHC II from plants under high light condition shows contributions of two additional carotenoids: anteraxanthin and zeaxanthin. It is well known that the loosely-bound violaxanthin is involved in the xanthophyll cycle, in which violaxanthin is de-epoxidized to form zeaxanthin under high-light conditions.

Complex	Chl <i>b</i>	Chl <i>a</i>	Phe <i>a</i>	β -Car	Lut	Vio	Neo
PSII RC	0	6	2	2	0	0	0
CP29	2	6	0	0	1	1	0.5
CP26	3	6	0	0	1	0.5	0.5
CP24	5	5	0	0	1	0.5	0.5
LHC II	5-6	7-8	0	0	2	0.3-1	1

Table 1.1. Pigment composition of PS II complexes.

Figure 1.12 shows the scheme of energy levels and energy-transfer pathways between carotenoids and Chl molecules in the LHC II complex. The double arrow depicts excitation into the S_2 state of a carotenoid. Intramolecular relaxation processes are denoted by wavy arrows, while the dashed arrow represents the long-lived Chl *a* fluorescence. Solid arrows represent the energy-transfer channels confirmed by time resolved studies. The dotted lines represent possible energy transfer channels involving energy transfer between thermalized carotenoid S_1 state and Chl *a* and back energy transfer from Chl *a* to the S_1 state of a carotenoid. The known energy-transfer pathways are labeled by the corresponding time constant.

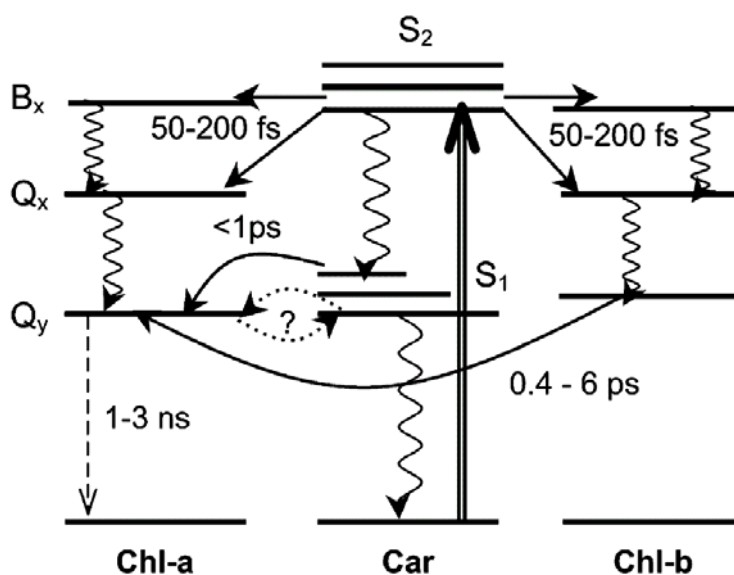


Fig. 1.12. Scheme of energy levels and energy-transfer pathways between carotenoids and Chl molecules in the LHC II complex (19).

A general aspect of the LHC II structure, which should be pointed out here, is its less organized nature, compared to the bacterial antenna, which will be described below. In LHC II, all Chls occupy clearly nonidentical sites. This inhomogeneity in environments and inter-pigment distances is reflected in the spectroscopic properties of the LHC II complex. At first sight, the absorption spectrum (Fig. 1.13) appears to have little fine structure, with one Chl *b* band at 650 nm, and one Chl *a* band peaking at 676 nm with a blue shoulder at ~670 nm.

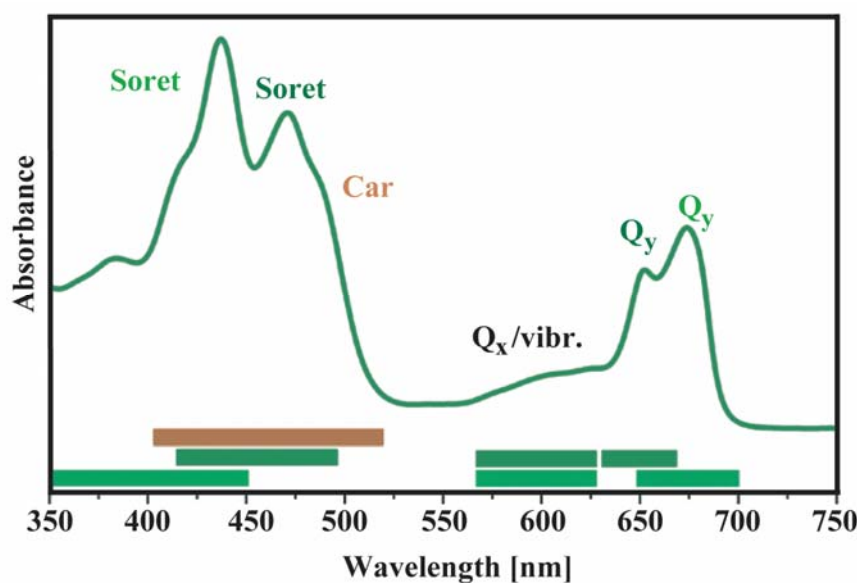


Fig. 1.13. Absorption spectrum of the LHC II complex with contributions of different molecular species to the particular spectral region denoted by horizontal bars. Carotenoids (orange), Chl *a* (light green), and Chl *b* (dark green).

With the use of various more sophisticated methods such as circular dichroism (CD), linear dichroism (LD), etc., twelve different bands could be identified. In time-resolved spectroscopic experiments, such as transient absorption difference spectroscopy, the excitation pathway upon photon absorption through these different energy levels can be followed. The transient absorption method, which was used for most studies, is especially suited for observation of such steps between different spectral forms. Thus, many downhill energy transfer processes have been identified in the LHC II complex (20-23). Spectrally, the observed processes fall into two categories: transfer from Chl *b* to Chl *a* and transfer from more blue absorbing Chl *a* to more red absorbing Chl *a*. Both were found to occur on several timescales from a few 100 fs to tens of ps (21, 24). After the equilibration within a LHC II monomer is completed, energy transfer between different LHC II monomers within one trimer can take place. This transfer is thought to be rather slow compared to the transfer within a single complex, as all the transfer times up to tens of ps were found to be unchanged upon monomerization (23). After several inter-trimer jumps, the excitation will arrive on one of the minor antennae, from where it will continue to a core antenna or to the RC directly. Altogether, the average time it takes an excitation to get trapped in the PS II RC, the trapping time, is about 150 to 200 ps (25).

1.4.2 Minor Peripheral Antenna Complexes (CP24, CP26 and CP29)

Besides the major trimeric peripheral antenna complexes LHC II, the outer antenna of PS II also contains the minor complexes CP29, CP26 and CP24. These proteins show large homology with LHC II, especially regarding the chlorophyll binding sites, and bind approximately 8-10 chlorophylls (*a* and *b*), besides several xanthophylls (Table 1). They also share many spectroscopic properties with LHC II (26), and their overall fold is thought to be similar to that of LHC II (27, 28). In general, one copy of each protein is found per PS II RC and together the minor complexes bind 15% of the chlorophylls in PS II. Therefore, their role in light harvesting seems to be less pronounced than the LHC II, although their role in regulatory mechanisms can be important in view of the location close to the PS II core. A possible role of these complexes in regulatory mechanisms is strengthened by the finding that a larger fraction of violaxanthin is converted to zeaxanthin in CP26 and CP29 than in trimeric LHC II (12). In addition, CP26 and CP29, but not LHC II or CP24, bind dicyclohexylcarbodiimide (DCCD), an inhibitor of NPQ (29, 30).

1.5 Bacterial Light Harvesting Complex 1 (LH1)

Unlike the plant light-harvesting systems, the bacterial light harvesting complexes are structures with a very high degree of symmetry. The LH1 is the only type of antenna embedded in the photosynthetic unit of the purple bacteria of *R. rubrum* and consists of a ring-like array of 16 $\alpha\beta$ -polypeptide subunits, each subunit binding a pair of BChls and one spirilloxanthin (Spx) (31). Actually the light harvesting antennae from this purple bacterium are well-characterized membrane proteins, because they possess a combination of properties that makes them particularly attractive for both biochemical and biophysical studies. This light-harvesting system is comprised of only two different pigments, BChl *a* and Spx with well defined and separated spectra. The BChl dimers embedded in LH1 absorb at 880 nm (Q_y) and 590 nm (Q_x), respectively, while the Spx absorption spans the spectral range between 500-560 nm (Fig. 1.14).

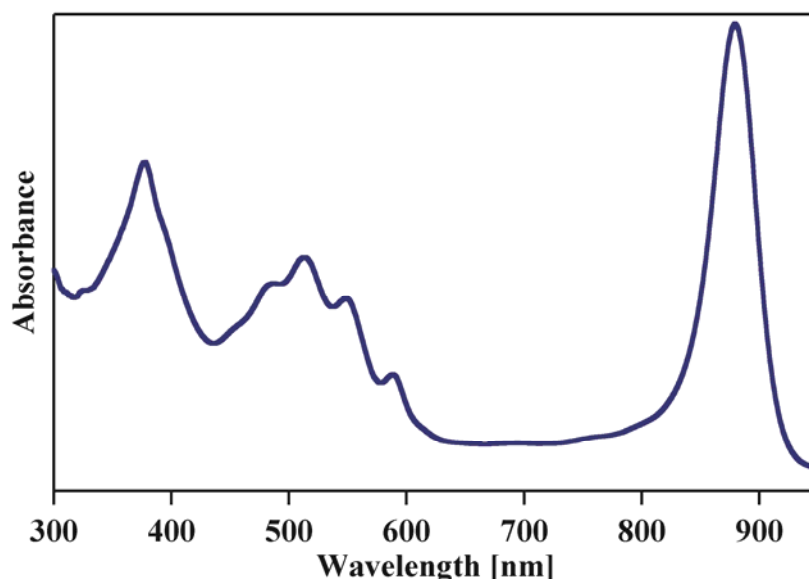


Fig. 1.14. Absorption spectrum of the LH1 complex from *R. rubrum*.

Although only a low resolution structure is available for LH1 from *R. rubrum*, it is evident that this antenna is organized as a ring, in analogy with the peripheral antenna complexes LH2 of *Rhodospseudomonas acidophila* (32), most probably with a 16-fold symmetry (31). The ring has an outer diameter of 116 Å and an inner diameter of 68 Å, enough to enclose the RC complex (Fig. 1.15).

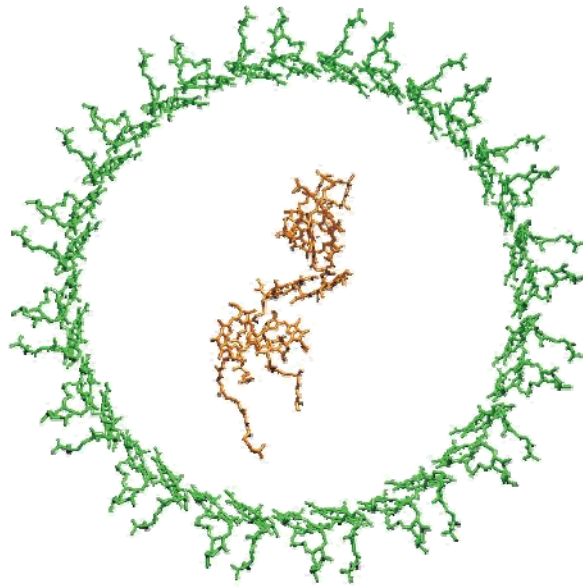


Fig. 1.15. Pigment model of the ring structure of the LH1 complex, enclosing the reaction center.

Details regarding the pigment arrangement could not be obtained from the low resolution structure of LH1, but, like in LH2, the heterodimeric subunits probably associate into a ring with the α -polypeptides on the inside, the β -polypeptides at the outside and the BChl dimers sandwiched between the two concentric rings of polypeptides. Also visible in the absorption spectrum (Fig. 1.13) are carotenoids bands, at 482, 512 and 548 nm. Each $\alpha\beta$ -dimer contains one molecule of spirilloxanthin, the longest naturally occurring carotenoid species (13 conjugated double-bonds). The spirilloxanthin was not identified in the 8.5 Å projection map, but, it is probably oriented almost perpendicular to the membrane plane.

2 Experimental Methods

Various processes in nature are accompanied by color changes. For example, when the visual pigment rhodopsin is excited by light, it undergoes a complex fast isomerization reaction, whereby the wavelength of maximum absorption shifts from about 500 nm to approximately 550 nm (33). Such (photo)chemical reactions lead to products with different absorption properties than the reactant species, thus offering a possibility for monitoring. Ultrafast transient absorption techniques directly explore these processes by accurate detection of absorption changes in time, to unravel the identity of the intermediates and the kinetics of these processes (34, 35). This technique involves contributions from a high-intensity pump pulse initiating a photo-induced process and a low-intensity broad-band probe pulse which scans the process at different delay times. This method is used extensively to examine the excited states dynamics of any molecule whose reaction to light is of interest.

As mentioned in the introduction (chapter 1), photosynthesis is the most important biological process on earth. Using transient absorption spectroscopy to study photosynthesis presents the great advantage that light, which is the investigating tool, constitutes the energy input of this process. The photosynthetic light reaction includes some of the fastest known chemical reactions. The most important events in a photosynthetic reaction occur in trillionths of a second. Measuring such short-lived events, and understanding the chains that link them together, demand some of the most precise experiments and exact measurement technologies currently available. This implies certain requirements for the light source used: a suitable wavelength within the absorption band of the sample, sufficient power, and, most importantly, short enough pulse duration compared to the studied reaction. Nowadays, one can achieve all these requirements using femtosecond-spectroscopic systems, which produce laser pulses shorter than 100 fs. I use here a commercially available femtosecond laser, a Ti:sapphire system running at a central wavelength of 775 nm (36).

In this chapter I will give a short description of such a laser setup, which was used to acquire the data presented in this thesis. I will start with the description of the femtosecond laser system, further the wavelength conversion/tuning and generation of multiple pulses for selectively pumping ground and excited states is presented, then the white light generation as well as the data acquisition/processing is explained.

2.1 The Femtosecond Laser System

The experimental setup is based on a commercial Ti:Sapphire amplifier with 1 kHz repetition rate, with a pulse width of about 150 fs (FWHM) and a pulse energy of 800 μJ at a central wavelength of 775 nm. Part of its output is used for pumping a non-collinear optical parametric amplifier (NOPA) with a tunable wavelength ranging from 480 nm to 1000 nm (a detailed description of the NOPA is presented below). The output pulse from the NOPA can be compressed to less than 30 fs in a two prism pair compressor unit and used as the pump pulse. For the multi-photon experiments, further 775 nm and 388 nm pulses were used, pulses generated simply by using the output of the Ti:Sapphire laser or, by using a BBO crystal. The samples are probed with single filament white light generated in sapphire substrates. Finally, the pump and the probe beams are focused on the sample using an off-axis parabolic mirror. For detection I use two vis-spectrometers (signal and reference) each with a 42 segment photo-diode array ($\Delta\lambda = 8$ nm). While the signal spectrometer records the actual spectrally resolved transmission of the sample at a certain delay time between the pump and the probe pulses, the reference spectrometer records the white light intensity. In order to improve signal-to-noise-ratios, photo-induced absorbance changes are detected in a referenced single shot measurement. As a result, a spectral range for probing from 400 nm to 1000 nm could be realized with this setup providing signal-to-noise-ratios up to $\sim 10^4$. A schematic outline of the setup is shown in Figure 2.1.

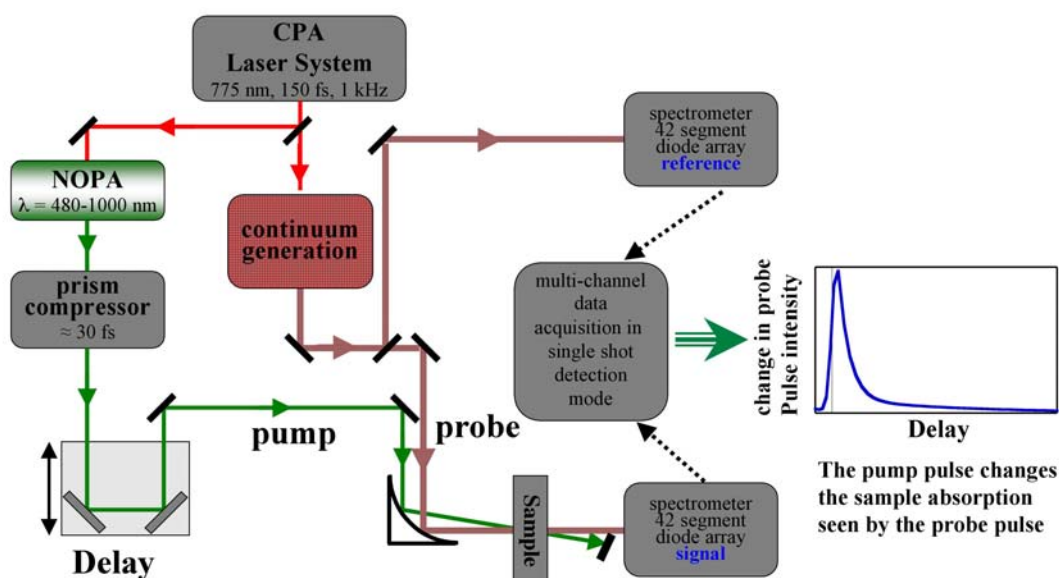


Fig. 2.1. Experimental setup of the pump-probe experiment.

Chirped pulse amplification (CPA) is one of today's wide-spread methods of creating intense ultrashort light pulses. Before amplification the pulse coming from the oscillator is temporally stretched from some hundred femtoseconds to some hundred picoseconds. After the amplification, the pulses are again compressed to minimum duration. Therefore, a complete femtosecond laser system needs in principle an oscillator, a regenerative amplifier consisting of a stretcher, a compressor and detectors. For this experiment a titanium sapphire laser of the model Clark MXR CPA 2001 was used as femtosecond light source. In principle, it contains a diode laser, an erbium glass fiber, an YAG pump laser, and a regenerative titanium sapphire amplifier as well as a compressor (37). In a stable condition, it is possible to achieve pulses lasting for about 150 fs with a central wavelength at 775 nm and a repetition rate of approximately 1 kHz. The output pulse energy is approximately 800 μJ .

2.1.1 Non-collinear Optical Parametric Amplifier (NOPA)

In order to access a variety of spectral regions, nonlinear optical processes can be employed. Optical parametrical amplification (OPA) in a nonlinear crystal (usually β -barium borate, BBO) is one of the most powerful tools to generate ultrashort pulses at different wavelength. The tuning range, in the case of this setup, is 480 to 1000 nm for pumping with a frequency doubled Ti:sapphire amplifier system. In more detail, the tunable NOPA pulses are produced by using a low energy seed pulse (SC), generated in a 1 mm sapphire plate, which is amplified by splitting up a high energetic pump photon into a signal and an idler photon, typically in a BBO crystal (Fig. 2.2). The noncollinear setup allows a matching of the group velocities of signal and idler, increasing the gain factor and preserving the fixed phase relation of the incident seed pulse.

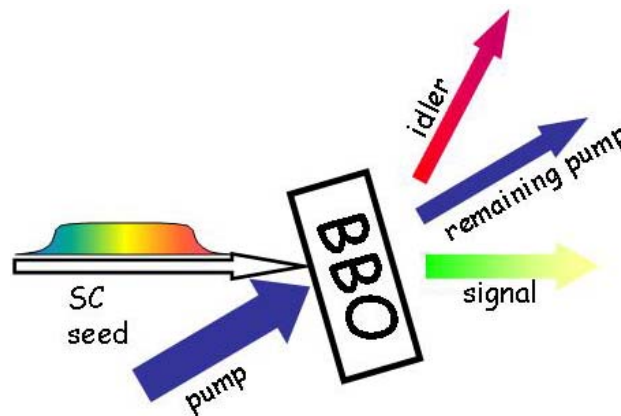


Fig. 2.2. Schematic representation of a non-collinear optical parametric amplifier (NOPA) (38).

In this experiment only a fraction of about 300 μJ is used. The main part of the power is split-off and frequency doubled in a BBO crystal (500 μm length), providing 50–110 μJ pulses at 388 nm. A small fraction (about 3–5 μJ) of the 775 nm output from the regenerative amplifier is focused via a $f=150$ mm quartz lens into a 5 mm thick sapphire plate to generate the white-

light, i.e the seed. With a combination of a variable filter and an iris diaphragm the energy and the beam profile can be influenced to provide a stable white light continuum. The 388 nm pump pulse with an intensity of 50–110 μJ is focused into the BBO by a $R=500$ mm mirror positioned below the seed light path. The BBO crystal used has a thickness of 5 mm and was cut at $\theta=32^\circ$ for type I phase matching. The pump beam is divided into signal and idler, thereby a parametric super-fluorescence ring is formed (Fig. 2.2). Now the white light beam is focused under a suitable angle with respect to the pump beam into the BBO crystal, where the amplification takes place. Finally, the desired excitation wavelength can be tuned by rotating the BBO-crystal to a desired angle and by changing the delay of the white light (38, 39). Using this method, I was able to generate NOPA pulses with excitation wavelengths of 490, 500, 546, 660, 880 and 935 nm, respectively. Spectra were measured with a commercial Ocean Optics S2000 multichannel spectrometer. For the near-IR NOPA pulses, the 775 nm fundamental was suppressed using a GG 830 filter. Pulse energies were measured with a commercial coherent “field master” using the heads LM2 and LM10.

2.1.2 Pulse Compressor

Since the chirp of the output signals coming from the NOPA is mainly linear, the compression of the output signal of the NOPA is possible. The broad bandwidth output pulses of the NOPA are chirped due to the initial chirp of the seed continuum and additional chirp caused by the dispersive properties of the BBO crystal, the optics, and the air. The chirped pulses can readily be compressed in a simple compressor made of two prisms that are passed twice (Fig. 2.3). With a small spacing of the prisms a pulse length below 30 fs can be reached throughout the tuning range.

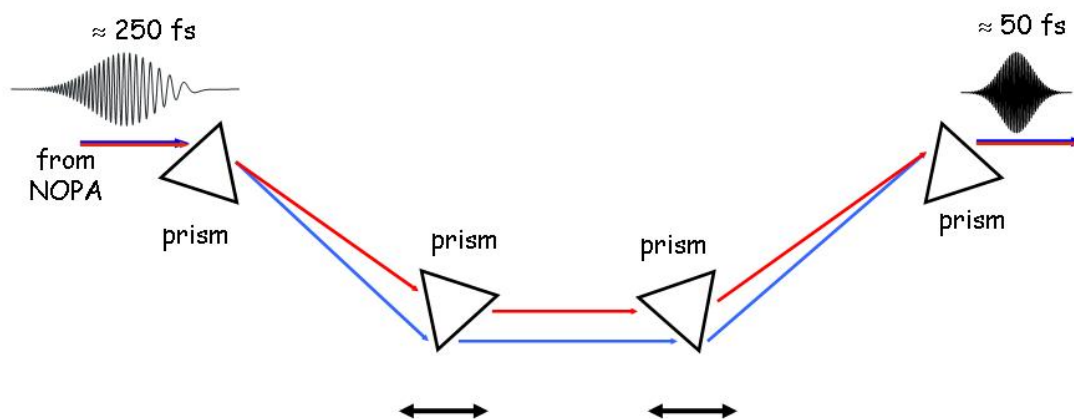


Fig. 2.3. Double-pass prism-pair compressor.

2.1.3 White Light Generation

The propagation of an ultrashort pulse through a medium can lead to considerable broadening of its spectrum. This effect, known as supercontinuum or white-light generation, has been observed in various media (40). The femtosecond continuum beam appears as a white disk that is surrounded by a distinct, concentric, rainbow-like pattern (conical emission). The term “white-light continuum” is usually reserved for the low-divergence, central part of the beam and excludes the conical emission. Self-phase modulation (SPM) (41, 42), ionization-enhanced SPM (41, 43), and four-wave mixing (42) are some of the mechanisms that have been invoked to explain the white-light continuum, and the extent of its spectral width. But it is fair to state that the physics is not properly understood. However, self-focusing is known to play an important role in generation of white light continuum (43-48).

In this work the white light is generated by passing laser pulses through a sapphire crystal. In order to avoid potentially undesirable effects that may result from exposure of the sample to the entire continuum, filters were used to select the desired probe wavelength prior to overlap with the pump pulses (49). Furthermore, the white light is divided into two parts. One part of the beam is focused via an off-axis parabolic mirror into the sample while the other part of the beam is used as reference and lead directly into the reference spectrometer. In the spectrometers the different portions of the beams are spectrally dispersed and recorded by a 42 segment photodiode array. This information is processed further in the computer and finally displayed as a signal.

2.1.4 Detector and Choppers

As already discussed, the probing pulse is separated by a variable beam-splitter into signal and reference pulse. The first part, the signal beam, is analyzed in the signal detector after it passes through the sample, while the other beam served as reference and is send directly into the reference detector to minimize the noise due to scattered light. Both beams are dispersed in the spectrometer, and are read by a 42 segment photodiode array. Each photodiode array (Hamamatsu S4114-46Q) is situated at the front of two circuit boards and are mounted back to back onto an insulating spacer. Each of these two boards carries 23 parallel sockets which hold the amplifier cards. The amplified signal finally reaches the output Darlington stage and the signal is then digitized in a gated analog to digital converter (ADC) (LeCroy model 1885F) (50). The 96 channels supplied by the ADC 1885F allow simultaneous parallel operation of two photodiode arrays. In combination with a suitably equipped spectrometer a spectral resolution of 8 nm for a usable spectral range of 336 nm was achieved.

The detected signal is proportional to the number of photons which hit the photodiode array ($N(\lambda)_{\text{sig}}$ and $N(\lambda)_{\text{ref}}$). In a first step, a dark-current correction is applied:

$$\begin{aligned} N(\lambda)_{\text{sig}} &= N(\lambda)_{\text{sig,uncor}} - N(\lambda)_{\text{sig,dark}} \\ N(\lambda)_{\text{ref}} &= N(\lambda)_{\text{ref,uncor}} - N(\lambda)_{\text{ref,dark}} \end{aligned}$$

In this case the absorption A of the sample will be defined as: $\frac{N(\lambda)_{sig}}{N(\lambda)_{ref}}$.

Taking the difference between the signal with pump and that without, the absorption difference is obtained:

$$\Delta A(\lambda) = \log\left(\frac{I_{Pmess}}{I_{Nmess}}\right) - \log\left(\frac{I_{Pref}}{I_{Nref}}\right)$$

where, P and N refers to pumped and not-pumped situation

To maximize the signal to noise ratio a set of choppers is used, which allows blocking the pump or the probe pulses one by one (Fig. 2.4)

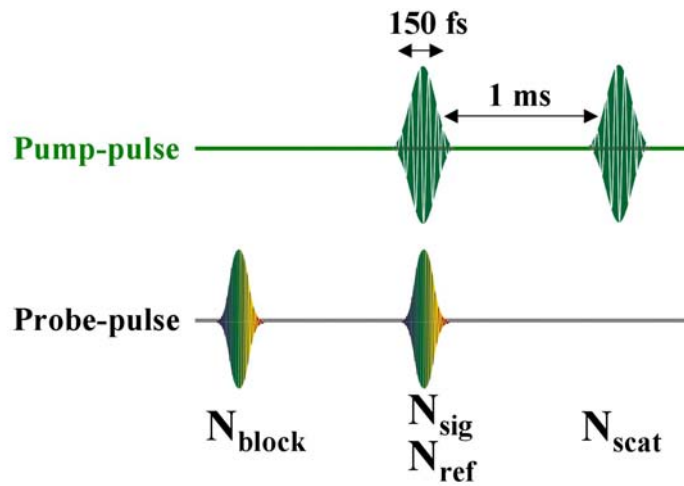


Fig. 2.4. Schematic representation of the pulse pattern caused by the chopper.

Within a single measurement the sample is scanned in three different modes of data acquisition. By blocking only the pump pulse the measurement of the unperturbed species is possible. The second mode involves the perturbed sample by both, pump and probe pulse, thus measuring the excited species. A third mode comprises only the pump pulse and contains mainly the scattered light, which is time independent.

The change of absorption of the sample is calculated according to the following formula:

$$\Delta A(t, \lambda) = \log\left(\frac{N(t, \lambda)_{block,ref} - N(t, \lambda)_{therm,ref}}{N(t, \lambda)_{block,sig} - N(t, \lambda)_{therm,sig}} * \frac{N(t, \lambda)_{sig} - N(t, \lambda)_{therm,sig} - N(t, \lambda)_{scat,sig}}{N(t, \lambda)_{ref} - N(t, \lambda)_{therm,ref} - N(t, \lambda)_{scat,ref}}\right)$$

ref = reference , sig = signal, block = blocked, therm = thermal noise, scat = scattered light

2.2 General Description of the Pump-probe Method

The pump-probe method is a technique designed to examine the excited states and molecular dynamics of any molecule, or complex of molecules, whose temporal evolution can be initialized by light. To achieve this, two laser pulses are used to first initiate the reaction by a strong pump beam and then monitor the temporal evolution of the system by the absorption signal of a weaker probe beam.

The quantity measured in pump-probe experiments is the absorbance change, $\Delta A(\lambda, t)$. The absorbance of a sample is defined as $A(\lambda) = \log(I/I_0)$, where I_0 is the incident light intensity and I the transmitted light intensity. At the time t upon excitation, the dependence of the difference-absorption on time and wavelength $\Delta A(\lambda, t)$ is obtained according to the formula:

$$\Delta A(\lambda, t) = A_P(\lambda, t) - A_N(\lambda)$$

where, P and N refers to pumped and not-pumped situation.

The absorption difference signal usually consists of several contributions. In the first place, the ground state absorption of the sample will be reduced, due to the transfer of some pigments to the excited state, or when they undergo a reaction and a different species is created with a different absorption spectrum, for instance, a reaction product, a molecule that has accepted or donated an electron. All those phenomena will result in a negative contribution to ΔA , the bleach (Fig. 2.5). Second, the excited state pigments can absorb the probe pulse and undergo a transition to a second excited state, which is seen as a positive ΔA contribution, the excited state absorption (ESA). Furthermore, the probe pulse can deexcite the pigments, and the resulting stimulated emission signal (SE) which leads to an increased intensity on the detector is again a negative ΔA contribution. Finally, when a chromophore is excited, a spectral response of a nearby chromophore can be observed as a result of electrostatic interactions, orbital delocalization, etc.

An easy picture of these contributions to the TA spectra, and how they evolve in time, is presented in an imaginary TA experiment below.

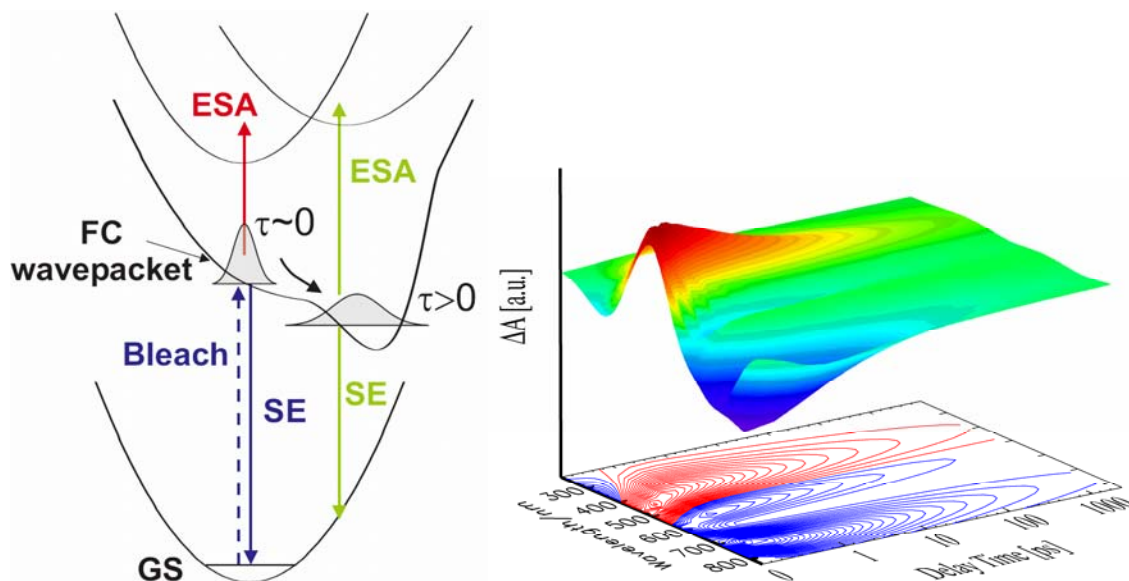


Fig. 2.5. Concept of the pump-probe transient absorption experiments showing various signal components during excited state evolution: ground state bleach, stimulated emission (SE) and excited state absorption (ESA).

Upon photoexcitation into the Franck-Condon region a wavepacket is formed in an optically allowed excited state. The difference spectrum at time zero is thus composed of a negative absorption around 550 nm, corresponding to the ground state bleaching, and a positive signal with maximum at 400 nm, representing the excited state absorption (ESA). At later times the wavepacket has moved into a lower lying excited state and a third component emerges in the difference spectrum, a negative signal around 700 nm representing the stimulated emission (SE). All those signals exhibit an exponential decay having the same rate determined by the bleach recovery and the decay of the intermediate excited state.

2.3 Data Analysis

In order to obtain information from the measured kinetics, it must be kept in mind, that meaningful results can only be extracted when the temporal width of the excitation and probe pulses are considerable smaller than the temporal response of the sample.

Transient absorption traces are most often fitted with a sum of exponentials, and the decay rates are related to the processes taking place. When a range of wavelengths is probed, all the decay curves can be fitted simultaneously to a minimum number of decay parameters in a "global analysis" according to

$$\Delta A(\lambda, t) = \sum_{i=1}^n a_i(\lambda) \exp\left(\frac{-t}{\tau_i}\right)$$

The change in absorption ΔA at wavelength λ and time t is written as a sum of exponentials with decay times τ_i and corresponding preexponential factors a_i . The decay times in such an analysis are taken to be the same at all wavelengths, whereas a_i varies with wavelength. The $a_i(\lambda)$ constitutes a spectrum associated with decay time τ_i . This is known as the decay-associated spectrum (DAS). Such a spectrum can give further information on the participating molecules and the processes occurring. In general, one can decide how many independent decay components are needed to describe the observed kinetics by closely inspecting the residuals (difference between measured and fitted curves). The singular value decomposition (SVD) method is a statistical tool to determine the maximum number of components that can be extracted with confidence from the experimental traces (51).

3 Excited State Dynamics of *Rhodospirillum rubrum* Reaction Center Mutants.

3.1 Introduction

Purple photosynthetic bacteria have proved to be excellent model systems for the study of light reactions in photosynthesis. This light reaction usually begins with the absorption of a photon by the light harvesting (LH) or antenna system (52). The absorbed energy is then rapidly and efficiently transferred to the reaction center (RC), where it is used to initiate the cyclic electron transport. These reactions take place in the photosynthetic membrane, where the RC is surrounded by two types of antenna complexes LH1 and LH2 (light-harvesting complex 1 and light-harvesting complex 2) in most phototrophic bacteria. Typically only one of these, LH1, is in close contact with the RC (53-60).

It is well-established (61), that the carotenoids of purple bacteria are exclusively bound to the protein components of the photosynthetic unit (PSU), which consists of a RC surrounded by the LH1. For many purple bacteria including the one employed in this study, *Rhodospirillum rubrum*, the RC is a heterotrimer, containing the membrane-bound subunits, L and M, which bind the bacteriochlorophyll (BChl) "special pair", two accessory BChls, two bacteriopheophytins (BPh), two quinone molecules, as well as one molecule of carotenoid (spirilloxanthin (Spx)) (61). The LM dimer associates strongly with the RC-H subunit, which consists of a single transmembrane helix attached to a large cytoplasmically located polar domain adhering to the cytoplasmically exposed surface of the LM dimer (Fig. 3.1).

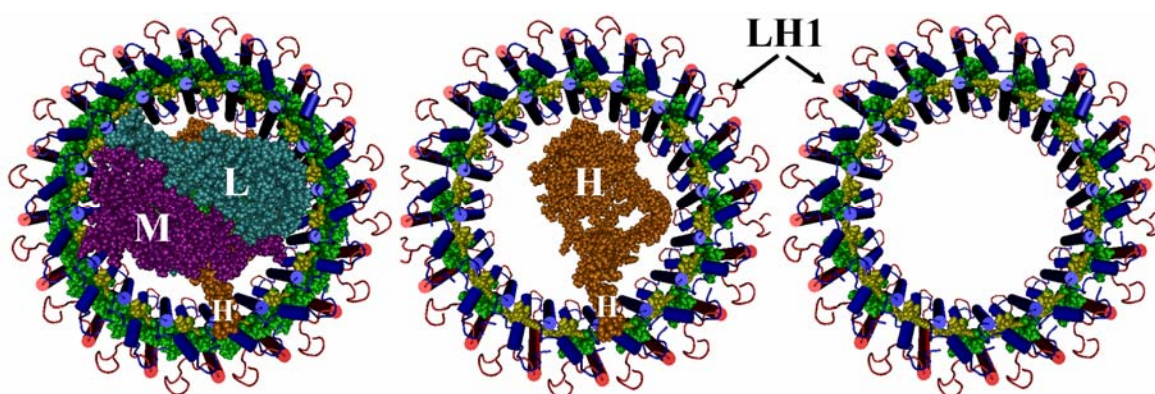


Fig. 3.1. Molecular models of the intact PSU (LH1+RC) and the putative PSUs of SK Δ LM and SPUHK1 mutants, as viewed from the periplasmic surface. The RC subunits L, M and H are indicated (62).

In *R. rubrum*, medium-resolution images of 2D crystals of the PSU have suggested that the RC is completely enclosed by the LH1 complex, which consists of a ring-like array of 16 subunits formed from the non-identical α and β polypeptides (61, 63). Biochemical evidence has indicated that each $\alpha\beta$ subunit binds a pair of BChls and one Spx molecule (63, 64). So far, the low resolution of the images obtained by cryo-electron microscopy (cryo-EM) (56, 65) does not allow the assignment of the 16 Spx molecules to the inner or outer surface of the LH1 ring. Both the cryo-EM data (56, 65) as well as current models (66, 67) of the PSU place the RC against the wall of the LH1 ring, without necessitating its structural distortion. However, the structural interaction of the *R. rubrum* LH1 complex with the RC is subject to some controversy. On the one hand, results obtained by atomic force microscopy (AFM) (66, 68) and low-resolution cryo-EM (65) from 2D-crystals of the RC-LH1 PSU indicate significant ellipticity of the LH1 ring, consistent with a single molecule (SM) spectroscopic study (69) of detergent-solubilized PSUs. However, the geometrical interpretation of the AFM studies may be based due to packing forces, since in the study of Fotiadis *et al.* (66), removal of the H subunit did not affect the ellipticity of the *R. rubrum* LH1, whereas in the AFM study of Scheuring *et al.* (68) performed on intact photosynthetic membranes of *Rhodobacter blasticus*, removal of the H subunit appeared to cause the LH1 complex to become circular. A complication here, in addition to the low resolution of the data, is that the *R. blasticus* PSU appears to be an RC-LH1 dimer, also containing the PufX polypeptide, which has been implicated in quinone transfer across the LH1 ring (70, 71), whereas the *R. rubrum* PSU appears to be a closed unit, lacking PufX (72). On the other hand, SM spectroscopic studies performed on PSUs isolated by the Ghosh group have indicated no perturbation of the LH1 circular symmetry due to the presence of an RC (73) either when solubilized in detergent or reconstituted into bilayer membranes. Nevertheless, both the low resolution (4 Å) crystal structure of a detergent-solubilized PSU from *Rhodospseudomonas palustris* (74) as well as AFM images of the PSU in intact membranes of *Rhodospirillum photometricum* (75) also indicate an elliptical geometry of the LH1 ring.

Consequently, if a significant distortion from LH1 circular symmetry is present, this should affect the relative distances between the BChl and Spx molecules, thus affecting also the rates of energy transfer between them. Since all PSUs are affected equally, even an ensemble measurement might highlight these differences. This consideration provided a major motivation to compare the ultrafast pathways of BChl-Spx energy transfer in chromatophores obtained from wild-type *R. rubrum* to those of mutants lacking either the complete RC (mutant SPUHK1 (76)) or the L and M subunits (mutant SK Δ LM (77)).

The wild-type carotenoid of *R. rubrum*, spirilloxanthin contains 13 conjugated double bonds and is so far the most unsaturated carotenoid known to be involved in photosynthetic light harvesting. It is well-accepted (78, 79), that the three major absorption maxima (at 485, 520, and 550 nm) of Spx correspond to vibronic levels of the second excited S_2 state, with the first excited states S_1 (also designated the $2A_g^-$ state) and S^* (see below) being symmetry-forbidden for the initial excitation process. Immediately following excitation, the S_2 state rapidly decays within 60-200 fs (78) to the S_1 and S^* state. From the S_1 state the system either decays to the ground state, or energy transfer to the Q_y of BChl can potentially occur (78). However, as a consequence of its extended conjugation, the S_1 state of Spx is short-lived and decays to the ground state in 1.4 ps both in solution and when bound to the LH1 complex of *R. rubrum* S1 (WT strain) in native membranes (78). In isolated LH1 complexes,

a slightly longer decay time of 1.6-1.7 ps has been observed (79). This indicates that no energy transfer can occur from the Spx S_1 state to the Q_y state of BChl, resulting in the low total efficiency of Spx to BChl energy transfer of 30% (78).

The groups of van Grondelle and Fleming (78) have also identified another excited state in carotenoids, designated S^* , which exhibits both a characteristic excited state absorption (ESA) in the visible region, and a lifetime clearly distinct from that of the S_1 state (~ 5.3 ps in intact photosynthetic units of *R. rubrum*), which is populated directly from the S_2 state, in competition with the S_1 state (78). For detergent-solubilized LH1 complexes of *R. rubrum* as well as in intact PSUs, S^* is on the pathway of ultrafast carotenoid triplet formation via the singlet fission mechanism, while in solution it decays to the ground state in 5 ps without detectable triplet formation (78, 80-82). On the other hand, pump-dump-probe experiments have suggested that the S^* states in light-harvesting complexes and in solution could be of different origins, and that the S^* state in solution might be a vibrationally hot ground state (83).

Efficient energy transfer via the S_1 state requires the S_1 energies of carotenoids to be higher than those of the acceptor states. Since it is known that S_1 energies are usually insensitive to solvent properties (84), it is reasonable to assume that the S_1 energies in LH1 complexes should be very close to those determined for carotenoids in solution. Under this assumption, the S_1 energy of Spx is expected to be low enough, so that no energy transfer to the Q_y state of BChl should occur. The efficiencies of S_1 -mediated energy transfer have been calculated from S_1 lifetimes of carotenoids in solution and in detergent-solubilized LH1 complexes, obtained from $S_1 \rightarrow S_N$ ESA decays. Evidence that Spx has no capability to transfer energy via the S_1 state was provided by studies of detergent-solubilized LH1 complexes from *R. rubrum*. Within experimental error, no difference between S_1 lifetimes in solution and in the LH1 complex was found (78, 79).

The availability of two independent RC-less mutant strains, both of which exhibit spectroscopic properties characteristic of intact LH1 complexes (see below), allows me to define the excitation energy transfer (EET) pathways between LH1 pigments more precisely than previously possible. In addition, I also describe here for the first time the ultrafast kinetics of the LH1 triplet state on the ps time scale.

3.2 Materials and Methods

Sample preparation. Chromatophore membranes were obtained from either the wild-type (S1) or the S1-derived deletion mutants SPUHK1 (containing a lesion in the *pufA* gene (76)) or SK Δ LM (which lacks both L and M subunits (77)). In the SK Δ LM a Tn908-derived kanamycin cassette was substituted for the BstEI-SalI fragment (which flanks both the L and M subunits) of the chromosomal *puf* operon (72) using site-directed mutagenesis. This strain completely lacks L and M subunits but retains the H-subunit, which localizes to the PSU (R. Ghosh, unpublished data). To facilitate a meaningful comparison, all strains were grown semi-aerobically using the medium M2SF, which induces photosynthetic membrane levels normally obtained only under low light conditions in the absence of oxygen (85).

Chromatophores were prepared as described (76) and diluted in 20 mM Tris-HCl (pH 8.0) containing 10 mM sodium ascorbate. The typical sample OD was 0.3–0.6/mm at 520 nm. Sample stability was confirmed by measuring the absorption spectra before and after the time-resolved measurements. Fused silica cuvettes with a pathlength of 1 mm were used for measurements. Determination of the BChl content of the wild-type and SPUHK1 chromatophores yielded a values of 32.7 ± 4.4 nmol of BChl/mg protein (76) and 32.66 ± 16 nmol BChl/mg protein, respectively. These values are almost identical to that (34.1 ± 4.73 nmol of BChl/mg protein) reported by Cheng *et al.* (86) for chromatophores from photoheterotrophically grown cells.

To minimize accumulation of photoproduct, the sample was translated continuously both horizontally and vertically in a direction normal to the bisector of the pump and probe beams at ~ 10 cm/s.

Stationary and Time-Resolved Spectroscopy Measurements. Absorption spectra were recorded with an Analytik Jena (Jena, Germany) S100 spectrometer using 1 mm fused silica cuvettes. The time resolved measurements using the femtosecond pump-probe technique were performed with a setup based on a CLARK CPA 2001 (Dexter, MI) laser/amplifier system operating at a repetition rate of ~ 1 kHz and at a central wavelength of 775 nm. The pulse width of the system was around 150 fs (FWHM). The laser served as pulse source for the following nonlinear processes. Excitation pulses were generated using a non-collinear optical parametric amplifier (NOPA) (37, 87) centered at a wavelength of 546 nm or 880 nm and focused to a diameter of 100 μ m inside the cuvette. The pulse length was compressed down to 50 fs, typical pulse energies were around 15 nJ, small enough to prevent multi-photon excitation of the sample. The sample was probed with a white-light continuum generated by focusing the 775 nm beam onto a 2 mm thick sapphire plate, whereby a spectral range of 400–1000 nm was used for probing. The continuum pulses were dispersed by two VIS-spectrometers, (sample and reference) and recorded with two 42 segment diode arrays. Data acquisition was performed in single shot detection mode as balanced and referenced measurement providing signal to noise ratios up to 10^4 (88). Excitation and probe pulses were polarized parallel. To account for long term drifts and possible degradation of the sample, the ratio between probe and reference signals for the non-excited sample was determined for every third shot.

3.3 Results

3.3.1 Steady-state Absorption Spectroscopy.

Figure 3.2 shows the absorption spectra of wild-type (S1) and the H (SPUHK1) and L+M (SK Δ LM) deletion mutants. All complexes show the characteristic three-peak structure of Spx with a Franck-Condon (0-0) transition at 550 nm. Additionally, antenna BChls contribute to the spectrum with three main bands, namely the Soret band (375 nm), the Q_x (590 nm) and Q_y (882 nm) absorption bands, respectively. The WT spectrum also shows two smaller additional peaks at 760 nm and 802 nm attributable to the Q_y transitions of the RC-bound BPh and accessory BChl, respectively (70, 71). The absorption maximum of the RC special pair, which normally contributes about 5% of the PSU absorption at 875 nm (70, 71) is hidden underneath the Q_y band of the LH1 complex. With the exception of a small (~ 2 nm) red shift of the LH1 band compared to the WT, the absorption spectra bands of both mutants are identical in form and relative amplitude. It has been also shown for both SPUHK1 (76) and for the SK Δ LM (R.Ghosh, unpublished data) that the near-IR CD spectra (which are a very sensitive measure of pigment-pigment interaction) are also identical to that of WT LH1. Thus, by these criteria, the LH1 complex appears to be unperturbed by the presence of an RC so that from a spectroscopic point of view, one can consider the WT sample as being an LH1+RC complex, and the SPUHK1 as a LH1 complex without the excitation energy acceptor RC. SK Δ LM contains the H subunit but lacks the pigment binding subunits L and M. A schematic representation of the PSU complexes is shown in Figure 3.1.

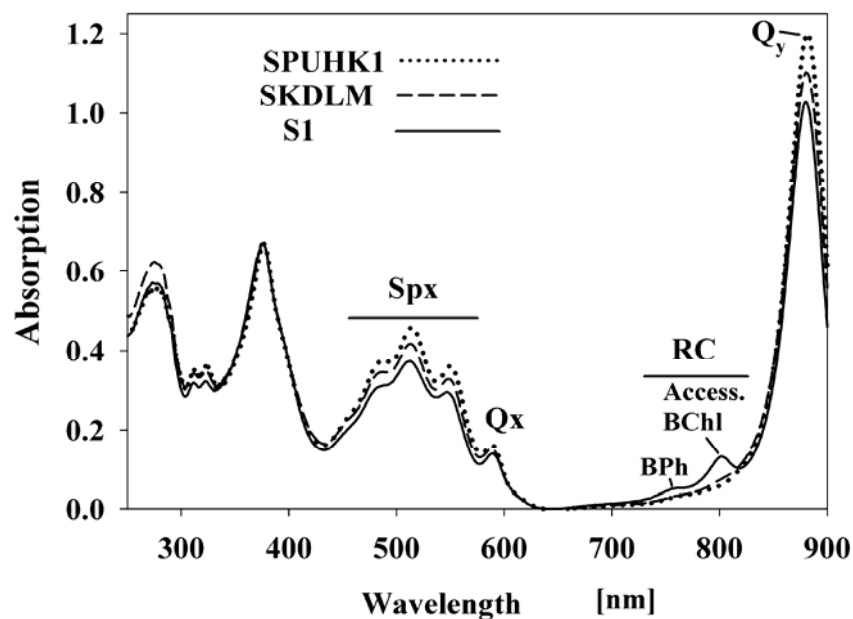


Fig. 3.2. Absorption spectrum of the chromatophore membranes from the WT (solid line) SPUHK1 and SKDLM mutants. The peaks at 760 and 802 nm correspond to BPh and the RC-accessory BChl (absent in the SPUHK1 and SK Δ LM).

3.3.2 Excited State Dynamics of Wild-type, SPUHK1 and SKΔLM Mutants of *Rhodospirillum rubrum* PSU Following Excitation of the Spx S₂ State.

To investigate the excited state dynamics of carotenoids and BChls in the photosynthetic unit complex of *R. rubrum* for both WT and SPUHK1, I performed time-resolved transient absorption (TA) experiments exciting the LH1 carotenoids to their S₂ excited state with a 550 nm laser pulse. Kinetic traces were measured over a broad spectral range for both visible as well as near-IR regions at a probing window from 400 to 1000 nm.

The excited state processes which occur upon carotenoid excitation in a LH1 are summarized in Figure 3.3. A depopulation of the carotenoid ground state occurs upon excitation, which causes a negative (bleach) signal in the difference transient absorption spectrum around 500 nm; a mirror image of the S₀→S₂ absorption band. At the same time, an ESA band arises in the spectral region above 950 nm; the S₂→S_N transition. Soon afterwards, the S₂ excited state is depopulated in about 0.2 ps through different processes: An internal conversion (IC) into intermediate lower excited states, which results in a transient population of the S₁ excited state, visible as an ESA (S₁→S_N transition) with a maximum at 620 nm, together with a population of the S* excited state leading also to a characteristic ESA around 600 nm. In parallel, excitation energy transfer to LH1 BChls can successfully compete with S₂→S₁/S₂→S* internal conversion, which will lead to a bleaching of the BChl band (880 nm) and concomitant an ESA signal will arise around 840 nm.

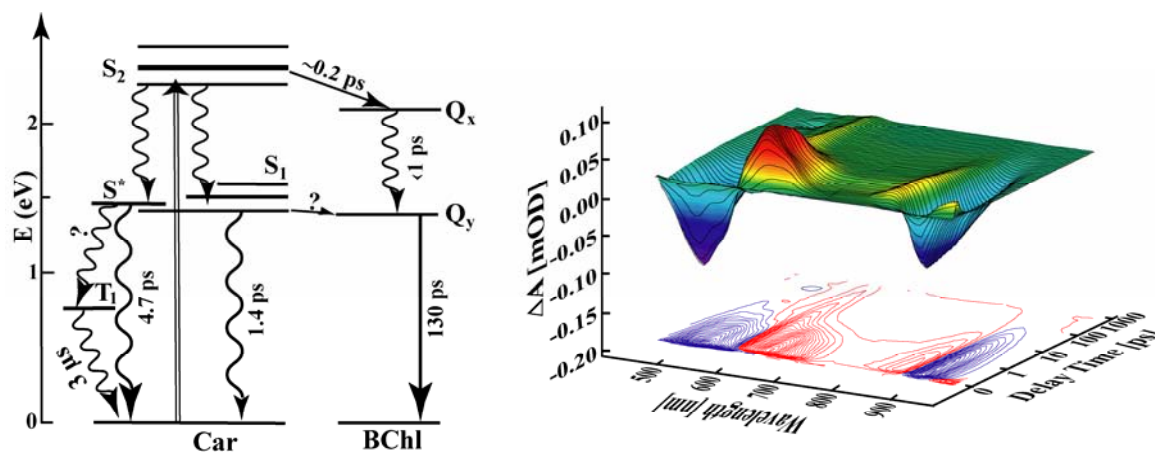


Fig. 3.3. Schematic representation of energy levels and energy-transfer pathways between carotenoids and BChl *a* in the LH1 complex (left). Transient absorption data of LH1, upon carotenoid excitation at 546 nm (right).

TA spectra recorded in the visible region (400-700 nm) were analysed by a global fitting routine and four decay components were sufficient to obtain an excellent global fit (Fig. 3.4).

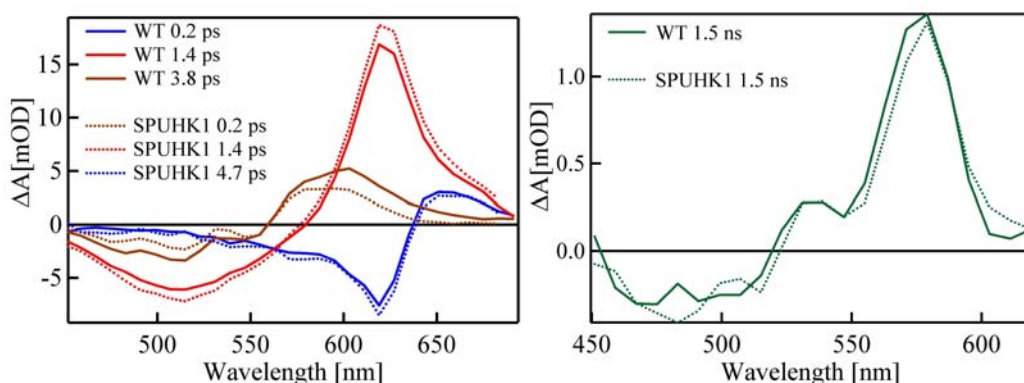


Fig. 3.4. Left: amplitude spectra (decay associated spectra) of the multi-exponential global fit analysis for wild-type (continuous line) and SPUHK1 mutant (dotted line). Right: transient spectra at 1.5 ns.

For both WT and SPUHK1 the fastest component (less than 200 fs), shows a negative amplitude between 500 and 620 nm and a positive signal with a maximum at 650 nm. The fast decay time allows me to assign this component to the decay of the S_2 state. The second component (Fig. 3.4, red line) exhibits a time constant of approximately 1.4 ps and shows the characteristic spectral signature of the S_1 state (78, 79), with an excited state absorption (ESA) at 620 nm as well as a ground state bleaching with a negative minimum at about 510 nm. The amplitude associated with the time constant of 1.4 ps of the WT ESA is slightly smaller than that of SPUHK1. The global fit yields values for the third time constant of 3.8 ps for the WT and 4.7 ps for the SPUHK1 sample. The WT sample shows a larger overall amplitude and for both samples the loss of bleach is accentuated and the ESA contribution dominates the spectra for λ_{probe} above 550 nm. The amplitude is negligible for wavelengths longer than 650 nm, and a small shoulder appears at 535 nm. Both the shape of the spectrum and the lifetime of this state are similar to those reported for the excited Spx S^* state (78). The last component (Fig. 3.4 right), represents a long-lived species not decaying on the time-scale of this experiment (1.5 ns). For both samples this last component shows a weak negative contribution around 500 nm, a positive signal with a maximum centred at 575 nm and a smaller shoulder at 535 nm. I interpret this component as corresponding to the Spx triplet state. All of the above-mentioned spectral components can also be observed for the LM-deletion mutant SK Δ LM. Taken together with the results for SPUHK1, this indicates that the spectral evolution of LH1 Spx after S_2 excitation is not affected by the presence of any RC components.

The near-IR transients contain information on energy transfer within LH1, from the carotenoid S_2 excited state to the LH1 BChls. Figure 3.5 shows transmission difference spectra in LH1 at five different time delays after photoexcitation at 546 nm.

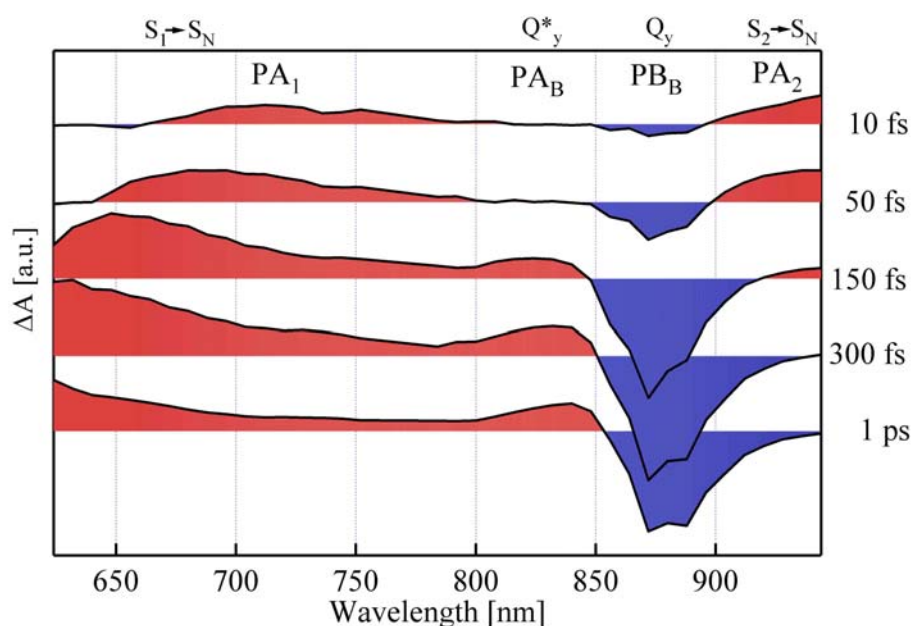


Fig. 3.5. Transmission difference spectra for wild-type sample at different time delays after photoexcitation at 546 nm.

After the pump pulse, the prompt appearance of a broad photoinduced ESA band, above 950 nm is observed (PA₂). Concomitant an ESA band termed PA₁ originally appearing at 750 nm shifts its maximum towards higher energies within 300 fs, displaying other kinetics than the previous one, indicating different origin. The PA₂ band decays very quickly and is replaced, within ~200 fs, by another ESA band peaking at 830 nm and a negative signal around 880 nm, the PA_B and PB_B bands. The PA₁ band is a well-known feature of carotenoids (89, 90), and is assigned to the S₁→S_N absorption, thus providing a spectral signature of the internal conversion process. The PA₂ band was also previously observed (91, 92) and attributed to transient absorption from the S₂ state. Furthermore, I assigned PA_B and PB_B to transient absorption from the BChl Q_y state, and bleach of the Q_y band respectively according to (93, 94). The very rapid decay of PA₂ and the corresponding rise of PA₁ and PA_B highlight the initial S₂→S₁ internal conversion process and the excitation energy transfer towards the BChls. The slight delay of PA_B compared to PB_B indicate the internal conversion of BChl from Q_x to Q_y (Fig. 3.3).

The most interesting part of the near-IR LH1 transient absorption spectrum is the spectral region between 800 and 1000 nm. In this region LH1 exhibits two ESA bands (PA_B and PA₂), a ground state bleach (PB_B), and for longer delay times an additional negative signal present only in the WT sample. A selection of characteristic transients showing the temporal response of the absorbance change of WT and SPUHK1 upon excitation at 546 nm are presented in Figure 3.6. The solid curves are the fitted curves resulting from the global fit analysis.

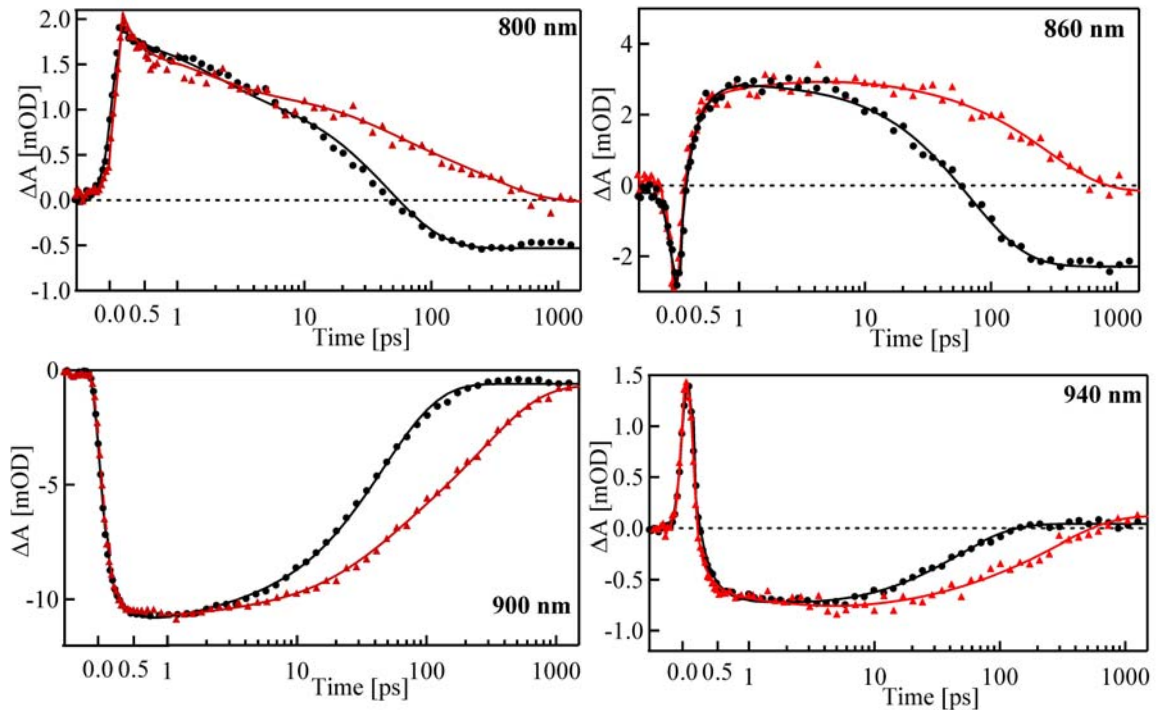


Fig. 3.6. Kinetic traces of the PSU of *R. rubrum* wild-type (black) and SPUHK1 mutant (red) measured after the excitation at 546 nm. Probing wavelengths are indicated for each curve. Solid lines represent the best fits obtained from multiexponential global fitting procedure.

The kinetic traces at 800 nm (Fig. 3.6), show solely the temporal evolution of the PA_B band for the SPUHK1 sample (red curve), displaying the exponential decay of this ESA. On the other hand, the WT sample show a faster decay of the PA_B state and an additionally offset for times longer than 100 ps.

The kinetics measured at 860 nm representing the evolution of the BChl ESA for WT and SPUHK1 following Spx excitation at 546 nm (Fig. 3.6). For both samples I observe a rapid absorption decrease which vanishes within the first few hundred femtoseconds followed by an absorption increase showing different kinetics for the investigated samples. The fast negative signal, which is similar for both samples, reflects the transition of the excitation energy into the lowest BChl excited state. For SPUHK1, the positive signal corresponds exclusively to the excited state kinetics of antenna BChl, while for the WT sample, the additional negative signal at longer delay times reflects the excitation transfer to the RC.

The 900 nm kinetic traces (Fig. 3.6) show a large absorption decrease and were selected at the minimum of the Q_y BChl band, reflecting characteristic contributions from the BChl bleach at 880 nm and BChl stimulated emission at 920 nm. The transients at these wavelengths are thus dominated by the LH1 BChl excitation dynamics. The onset of the BChl bleach signal appears exclusively due to the energy transfer from Spx S_2 /hot S_1 states to the BChl $Q_{x/y}$ states, since the 546 nm excitation pulse does not directly excite the BChls. The TA signal exhibits a different exponential decay for WT and SPUHK1 samples. The bleach signal grows within the first few hundred femtoseconds, i.e. the time needed for the

excitation energy to reach the BChl. Note the same transfer rate, Spx to BChl, for both samples. The TA kinetics is followed by a significant loss of signal on the time scale of tens to hundreds of picoseconds. The observed loss is exclusively due to BChl dynamics which is spectrally separated from Spx. Clearly, SPUHK1 shows a longer lifetime of the excited state compared to WT, due to the lack of photochemical quenching pathways, i.e. excitation energy transfer to the RC.

Last, the kinetic trace at 940 nm shows, additionally to the pattern presented for $\lambda_{pr}=900$ nm a fast rise and decay of the PA₂, which is similar for both samples.

A global fit routine was applied to the data obtained in the near-IR spectral range (600-1000 nm) and revealed the presence of four components for WT (Fig. 3.7), and SPUHK1 mutant.

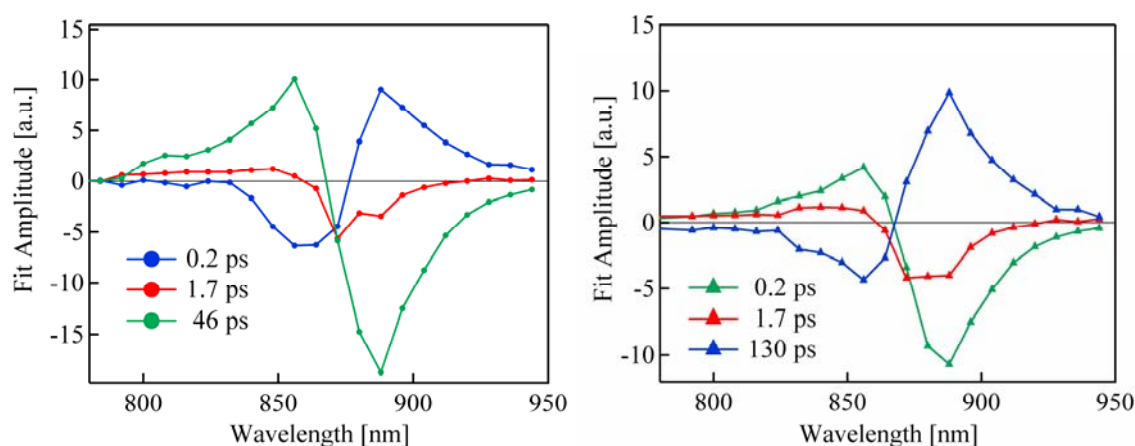


Fig. 3.7. Fit amplitudes characterizing the spectral evolution of the transient absorption for WT (left) and SPUHK1 (right) in the near-IR region after excitation at 546 nm.

Both samples have the first two components of < 200 fs and 1.7 ps in common, which correspond to the time constants characteristic for excitation energy transfer towards BChls and Spx S₁ excited state dynamics. The third component of WT (46 ps) and SPUHK1 (130 ps) are mainly contributions of the excited BChl and the WT sample decays 3 times faster than the SPUHK1 sample, which can be attributed to excitation energy transfer to the RC, i.e. photochemical quenching. Other processes occurring in the LH1-RC complexes such as equilibration among BChls and vibrational relaxation of BChl cannot be the main cause for these signals, as they occur on faster time scales and would manifest themselves as spectral changes (distribution of energy) whereas I observe an overall loss of electronic excitation. The slower processes are mainly associated with excited state decay via quenching channels (95-97). Singlet-singlet annihilation of excitation among and within LH1 rings can be also excluded because of the low excitation energy (98). The loss of signal for SPUHK1 can be assigned to the natural decay of the Q_y level of BChl (99).

The last component describes a long time offset, i.e. the spectral amplitude at 1.5 ns. As seen in Figure 3.8, the spectral amplitudes exhibit a well defined shape for the WT, whereas for both mutants SKALM and SPUHK1 the defined structure is absent.

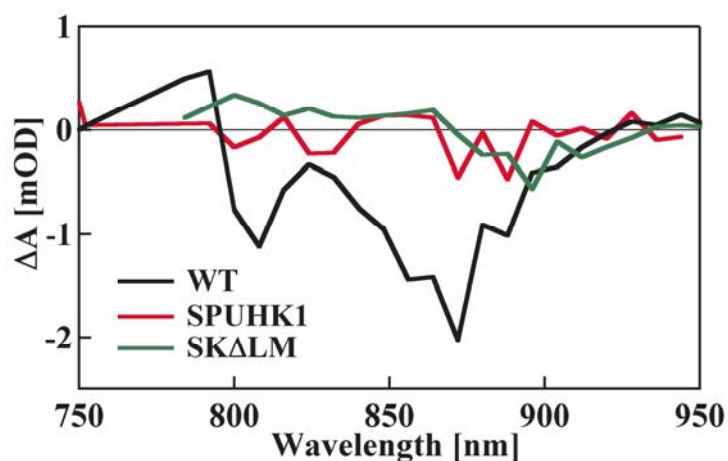


Fig. 3.8. Transient absorption difference spectra taken at 1.5 ns for WT (solid line), SPUHK1 (dotted line) and SK Δ LM (dot-dashed line) chromatophores of *R. rubrum*.

At long delay times, almost all of the energy transfer and charge separation processes are expected to be completed. Therefore, the spectra reflect the differences in absorption between the charge-separated and the ground state. The main features in such a difference spectrum are caused by the photo-oxidation of the primary electron donor in the RC: i.e. bleach of the BChl dimer P band at around 880 nm. The electrochromic blue-shift of the monomeric BChl *a* absorption band in the 800 nm region is reflected by an absorbance increase on the short-wavelength side of this band and a decrease at longer wavelengths. The loss of the interactions of the special pair of BChls with BChl *a* and the disappearance of the upper (i.e. higher energy) exciton transitions of the special pair may also add to the difference spectrum in this spectral range. No residual signal for long delay time was found for either of the mutants SPUHK1 or SK Δ LM (Fig. 3.8), as expected from their RC-less phenotypes.

Summarizing, the main differences between WT and SPUHK1 mutant were found in the BChl excited state and RC dynamics; whereas no major difference was observed for the spirilloxanthin excited state dynamics.

3.3.3 Photo-protection via Triplet Energy Transfer from $^3\text{BChl}$ to ^3Car .

One of the well established photo-protection mechanisms of carotenoids involves triplet energy transfer from BChl to carotenoids, which efficiently competes with energy transfer to oxygen and thus prevents the formation of dangerous reactive singlet oxygen. This efficiency was tested by monitoring the transient absorption of ^3Spx upon optical excitation into the Q_y band of LH1 BChls. Since I was interested in selectively observing triplet energy transfer $^3\text{BChl}^* \rightarrow ^3\text{Spx}$ solely within the LH1 antenna, the SPUHK1 mutant was chosen for this study. I performed a global fit analysis for data obtained in the 400-700 nm spectral range upon direct excitation of BChl Q_y at 880 nm (Fig. 3.9).

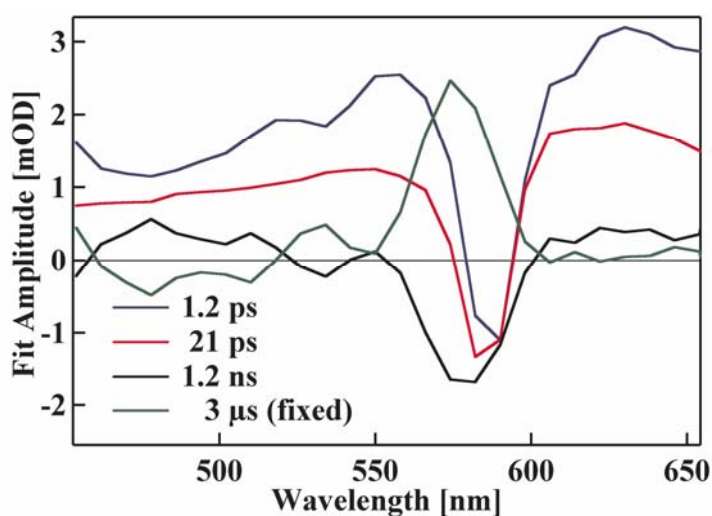


Fig. 3.9. Amplitude spectra (decay associated spectra) of the multiexponential global fit analysis upon excitation at 880 nm.

Four components were necessary for a satisfactory global fit. The first component has a lifetime of 1.2 ps and exhibits a broad spectrum covering the entire investigated spectral range. The main feature is a bleach at 590 nm attributed to the Q_x band. Moreover, this component may reflect an EET toward Spx for two reasons: first, the spectral shape superimposed to the broad, unstructured BChl ESA reflects a Spx bleach-like spectrum below 550 nm and a Spx ESA above 600 nm and second, the lifetime of this component is close to the S_1 lifetime observed upon direct Spx excitation. However, to substantiate this conclusion further experiments need to be performed. The second component reflects a pure BChl excited state (with a broad ESA contribution over the entire spectral range and a Q_x bleach at 590 nm) and has a lifetime of 21 ps. Note the faster lifetime compared to the carotenoid excitation (previous section), which is presumably due to exciton-exciton annihilation, since here the BChls were excited directly. The third component (with a lifetime of 1.2 ns) shows two minima, at 535 nm and 575 nm and positive signals around 500 nm and above 625 nm. This component strongly resembles a mirror image of the fourth component, thereby indicating that this amplitude represents a growing signal of a species which is not decaying within the temporal observation limit of our setup. The lifetime and the spectrum of the fourth component (3 μs) were determined by a ns time-resolved setup (data not shown).

The fourth component, exhibits an identical spectral shape with the triplet state observed upon Spx excitation (Figure 3.9). This is not surprising since previous studies with μs time-resolution showed triplet state spectra upon BChl excitation, via the mechanism $\text{BChl}^* \rightarrow {}^3\text{BChl} \rightarrow {}^3\text{Spx}$. Despite the fact that many studies have addressed the problem of triplet excitation energy transfer from BChl to carotenoids, to my knowledge, the time constant of this process has not been reported. Here I present for the first time the formation of the Spx triplet state with femtosecond time resolution. Figure 3.10 shows TA kinetics observed upon excitation of the Q_y BChl of the SPUHK1 sample, with the probe wavelength centred at 575 nm, i.e. at the maximum absorption of the Spx triplet.

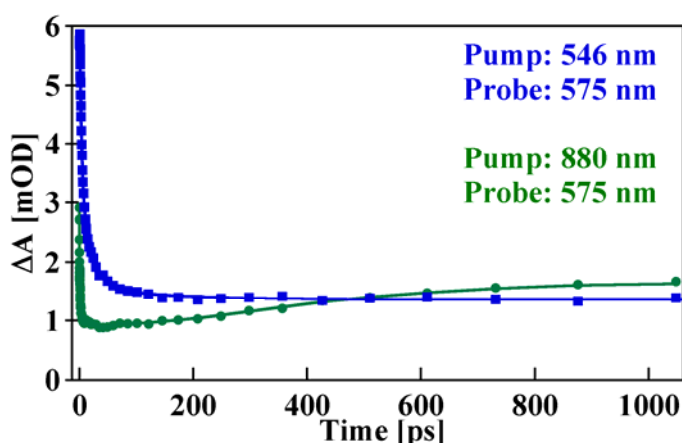


Fig. 3.10. Kinetic trace of the *R. rubrum* SPUHK1 mutant measured after excitation at 546 nm (carotenoid moiety) and 880 nm (Bchl Q_y transition). The probing wavelength was centred around 575 nm.

At early times, up to 30 ps, the instantaneously positive TA signal shows a decay associated with the depopulation of the BChl excited state. Subsequently, the TA signal then increases again for longer delay times and grows exponentially with a time constant of 1.2 ns, i.e. the third component in the global fit analysis (Fig. 3.9). This third component can be associated with triplet energy transfer from BChl to Spx, since at the probing wavelengths the spectrum is free of ${}^3\text{BChl}$ contributions and the ${}^1\text{BChl}$ excited state vanishes within the first 100 ps. Figure 6b shows an excitation wavelength-dependent comparison between the residual long-lived signals of SPUHK1 samples. The signals after BChl or Spx excitation exhibit identical spectral shape, a bleach between 400-520 nm and two positive maxima at 535 and 575 nm, showing a clear signature of Spx triplet state. Previous reports indicate that the Spx T_1 state is formed via singlet-excitation fission from the S^* excited state (78). However, I have shown that upon direct excitation of BChl, the first component exhibits a weak Spx signature (Fig. 3.9). Thus, the question remains if there is an EET from BChl to Spx S_1 upon optical excitation of the Q_y transition.

Figure 3.11 shows an excitation wavelength dependent comparison between residual long lived signals of SPUHK1 samples. The signals after BChl or Car excitation exhibit identical spectral shape, a bleach between 400-550 nm and two positive maxima at 535 nm and 575 nm, showing a clear signature of spirilloxanthin triplet state.

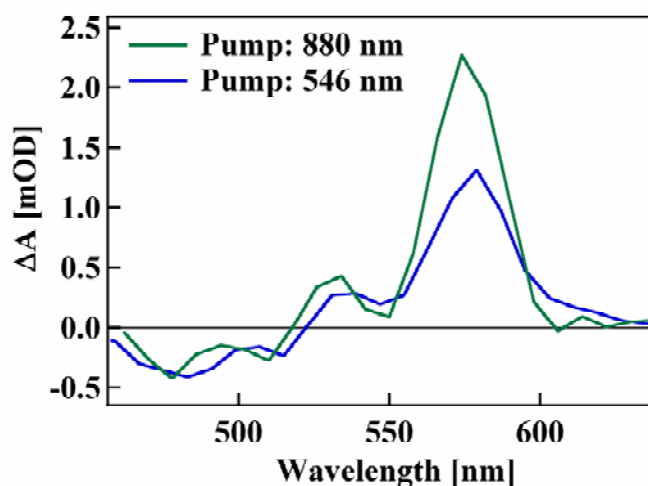


Fig. 3.11. Transient triplet state absorption spectra of SPUHK1-sample detected at 1.5 ns upon excitation of carotenoid (blue curve), and BChl (green curve).

Figure 3.12 illustrates the calculated fitting curves along with the experimental data points at 575 nm for the LH1 complexes excited in the carotenoid region (546 nm) or the BChl region (880 nm). The fit of the curves reveals time constants of 2.4 and 3 μ s. The excitation energies used in this experiment are: 400 μ J for the 546 nm excitation and 600 μ J for the 880 nm excitation. This can explain the difference in amplitude between the femtosecond and the nanosecond studies.

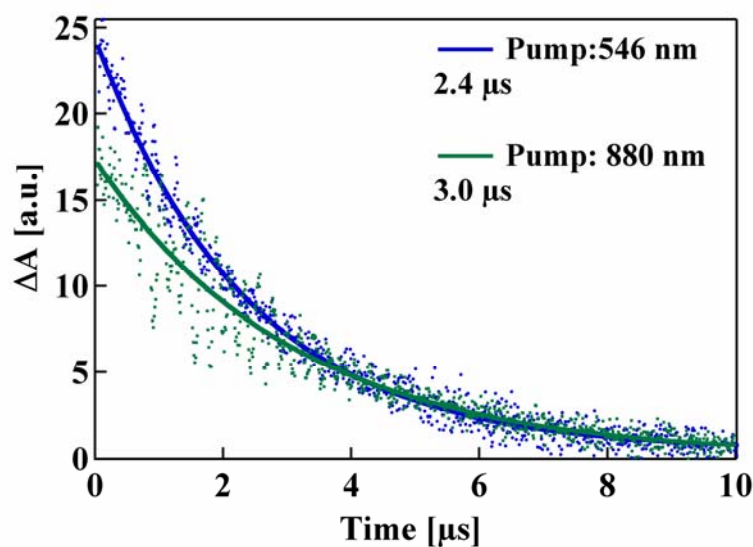


Fig. 3.12. Kinetics traces for SPUHK1 upon excitation at 546 nm (blue) and 880 nm (green), while the probing wavelength was centred at 575 nm. Solid lines are fit curves.

Previous reports show that spirilloxanthin T_1 state is formed via singlet-excitation fission from S^* state (100). Moreover, I have shown that upon direct excitation of BChl, the first component exhibits a weak Car signature (Fig. 3.9). Thus, the question remains, if there is an EET from BChl to Car S_1 upon optical excitation of the Q_y transition.

We thus performed a near-IR experiment, in which by pumping at different wavelengths (namely the Car or BChl transitions) the spectral region of Car S_1 excited state absorption was traced, more specifically the $S_1 \rightarrow S_2$ transition, visible around 1000 nm.

Upon Car excitation at 546 nm, a clear signature of $S_1 \rightarrow S_N$ and $S_1 \rightarrow S_2$ transition can be seen (Fig. 3.13, blue curve). On the other hand upon excitation at 880 nm (the BChl Q_y transition) no S_1 signal has been observed (Fig. 3.13, green curve). I can thus conclude that the $BChl^*(Q_y) \rightarrow Car(S_1)$ pathway is inactive and can thus not be utilized for the photosynthetic light reaction. However, since the S^* is the precursor of T_1 , the possibility that spirilloxanthin lower excited states involved in the Car triplet formation can not be completely ruled out.

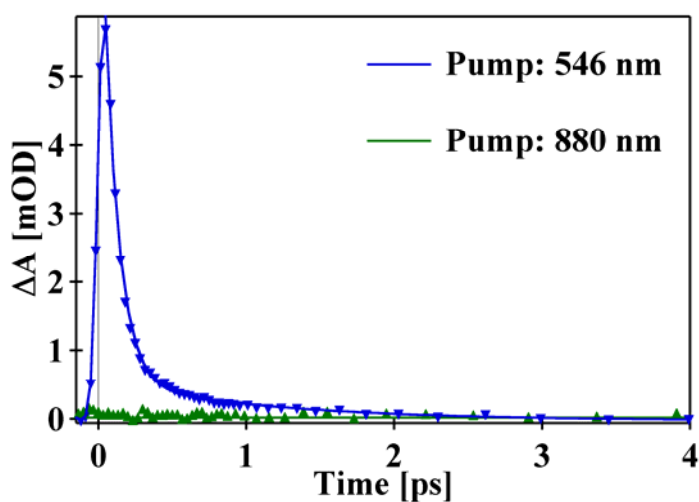


Figure 3.13. Carotenoid S_1 signature probed at 1000 nm upon carotenoid excitation at 546 nm (blue curve) or BChl excitation at 880 nm (green curve).

3.4 Discussion

The kinetics of excitation energy transfer between protein-bound pigments can be a very sensitive measure of the local environment. In this study I have employed ultra-fast spectroscopy to probe possible changes in the LH1-pigment organization in different mutants of *R. rubrum* lacking a functional RC, either due to the lack of the H-subunit, which is essential for RC-LM insertion into LH complexes, or due to site-directed deletion of the L and M subunits.

The decay kinetics of Spx for WT (S1) and the mutant samples following excitation at 550 nm show a very similar behaviour. In particular, for both RC-less mutants, the excitation to the S_2 state is followed by the simultaneous population of the lower singlet excited states S_1 and S^* , which then decay with lifetimes of approx. 1.4 and 4.7 ps, respectively, very close to the results found for WT (1.4 and 3.8 ps, respectively). The 4.7 ps lifetimes of S^* in the mutants is similar to the ones found by Gradinaru *et al.* (78) (5 ps) and Gärtner *et al.* (101) (3 ps), and is very close to the 7 ps found in the B850:Spx complex (69), and 3.8 ps for the WT sample, suggesting that its dynamic properties in those complexes do not differ significantly. The S_1 and the S^* states are thus temporally well-separated, and therefore the determination of the formation yields of S^* and the triplet by a direct comparison of their amplitudes in the two different samples is possible. By comparing the magnitude of the respective fit amplitudes in the WT and SPUHK1 (Figure 6(b)), I find similar amplitudes for the triplet signal. Therefore, I can conclude that there is no significant difference between the two samples in the generation of Spx triplet state.

Employing femtosecond spectroscopy I was able to track not only Spx excited states (S_2 , S_1 and S^*), triplet state (T_1) and to monitor the excitation energy transfer from Spx to BChl within the LH1 antenna, but also the energy transfer from LH1 to RC. The time-resolved difference absorption at 864 nm (Figure 3a) in a region where mostly ESA due to BChl is present, show significantly different temporal behaviour of SPUHK1 and WT. The ESA grows instantaneously within 100 fs followed by a significant loss of signal on the time scale of tens to hundred of picoseconds. The observed loss derive exclusively from BChl dynamics which are separated from Spx. For SPUHK1, the BChl ESA signal (Figure 3a) decays with the same time constant as the BChl bleach/SE (Figure 3b) denoting that this ESA raises from the lowest BChl excited state, which relaxes directly into the ground state. The longer lifetime of the excited state for SPUHK1 in comparison to WT can be explained by the absence of the photochemical quenching channel. For long delay times a negative signal remains for the WT sample (Figure 3a) due to the electrochromic blue shift of the monomeric BChl *a*.

Upon direct excitation of BChl I was able to follow the time evolution of the Spx triplet state (Fig. 6). The Spx triplet spectrum (last component Figure 5) is characterized by a positive peak, which arises from $T_1 \rightarrow T_N$ transition, and the negative bleach from the loss of Spx^0 (ground state) molecule due to their conversion into excited Spx^* molecule.

The initial building-up phase of $T_1 \rightarrow T_N$ absorption, which reflects the process of $^3\text{BChl}$ -to- ^3Car energy transfer, was clearly observed at 575 nm (Figure 6). As revealed by the global fit analysis for the SPUHK1 data (Figure 5), the third component has a time constant of 1.2 ns, suggesting that $^3\text{BChl}$ transfers triplet excitation to ^3Spx . Similar triplet excitation transfer has been observed for LH2 complex of *Rhodospseudomonas palustris*, where the ^3Car

absorption increases with a time constant of 0.16 μ s at 77 K. However, the raise of carotenoid triplet absorption could not be resolved at room temperature due to the limited instrumental resolution (102). Faster ^3Car -to- $^3\text{BChl}$ excitation energy transfer at room temperature compared to measurements at 77 K show that these processes are temperature-dependent. In summary, the present study allowed to follow the complex dynamics of isolated photosynthetic membranes obtained from wild-type and different reaction center (RC)-subunit deletion strains. It could be shown that deletion of H or (L+M) subunits has no effect upon the Spx S_1 , and only a very small effect upon the S^* (from 4 ps WT to 5 ps SPUHK1) lifetimes of the overall LH1 complex. Moreover, the energy transfer from the excited Spx to the RC in the case of WT strain could be observed with a transfer time of about 46 ps. The absence of this deactivation channel for the RC-subunit deletion strains confirms the assignment of this essential quenching mechanism. For all investigated strains, a triplet energy transfer from BChl molecules to Spx occurred. Although this had been reported before, the current study allows for the first time to follow this process and determine associated time constant to be 1.2 ns. Taken together, these results also argue strongly that for the *R. rubrum* PSU, the presence of a RC has no effect upon the overall pigment organization of the LH1 complex *in vivo*.

In summary, the present study has shown that deletion of H subunit inhibits the formation of the RC but shows no difference for the spirilloxanthin S_1 lifetime and only very small difference for S^* (from 4 ps WT to 5 ps Spuhk1). Moreover, I observed energy transfer from the photoexcited Cars to the RC in the case of the WT sample, and a transfer of the triplet excitation energy from BChl to Cars within nanoseconds.

4 Carotenoid Radical Cation as a Probe for Non-photochemical Quenching

4.1 Introduction

Non-photochemical quenching (NPQ) is a fundamental mechanism in photosynthesis which protects plants against excess excitation energy and is of crucial importance for their survival and fitness. Feedback deexcitation (qE), a component of NPQ, is an important process in the photo-protection of plants by which excess excitation energy of chlorophylls is dissipated as heat (6). The activation of qE is linked to an increase in the pH gradient across the thylakoid membrane upon light saturation of the photosynthetic electron transport (4, 6, 103). Violaxanthin is converted to zeaxanthin in the xanthophyll cycle, and PsbS, a protein subunit of photosystem II for which a central role in qE has been reported (104), is protonated (104, 105). Although the interconversion of violaxanthin to zeaxanthin in the xanthophyll cycle is a prerequisite for complete qE induction, the detailed molecular mechanism of qE remains elusive. Today even the exact role of carotenoids in this process is unclear and thought to be either direct (106), indirect (107), or both (15).

According to the so-called "gear-shift" model (106), zeaxanthin acts as a direct quencher of electronically excited chlorophylls, since its first singlet excited electronic state (S_1) is supposed to be lower than the lowest excited chlorophyll state (Q_y). Excitation energy transfer (EET) from Chl *a* to zeaxanthin is thus in principle possible and dissipation at zeaxanthin can take place (106, 108). In contrast, the S_1 state of violaxanthin is supposed to be above the Q_y level of Chl *a* and thus cannot quench the Chl *a* excited state. This mechanism has been recently verified in artificial light-harvesting dyads (109).

An indirect role of the carotenoids is postulated in the aggregation model, suggesting the LHC II as the quenching site (107, 110). This model predicts that the conversion of violaxanthin to zeaxanthin induces conformational changes of the proteins, by which new pigment configurations capable of quenching arise. Recently, the formation of chlorophyll dimers as quenching sites has been suggested (107).

A model that combines both direct and indirect roles of the carotenoids is the hypothesis that a quenching complex between Chl *a* and zeaxanthin is formed during the induction time of qE, in which zeaxanthin also acts as the terminal quencher (17, 111-113).

Apart from elucidating the molecular mechanism, it remains to be shown exactly where and in which pigment-protein complex of the photosynthetic apparatus qE actually occurs. Studies on the qE deficient *Arabidopsis thaliana* npq4-1 mutant that lacks the protonation-induced absorption change at 535 nm strongly suggest that the PsbS protein contributes to photoprotective energy dissipation (104). This implies that the quenching site might be PsbS, since binding of zeaxanthin to PsbS *in vitro* has been reported to give rise to a strong red shift

in the absorption spectrum (114), providing a possible explanation for the absorption change observed at 535 nm when qE is active (115, 116). Moreover, the resonance Raman spectrum of the *in vitro* Zea-PsbS complex has the same features as found *in vivo* during qE (114, 117).

However, another recent qE model proposes an indirect role of PsbS (107). According to this model, PsbS interacts with LHC II in the photosynthetic membrane at low luminal pH, inducing a conformational change and resultant quenching in the same way as observed *in vitro* upon crystallization of the antenna complex. It was reported that PsbS has two different aggregation states with different affinities for the core and the LHC antenna (118). At pH 4, the protein exists as a monomer and preferentially associates with the antenna LHCs. At pH 7, a PsbS dimer, the favored aggregation state, mainly co-migrates with the photosystem II core. Coupling this information with the observation that dimers monomerize upon qE induction in intact systems (118-120), because of acidification of the thylakoid lumen, leads to the conclusion that monomers associated with the LHC antenna are responsible for *in vivo* energy dissipation (13).

On the other hand, an appealingly simple mechanism, based on the recently determined molecular structure of LHC II (121, 122), reconsidered LHC II as the location of qE (122). This was based on the consideration that replacement of violaxanthin by zeaxanthin in its binding pocket of LHC II should enable quenching via EET from chlorophyll to zeaxanthin or via electron transfer (ET) from zeaxanthin to chlorophyll. The latter possibility is predicted by theory and indeed it has been confirmed experimentally that carotenoid radical cations are formed during qE (15, 17, 111). As a consequence, if ET and not EET is the main component of qE, the efficiency of qE depends on the ionization potential of the carotenoids and the properties of the detected carotenoid radical cations rather than on the energetic position of S_1 . In general, there are few studies addressing the properties of carotenoid radical cations directly. Although $\beta\text{-Car}^{\bullet+}$ in RC has been studied for over 20 years (see e.g. (123, 124)), only recently, spectroscopic investigations of such cations generated electrochemically in solution have been reported (125, 126). Carotenoid radical cations have also been observed in LH2 from purple bacteria upon direct carotenoid excitation (127).

In this chapter, I first give a brief summary of the sample preparation followed by ultrafast time resolved studies of Chl excited state dynamics comprising both EET and ET deactivation mechanisms. Finally, I use multiple light pulses to investigate the ultrafast dynamics of carotenoid radical cation formation both in solutions of the pure compounds and in LHC II isolated from plant thylakoids. The three-pulse technique involves contributions from two high-intensity pulses initiating a resonant two-photon, two-color ionization (R2P2CI) process and a low-intensity broad-band probe pulse. The R2P2CI measurements reveal the spectroscopic properties of $\text{Car}^{\bullet+}$ and the spectral characteristics of zeaxanthin and violaxanthin radical cations in LHC II, which are crucial for understanding the qE protection mechanism in higher plants.

4.2 Sample Preparation

For the measurements in solution, Vio, Lut, Zea, and β -carotene powders were dissolved in ethanol to an optical density (OD) of 1 at the red wing of the 0-0 vibronic band of the $S_0 \rightarrow S_2$ transition. The Vio, Lut, and Zea were purified from spinach by HPLC (128), whereas β -carotene was purchased from Sigma.

Thylakoid membranes from pea leaves were prepared as described (129, 130). All thylakoid isolation procedures were performed in a darkened cold room (7° C) under dim green light using chilled wares. The leaves (8-10 g) were cut into 2-3 cm pieces and ground using two to three 1-s bursts in a Waring blender in 100 mL of a slushy grinding buffer containing 0.33 M dextrose, 50 mM $\text{Na}_2\text{HPO}_4 \cdot 7\text{H}_2\text{O}$, 50 mM KH_2PO_4 , 25 mM KCl, 5 mM MgCl_2 , 0.1% BSA, and 0.2% sodium ascorbate, pH 6.5. The brie was gently vacuum filtered through a 41 μm nylon filter (Spectra/Mesh). The filtrate was centrifuged for 10 min at 1500g in an SS-34 (Sorvall) rotor at 4° C. The pellet was gently resuspended in buffer A containing 0.33 M sorbitol, 4 mM EDTA, 5 mM MgCl_2 , 2 mM MnCl_2 , 0.1 M HEPES, and 0.2% BSA, pH 7.6. The reaction mixture (buffer B) contained 0.1 M sucrose, 10 mM NaCl, 10 mM KCl, 5 mM MgCl_2 , 10 mM Tricine, 1 mM KH_2PO_4 , and 0.2% BSA, pH 8.0. The Chl concentration was determined according to the equations of Porra *et al.* (131).

By incubation of the thylakoid membranes at pH 5.3 in the presence (40 mM) or absence of ascorbate, samples with or without zeaxanthin have been prepared. LHC II isolation was subsequently performed as in ref (122). For preparation of the light-harvesting complex, the pelleted chloroplasts were thoroughly dispersed in 35 ml of 5 mM EDTA (pH 7.8) containing 0.1 M sorbitol. The pH of the resuspended sample was then adjusted to 6.0 with 1.0 N HCl, and the sample was centrifuged at 10,000 g for 10 min. The membranes were resuspended in 30 ml of 0.1 M sorbitol and then repelleted by centrifugation at 10000g for 10 min. This washed pellet was resuspended in 0.5% Triton X-109 (in deionized H_2O) to a chlorophyll concentration of 0.5 mg/ml. The mixture was incubated with stirring for 30 min at 25° C, and centrifuged at 41000g for 30 min. The small pellet which formed was discarded and 8.0 ml of the dark-green supernatant was loaded on linear 0.1-1.0 M sucrose gradients containing 0.5% Triton X-100. The gradients were centrifuged for 15 h in a Beckman SW-27 rotor at 100000 g.

Recombinant CP24, CP26 and CP29 from *Arabidopsis thaliana* were refolded in the presence of isolated pigments (neaxanthin, lutein, violaxanthin, Chl *a* and Chl *b*) with adjusted chlorophyll content in order to resemble native CP29. Exposure of CP24, CP26 and CP29 to zeaxanthin led to zeaxanthin-enriched samples (CP24-Zea, CP26-Zea and CP29-Zea) without the necessity to vary other parameters like light or pH gradient.

Pigment composition of LHCs samples was determined by high performance liquid chromatography (HPLC), by the integration of HPLC peaks measured at 440 nm (132). Every sample was measured once. For the spectroscopic experiments, the typical sample OD was 0.8/mm at 660 nm. Sample stability was confirmed by measuring the absorption spectra before and after the time-resolved measurements.

4.3 Chlorophyll Excited-State Dynamics in LHC Proteins

4.3.1 Excitation Energy Transfer.

Several models for the qE component of NPQ have been proposed and are still discussed controversially. A recent model for qE suggests that the replacement of Vio by Zea in its LHC II binding pocket can in principle result in qE via the so-called "gear-shift" mechanism. The latter requires the Vio S_1 state to be higher in energy than the Q_y of Chl *a*, and the S_1 state of Zea to be lower. To confirm the proposed model, ultrafast pump-probe measurements were performed on native LHC II and on LHC II in which Vio has been biochemically converted to Zea as indicated above. The experimental approach employs excitation of LHC II chlorophylls at 660 nm into the first excited state when Vio or Zea was present. The lifetime of Chl *a* was probed by measuring the kinetics corresponding to ESA of the Chl Q_y excited state at 900 nm (Fig. 4.1).

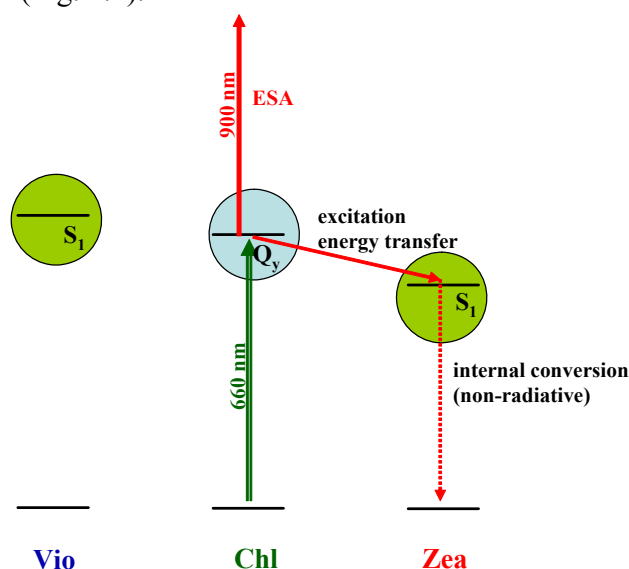


Fig. 4.1. Schematic representation of the gear-shift model.

When Vio is present in LHC II (left side of Fig. 4.1), EET from Q_y to S_1 is not possible. On the other hand, in the case of Zea (right side of Fig. 4.1) the excitation energy located on Chl can be transferred to Zea S_1 , which finally decays non-radiatively by internal conversion back to the electronic ground state.

The presence of Zea in LHC II was verified by HPLC analysis (Fig. 4.2). For the LHC II-Vio sample a maximum content of Vio was achieved, and no trace of Zea was detected. In the Zea-enriched LHC II sample (LHC II-Zea) the maximum Zea level exceeds the Vio content almost by a factor of 2 (Fig. 4.2). It should be noted that a part of Vio is lost during the conversion.

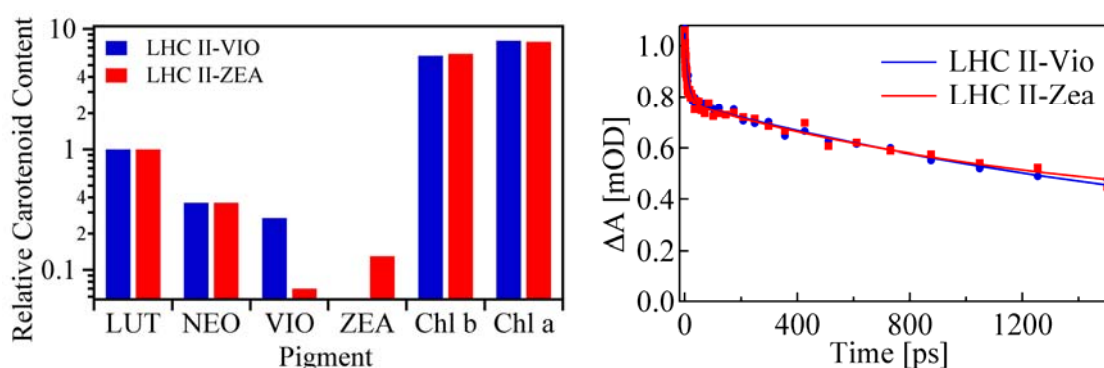


Fig. 4.2. Carotenoid composition in native and Zea-enriched preparations of LHC II (left). TA data for LHC II-Vio (blue) and LHC II-Zea (red) detected at 904 nm upon excitation at 660 nm. The solid lines correspond to the fit curve obtained by a global fitting routine (right).

The data in Figure 4.2 are normalized to one lutein molecule. They represent integration of HPLC peaks measured at 440 nm and correspond to relative values, though direct comparison between the same carotenoids in the two different samples is possible. Within the experimental accuracy the neoxanthin content of both samples remains unchanged, the violaxanthin content decreases upon the presence of zeaxanthin.

To study the kinetics of the first excited Chl state in LHC II, the Q_y transition was excited at 660 nm and TA spectra were acquired in the near-IR region from 800 to 1050 nm, where the broad ESA of Chl can be detected. The TA spectra were analyzed using a global fitting routine revealing two major decay components, a fast decay (~ 10 ps) and a slower decay, with a time constant beyond 1.5 ns, that is, beyond the time scale of the experiment. The kinetics observed for both LHC II samples, LHC II-Vio and LHC II-Zea, are essentially identical over the entire spectral range investigated, displaying only minor differences, which are not significant within the experimental errors. The transient characteristics in the Q_y region are illustrated by the kinetic traces measured at 904 nm (Fig. 4.2). It is important to note that LHC II-Zea samples show no additional rise and decay as reported for thylakoid membranes upon qE induction (15).

Furthermore, to determine whether zeaxanthin may induce chlorophyll quenching in isolated LHCs, near-IR TA kinetic traces were measured by photoexcitation at 660 nm of the light harvesting minors (CP29, CP26 and CP24) displaying specific xanthophyll compositions. Figure 4.3 shows TA (left) and HPLC analysis (right) of the investigated light harvesting minors. Recombinant LHC minors from *Arabidopsis thaliana* were refolded in the presence of isolated pigments with adjusted chlorophyll content in order to resemble native CP24, CP26 and CP29. Exposure of CP24, CP26 and CP29 to zeaxanthin led to zeaxanthin-containing samples (CP24-Zea, CP26-Zea and CP29-Zea) without changing any other parameters like light or pH gradient. The near-IR TA kinetic profiles at 904 nm (Fig. 4.3) exhibit two decay components for all investigated samples, which originate solely from chlorophyll excited state absorbance dynamics (15, 88, 133). Comparing the TA measurements of all light harvesting samples I find kinetic differences between the various species, while the TA measurements of native and Zea enriched sample of the same light

harvesting species are practically identical. These data are consistent with the results obtained for LHC II binding Vio or Zea (Fig. 4.2).

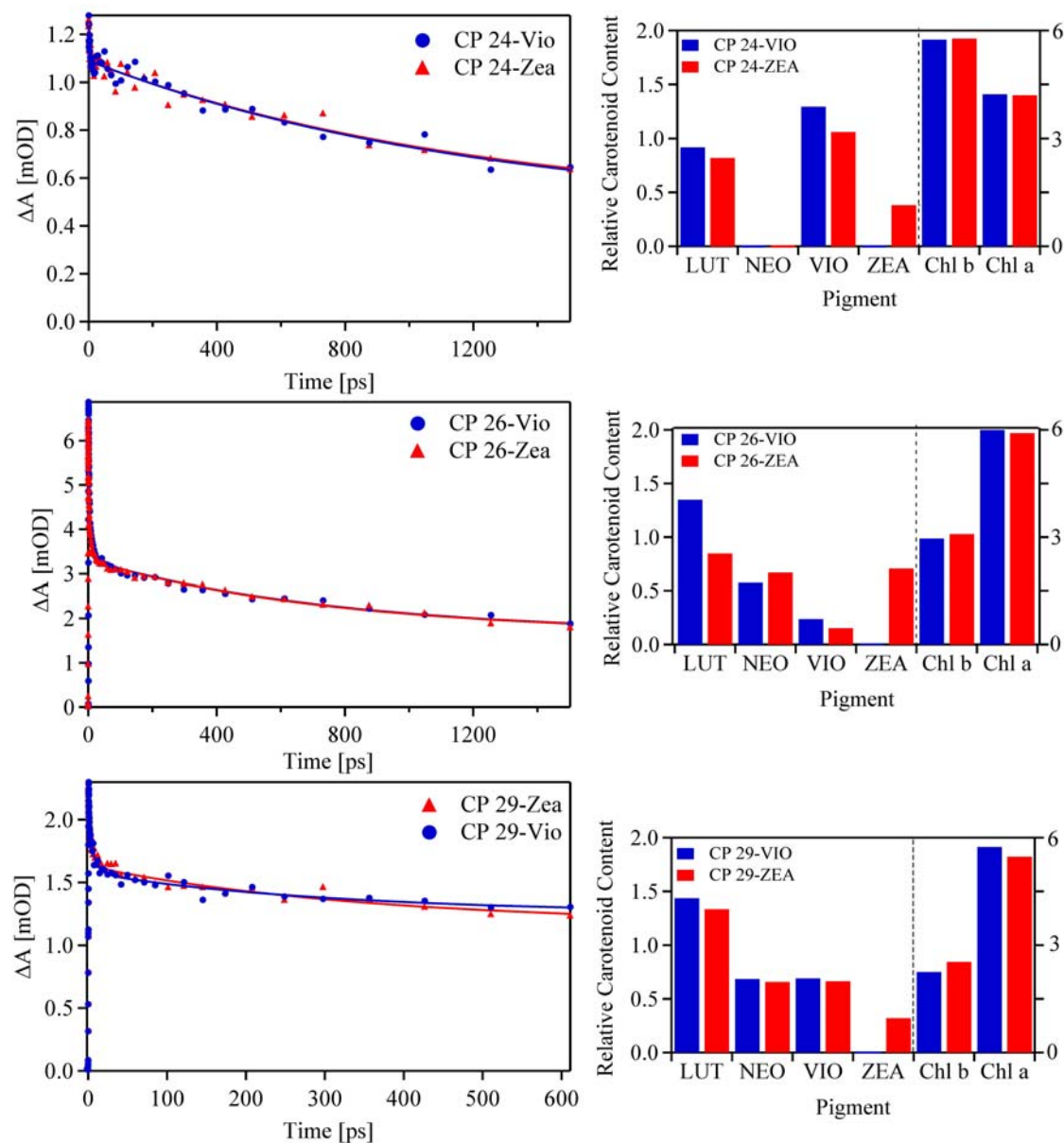


Fig. 4.3. TA data detected at 904 nm upon excitation at 660 nm (left) and HPLC analysis (right) for native (blue) and Zea enriched (red) CP24, CP26 and CP29. The solid lines correspond to fit curves obtained by a global fitting routine.

The analysis of my TA measurements on LHC II samples upon Q_y excitation revealed two kinetic components, a fast 10 ps and a slow >1.5 ns component necessary to describe the ESA dynamics at a probe wavelength of 904 nm (Fig. 4.2 and Fig. 4.3). Earlier time-resolved pump-probe measurements of trimeric LHC II have revealed EET from Chl *b* to Chl *a* which

occurs with kinetic components of ~150 fs and 600 fs at room temperature and at 77 K (20, 23, 133, 134), and equilibration among the Chl *a* molecules taking place with time constants longer than 10 ps (23, 24, 133). In agreement with these earlier measurements I assign the fast 10 ps component to equilibration processes between Chl *a* molecules. The slow decay >1.5 ns can be attributed to the excited state lifetime of Chl *a* molecules.

Mullineaux *et al.* show that the Zea/Vio ratio in LHC II has no influence on the time-resolved fluorescence emission spectrum (135). However, the authors report a decrease of the fluorescence lifetime from 4.3 ns in the solubilized LHC II to 110 ps in a semicrystalline aggregated state. They also state that the quenching species is a nonfluorescent pigment, which cannot be resolved by time-resolved fluorescence measurements. This difficulty is overcome by my measurements since here I measure ESA and can thus detect also nonfluorescent (dark) states. My experiments reveal no change in lifetime of the excited state absorption signal of the initially excited Q_y states. Both the native and Zea containing samples exhibit the same excited state dynamics and no evidence of chlorophyll quenching has been found. Since the chlorophyll fluorescence lifetime is typically 2.5 ns, it is unlikely that relevant changes occur beyond the experimentally covered time range of 1.5 ns. Thus, Zea is not capable of quenching either isolated LHC II complexes if it replaces Vio in its binding pocket nor light harvesting minors (CP29, CP26 and CP24). As a consequence, this originally proposed simple mechanism for qE of NPQ is not sufficient to invoke efficient quenching.

4.3.2 Electron Transfer.

Experiments on Vio and Zea solubilized in organic solvents and bound to recombinant LHC II have shown that the S₁ energies exhibit no major difference and lie below the excited-state of Chl *a* (136-138). According to TA measurements, the S₁ energies of Vio and Zea have values of 1.79 and 1.74 eV in solution and 1.70 and 1.71 eV in recombinant LHC II, while fluorescence measurements give 1.84 and 1.80 eV. The difference in the values obtained from TA and fluorescence is consistently explained by geometry relaxation effects (139). Recent theoretical (17), and experimental studies (15), show that zeaxanthin plays a direct role in quenching the excitation energy: a quenching complex forms between Chl *a* and zeaxanthin during the induction time of qE, and zeaxanthin acts as terminal quencher via electron transfer leading to carotenoid radical cation formation. As a consequence, if ET and not EET is the main component of qE, the efficiency of qE depends on the ionization potential of the carotenoids and the properties of the detected carotenoid radical cations rather than on the energetic position of S₁.

A recent experiment performed on intact spinach thylakoid membranes show spectral differences observed between the quenched and unquenched states ascribed to the formation of zeaxanthin radical cations when the near-IR region was probed after excitation at 664 nm (15). To observe if isolated light harvesting complexes provide sites for charge transfer quenching, ultrafast pump-probe measurements were performed on native and Zea enriched light harvesting samples. I performed ultrafast TA measurements upon excitation of bulk chlorophyll of LHCs at 660 nm in the presence or absence of Zea and the near-IR region (850-1050 nm) was scanned for carotenoid radical cation formation. The TA spectra measured in the 850 to 1050 nm region at a delay time of 20 ps are presented in Figure 4.4.

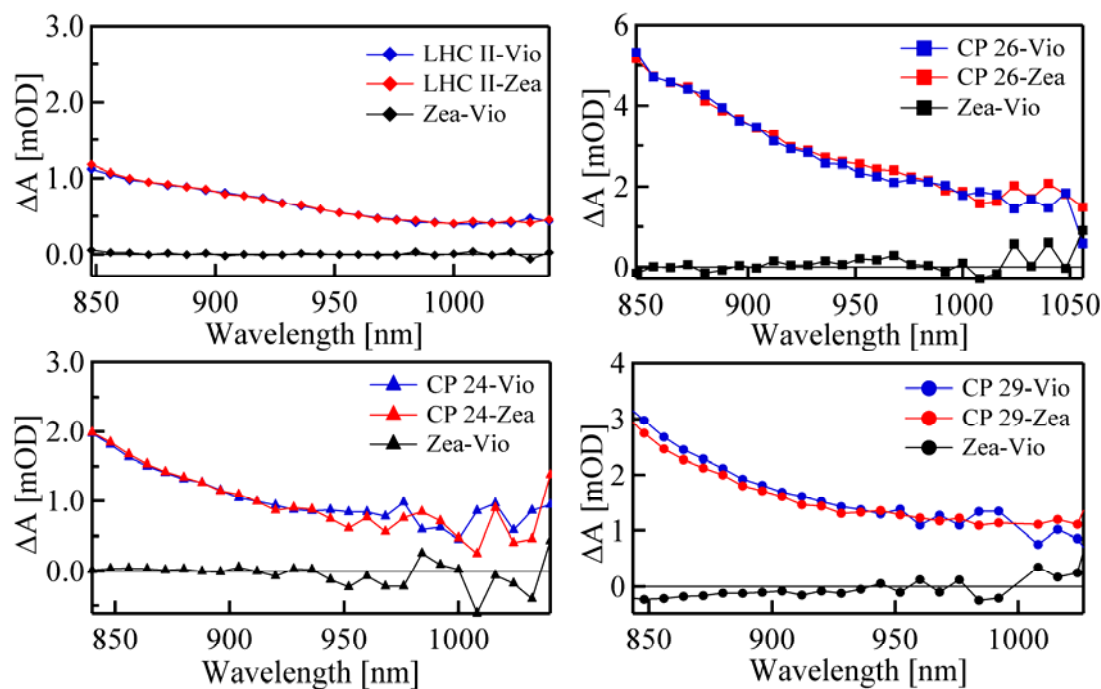


Fig. 4.4. Near-IR spectrum of native (blue) and Zea enriched LHCs (red) recorded 20 ps upon excitation of Chl bulk at 660 nm.

In my experiments, upon Q_y excitation of Chls, no additional rise and decay attributed to $\text{Car}^{\bullet+}$ during qE was detected throughout the entire investigated spectral range (800-1050 nm). The TA spectra within the same light harvesting complex are similar over the entire investigated spectral range, displaying only minor differences, which are not significant within the experimental errors. The difference spectra (native-Zea enriched LHCs) do not show absorption spectra expected for zeaxanthin radical cation.

We have shown that replacement of Vio to Zea in the LHC II binding site of Vio has no effect on Chl excitation lifetime (Fig. 4.2), and show no absorption spectra indicative for zeaxanthin radical cation formation. In any case, experiments performed on intact spinach thylakoid membranes show formation of a zeaxanthin radical while qE is active. Thus, the simple quenching model mentioned above, assuming LHC II as site of qE (122), has to be revised, and other factors have to be taken into account. For example, if PsbS is indeed necessary for maximum qE, its absence in the preparations may explain why quenching does not occur. If indeed the protection mechanism involves carotenoid radical cation formation, the properties of the detected radical are essential not only for understanding of the qE protection mechanism in higher plants but also to localize the quenching site. In the next section of this chapter, I will specifically generate and characterize carotenoid radical cations by means of resonant two-photon two-color ionization spectroscopy (R2P2CI).

4.4 Generation of Carotenoid Radical Cations in Solution

Four different carotenoids violaxanthin, lutein, zeaxanthin, and β -carotene were studied by R2P2CI spectroscopy. The first pump pulse centered at 490 nm excites the carotenoids to the S_2 state, whereas the second pump pulse with a delay time τ_1 has a center wavelength of 775 nm and is resonant with the $S_2 \rightarrow S_N$ transition (Fig. 4.5).

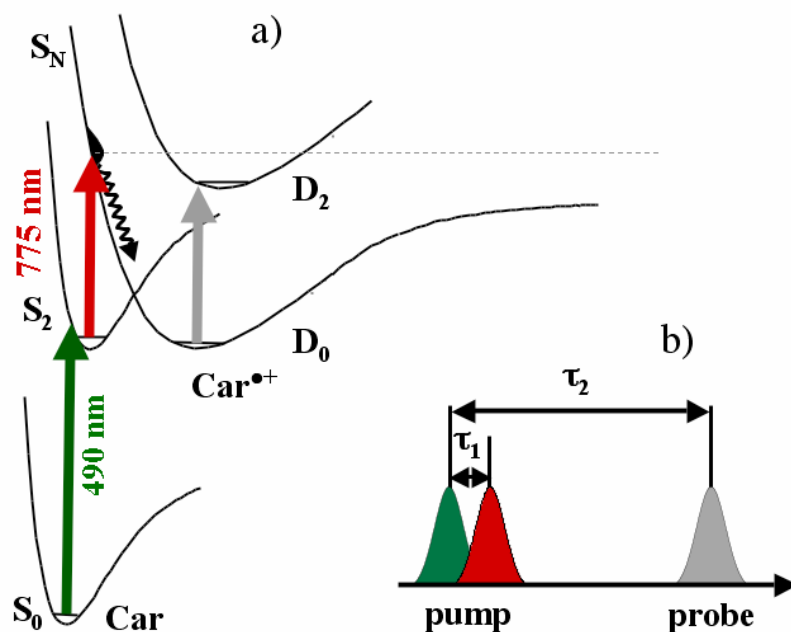


Fig. 4.5. Schematic diagram of the resonant two-photon two-color ionization (R2P2CI) experiment on carotenoids.

Upon carotenoid excitation at 490 nm, the generated S_2 state of all carotenoids exhibits a strong ESA in the near-IR region. Applying the 775 nm pulse while the S_2 state is occupied results in a further excitation of the molecules into the S_N state. The relaxation of this higher excited-state can occur either back to S_2 , or a free electron can be released and a carotenoid radical cation is formed. The second pathway is supported by previous studies (140), and by my experiments, since the second pulse leads to ESA decrease in favour of a new long-lived species attributed to $Car^{\bullet+}$ (Fig. 4.6). Transient absorption (TA) spectra were measured for different time intervals τ_2 between the second pulse and the probe pulse (Fig. 4.5b).

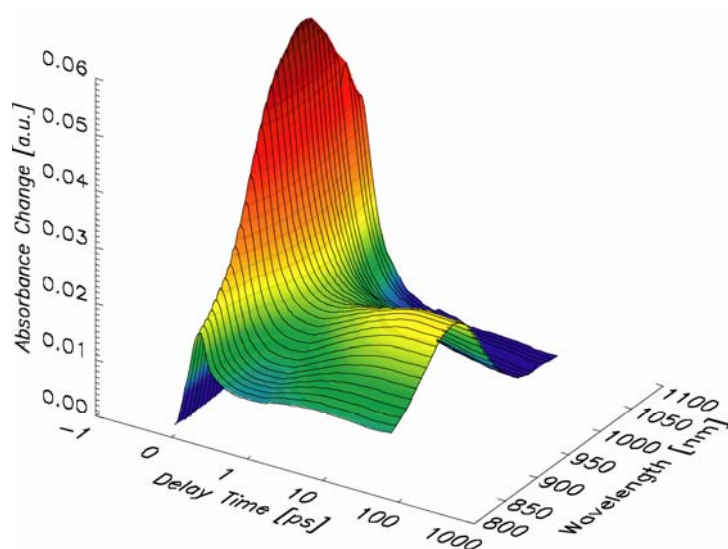


Fig. 4.6. Temporal evolution of $\beta\text{-Car}^{\bullet+}$ upon generation by R2P2Cl.

The TA spectra exhibit a transient signal in the near-IR region from 800 to 1000 nm associated with the $\text{Car}^{\bullet+}$ (Fig. 4.6). The spectral amplitude of the cation absorption strongly depends on the time delay between the first two pulses τ_1 (Fig. 4.7). The maximum yield of the transient $\text{Car}^{\bullet+}$ signal was achieved by tuning the delay time τ_1 to approximately 40 fs. However, the time delay cannot be unambiguously detected since the pulse lengths, which are 100 fs for the first pulse and 250 fs for the second pulse, directly influence the time resolution.

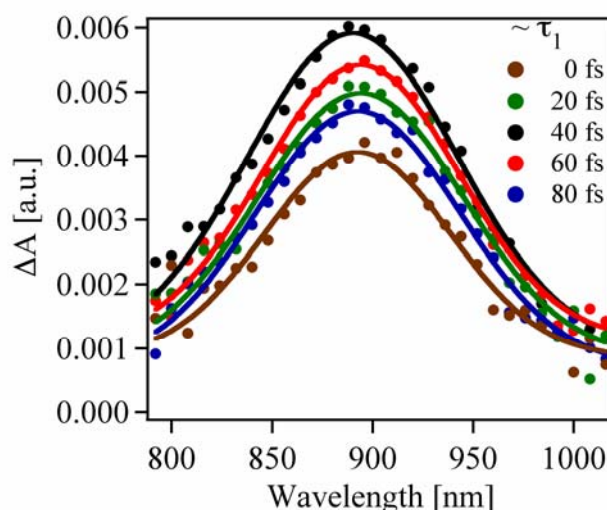


Fig. 4.7. Absorption spectra of $\text{Lut}^{\bullet+}$ in ethanol for different time delays (τ_1).

When the maximum yield of the $\text{Car}^{\bullet+}$ signal was achieved for violaxanthin, τ_1 was kept fixed for all carotenoids, and TA measurements were performed by varying τ_2 . The temporal and spectral evolution of the optically generated $\text{Car}^{\bullet+}$ species is presented in Figure 4.8. For

simplicity only the Vio data are shown, since the trend is practically identical for all investigated carotenoids.

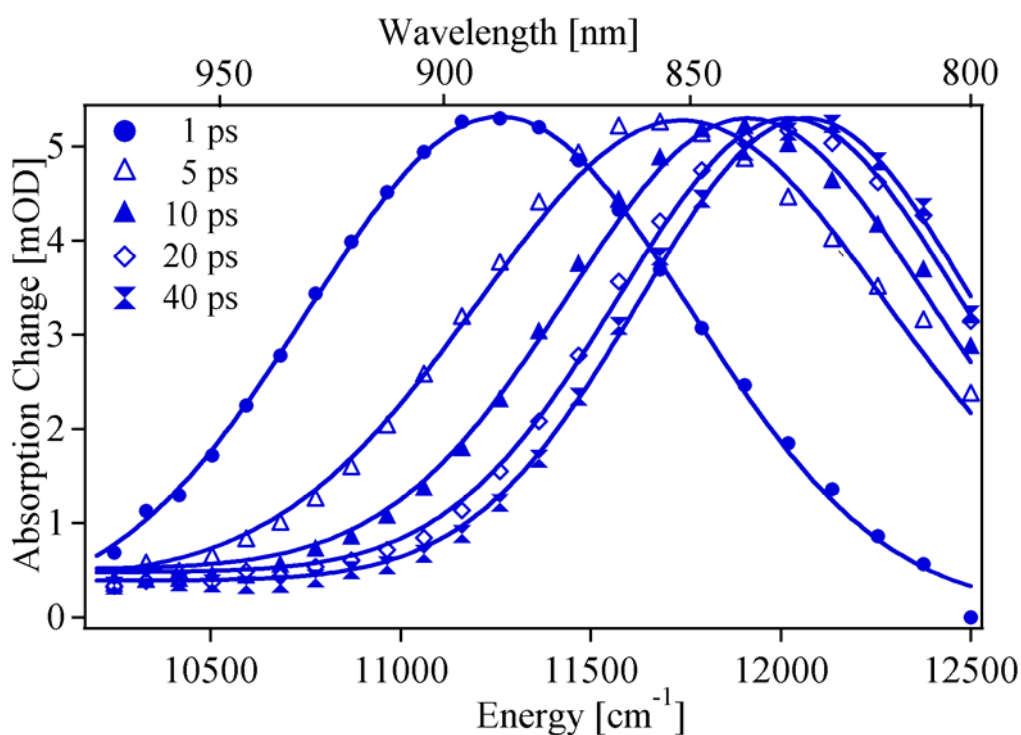


Fig. 4.8. Absorption spectra of $\text{Vio}^{\bullet+}$ in ethanol for different time delays (τ_2) after cation generation.

Upon increasing τ_2 a blue spectral shift concomitant with a narrowing of the $\text{Car}^{\bullet+}$ spectrum was observed, indicative of a cooling process in the $\text{Car}^{\bullet+}$ ground state. The cooling dynamics was monitored by plotting the bandwidth versus time delay, and an exponential fit results in a time constant of ~ 6 ps (Fig. 4.9). It should be noted that without the second pulse no transient $\text{Car}^{\bullet+}$ signal was detected.

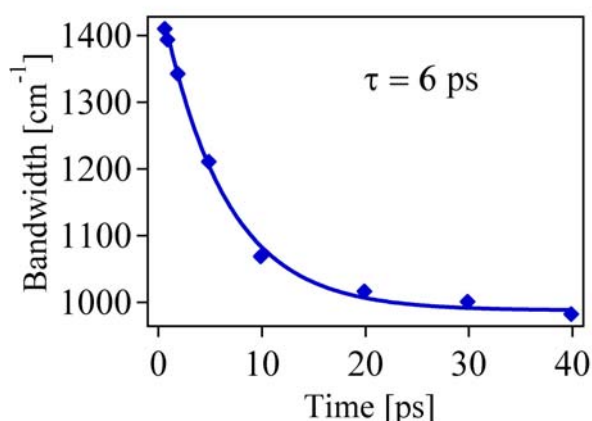


Fig. 4.9. Bandwidth at FWHM vs. time delay of $\text{Vio}^{\bullet+}$.

The TA spectra for $\tau_2 = 40$ ps of all four carotenoids studied are shown in Fig. 4.10. At this point, the dynamic evolution of the $\text{Car}^{\bullet+}$ spectra was completed, indicating that the cations are in their respective ground states and that the cooling processes are finished.

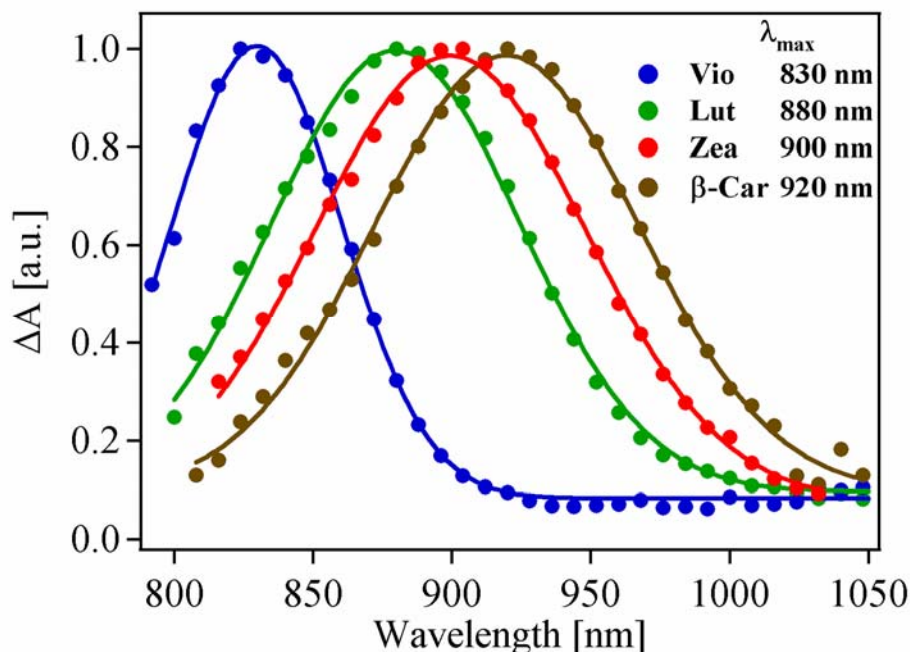


Fig. 4.10. Transient absorption spectra of the investigated $\text{Car}^{\bullet+}$ in the near-IR region in ethanol, taken 40 ps after generation. From left to right: violaxanthin, lutein, zeaxanthin, and β -carotene.

For ease of comparison, the $\text{Car}^{\bullet+}$ spectra are normalized to the same maximum absorbance value. The $\text{Car}^{\bullet+}$ bands have maxima located at 830 nm (violaxanthin), 880 nm (lutein), 900 nm (zeaxanthin), and 920 nm (β -carotene). A shift of the $\text{Car}^{\bullet+}$ absorption band toward lower energies in the order violaxanthin \rightarrow lutein \rightarrow zeaxanthin \rightarrow β -carotene according to the increase in conjugation length from violaxanthin (9 C=C) to lutein (10 C=C) to zeaxanthin and β -carotene (11 C=C) was observed. Surprisingly, although having the same number of C=C double bonds, the excited-state absorption (ESA) observed for β -carotene is slightly red-shifted compared to zeaxanthin. Comparison of violaxanthin and zeaxanthin, the relevant carotenoids for qE, yields an energy difference for the $D_0 \rightarrow D_2$ transition for $\text{Vio}^{\bullet+}$ and $\text{Zea}^{\bullet+}$ in ethanol of $\sim 937 \text{ cm}^{-1}$ or 0.12 eV.

TA spectra of β -carotene radical cations generated as mentioned above in increasingly polar solvents (acetonitrile, ethanol, acetone, dichloromethane, chloroform and CS_2) are presented in Fig. 4.11. The spectra are taken at a delay time of 40 ps. For easy comparison, the $\text{Car}^{\bullet+}$ spectra are normalized to the same maximum absorbance. The β -carotene cation radical shows a strong solvent dependent spectral change; its λ_{max} shifts to lower energy upon decreasing polarity, i.e. from acetonitrile to CS_2 by about 130 nm, reflecting the carotenoid-to-solvent dispersive interaction (Fig. 4.11).

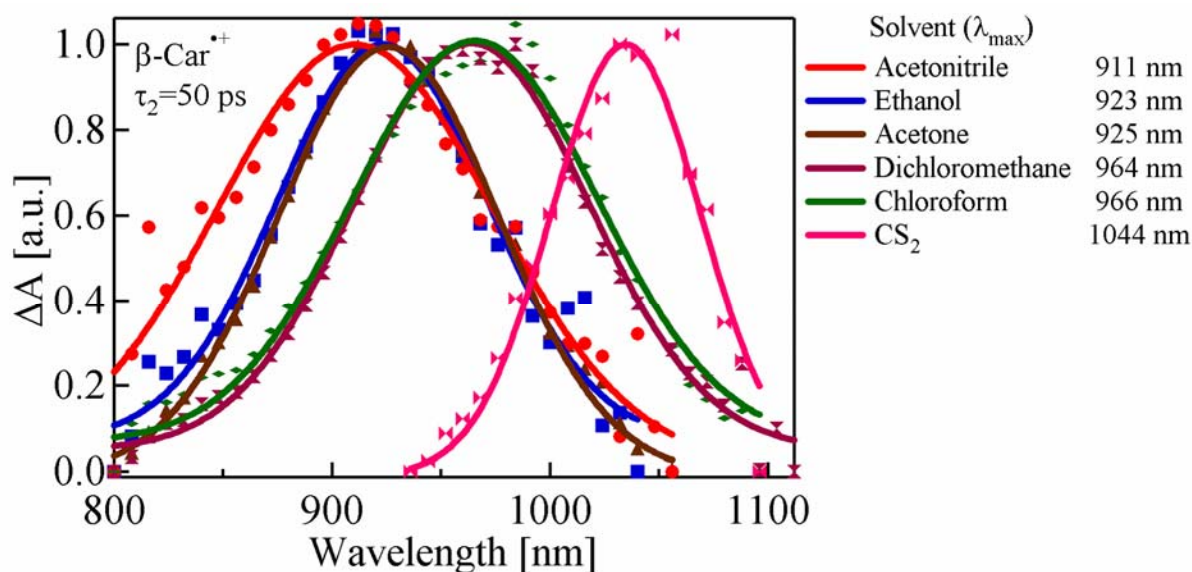


Fig. 4.11. Transient absorption spectra of $\beta\text{-Car}^{\bullet+}$ in acetonitrile, ethanol, acetone, dichloromethane, chloroform and CS₂.

Concomitant with the spectral shift a narrowing of the spectra towards less polar solvents is also observed (Fig. 4.11). Carotenoid radical generation by chemical oxidation display the same tendency of λ_{\max} solvent dependency, though the spectral shift is less pronounced (see Fig 5.3 and (141)).

Since, the formation of $\beta\text{-Car}^{\bullet+}$ upon R2P2CI occurs on a femtosecond time-scale by direct electron ejection into the solvent, it's not surprisingly the observed difference between R2P2CI and chemical oxidation (Chapter 5). The ejected electron provides a strong environmental change that strongly affects the optical properties of the $\beta\text{-Car}^{\bullet+}$.

4.5 Carotenoid Radical Cation Detection in LHC II

The R2P2CI measurements on carotenoids in solution revealed a transient species identified as $\text{Car}^{\bullet+}$ signal in the near-IR region (Fig. 4.10). However, R2P2CI measurements on LHC II (Fig. 4.12), lead to a chlorophyll ESA signal as a consequence of EET from S_2 (Car) to Q_y (Chl) which interferes with the detection of $\text{Car}^{\bullet+}$. The pump-probe (PP) TA spectra recorded at a delay of 40 ps upon carotenoid excitation into S_2 at 490 nm are dominated by a structureless ESA signal, which originates from excited Chls and cover the entire investigated spectral range. After 40 ps, a large part of the excitation energy is already transferred to Chls as a result of direct EET from the carotenoids. Remaining carotenoid contributions, for instance ESA from S_1 , disappear with a time constant around 10 ps as a result of the fast internal conversion (IC) to the ground state (138). As a consequence, the PP spectrum at 40 ps contains exclusively Chl ESA, while a corresponding R2P2CI spectrum contains both Chl ESA and $\text{Car}^{\bullet+}$ contributions. The difference between R2P2CI and PP spectrum at 40 ps should thus reflect only the remaining spectral contribution of the thermalized $\text{Car}^{\bullet+}$ species. However, also the Chl ESA signal differs in the R2P2CI experiment slightly from the conventional PP experiment, since further excitation of the S_2 state with the second laser pulse results in a loss of potential carotenoid donors for the EET toward the Chls, and consequently the Chl ESA signal will decrease. On the other hand, hot S_2 states may be produced in the R2P2CI experiment, which can have an increased $\text{Car} \rightarrow \text{Chl}$ transfer rate. In any case these phenomena only result in a shift of the baseline and do not disturb the analysis.

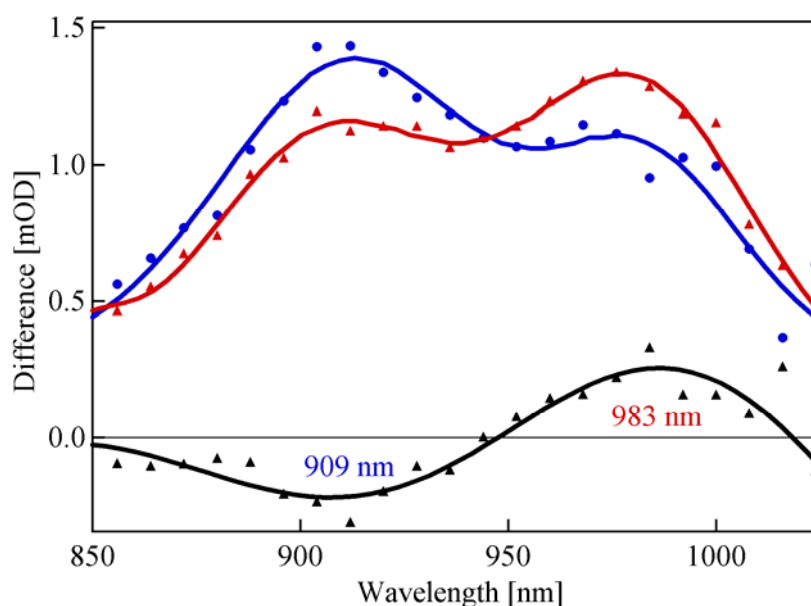


Fig. 4.12. Difference transient absorption spectra between R2P2CI and PP revealing all $\text{Car}^{\bullet+}$ in LHC II-Vio (circles) and LHC II-Zea (triangles). The solid line corresponds to Gaussian fits of the data points. The difference between Zea and Vio LHC II (black triangles) and the respective Gaussian fits with extrema at 909 and 983 nm reflects the decrease in $\text{Vio}^{\bullet+}$ and the increase in $\text{Zea}^{\bullet+}$.

The transient difference spectra at 40 ps time delay obtained by this procedure for the LHC II-Vio and LHC II-Zea samples are presented in Figure 4.12. This is a sum of all carotenoid radical cations spectroscopically generated in LHC II (Fig. 4.2). A Gaussian fit of the difference TA spectrum Zea-Vio results in a negative contribution at 909 nm and a positive one at 983 nm. The energy gap between them is 828 cm^{-1} or 0.10 eV, close to the energy gap of 0.12 eV between Vio^{•+} and Zea^{•+} found in solution. Recent voltammetric oxidation studies (142), reveal the energy difference between the oxidation potential of Vio and Zea (0.29 eV). Since I probe the $D_0 \rightarrow D_2$ transition, a comparison between electrochemical data and my values has to take the S_0-D_2 energy difference for Vio and Zea into account. A deviation of $\Delta E (S_0-D_2)$ should be responsible for the observed difference.

In comparison with the solution spectra, the absorption maxima of Car^{•+} in LHC II are generally red-shifted by about 80 nm.

4.6 Discussion

In the R2P2CI experiments a long-lived species with a TA signal in the near-IR region was observed for all four investigated carotenoids in ethanol. In previous experiments, transient $\text{Car}^{\bullet+}$ species were created by ionization, which vanish only after charge recombination, a process which occurs typically within ps to μs (143). Previously reported pump deplete probe (PDP) experiments on lycopene showed a persistent loss of excited-state population after re-excitation of the S_2 ESA at 795 nm (144). No product state was observed, and the re-pumped population disappeared, most probably deposited in a long-lived $\text{Car}^{\bullet+}$ state with no clear spectral signature in the probed region. Similarly, double-pump techniques have been applied to peridinin, where an 800 nm pulse was applied soon after carotenoid excitation. Thereby, a part of the S_2 population was transferred to a higher excited state obtaining a photoproduct state persisting on a nanosecond time scale, and attributed to peridinin cations based on their $\text{D}_0 \rightarrow \text{D}_2$ transition detected in the near-IR region (140). The R2P2CI experiments performed on carotenoids solubilized in ethanol show a similar transient species, which can unambiguously be assigned to $\text{Car}^{\bullet+}$, in agreement with previous measurements.

The evolution of the transient absorption bands of the $\text{Car}^{\bullet+}$ between 1 and 40 ps (Fig. 4.8) is in all cases dominated by a substantial narrowing of the ESA band and by a significant blue shift (e.g. from 885 nm to 830 nm for Vio in ethanol) of the absorption maximum. This is typical for cooling processes which are due to energy transfer from the $\text{Car}^{\bullet+}$ to the solvent (vibrational cooling).

As illustrated by my measurements of the various $\text{Car}^{\bullet+}$ species in ethanol (Fig. 4.10) and the quantum chemical calculations (88), the order of the excitation energies of the lowest strongly absorbing states in the near-IR region is $\text{Vio} > \text{Lut} > \text{Zea} > \beta\text{-Car}$. The decrease in excitation energies from Vio to Lut and Zea goes parallel with the increasing number of conjugated double bonds in agreement with a simple particle-in-a-box model. It is, however, astonishing that compared to $\text{Zea}^{\bullet+}$, $\beta\text{-Car}^{\bullet+}$ is red-shifted by 20 nm in ethanol and 5 nm in the quantum chemical calculations, respectively, since both contain eleven conjugated double bonds. The small energetic difference in the calculation disregarding any solvent effects can probably be attributed to the additional OH groups in Zea, which are the only major chemical difference, whereas all other geometrical parameters are essentially the same in the two compounds. In ethanol, the difference in the excitation energies is a factor of four larger than the quantum chemical calculation values, which could be due to a better stabilization of the excited state of Zea compared to the one of $\beta\text{-Car}$. In contrast to $\beta\text{-Car}$, Zea can form hydrogen bonds with ethanol via the additional OH groups, and the polar solvent may interact favorably with the local dipoles of the Zea hydroxyl groups. Preliminary calculations of the excited states of Zea bound to one ethanol molecule via a hydrogen bond indicate that the excited state increases in energy from 1.476 eV (840 nm) to 1.493 eV (829 nm). Similar explicit solvent effects can be expected to be responsible for the different shifts in the quantum chemical calculations and the experimental values obtained in ethanol when the other carotenoids are compared.

In general, $\text{Car}^{\bullet+}$ absorption strongly depends on the solvent as previous $\beta\text{-Car}$ studies illustrate. For example, $\beta\text{-Car}$ absorbs at 935 nm in acetonitrile (125), and 970 nm in dichloromethane (16). However, since the overall structure of the carotenoids is very similar, one can expect differences due to implicit solvent effects to be quite similar for different

species, while direct interactions like H-bond formation are more important to explain small differences between similar carotenoids. In summary, the general position of the absorption band is determined by the polarizability of the solvent and the number of conjugated double bonds of the carotenoid, while small differences in the absorption spectra of similar carotenoids of the same length are due to subtle differences in the molecular structure of different carotenoids as has been pointed out for Zea and β -Car.

One goal of the present work was to investigate and characterize possible carotenoid cations in LHC II and to understand their role in qE. Figure 4.12 presents the R2P2CI-PP difference spectra of LHC II-Vio and LHC II-Zea samples which correspond to sums of all different carotenoid cations spectroscopically generated in the R2P2CI experiment (Vio, Neo, Lut, Zea). For the analysis of Figure 4.12, variable contributions of the different carotenoids are anticipated according to their relative amount generated in the corresponding samples. The cation signal of Lut can thus be expected to be approximately three times larger than that of Vio in the LHC II-Vio sample (see pigment analysis in Fig. 4.2). On the other hand, the transiently populated S_2 states of the different carotenoids interact differently with the second pulse. For example, the S_2 population of Vio may have a larger spectral overlap with the second pulse, since its $S_2 \rightarrow S_N$ band is blue-shifted compared to that of Lut. Thus, assuming that the first pulse excites approximately the same amount of carotenoids, the amount of cation generation is strongly dependent on the second pulse. As a result, the correlation between the amount of neutral carotenoids and the amount of cations generated by means of R2P2CI is lost. Nevertheless, all these phenomena have influence only on the amplitude of the cation band and not on λ_{\max} . Therefore, subtraction of LHC II-Vio cations generated by R2P2CI from LHC II-Zea results in a cancellation of Neo and Lut cation contributions whose amounts are identical in Vio and Zea LHC II samples, and only a negative and a positive signal remains corresponding to the decrease of Vio and the increase of Zea cations.

Because of the difference in the amount of Zea and Vio bound to those samples, and the differences observed also in my TA measurements, I was able to attribute the transient spectral maximum at 909 nm to $\text{Vio}^{\bullet+}$ and at 983 nm to $\text{Zea}^{\bullet+}$. In LHC II the absorption bands of the cations are shifted to lower energies compared to ethanol which is a result of interactions with the protein environment in LHC II. The observed shift of the carotenoid radical absorption band in LHC II toward lower energies from Vio to Zea is similar to their shift in solution and to corresponding quantum chemical calculations. This is also in agreement with earlier measurements on photosystem II core complex mutants from *Synechocystis* sp. PCC 6803, where upon replacement of the natural β -carotene (11 C=C) by β -zeacarotene (β -Zea) (9 C=C), a blue shift for the corresponding carotenoid cations from 984 nm (β -Car $^{\bullet+}$) to 898 nm (β -Zea $^{\bullet+}$) has been observed (145).

The energy difference between the allowed excited states in the near-IR of $\text{Vio}^{\bullet+}$ and $\text{Zea}^{\bullet+}$ is $\sim 1370 \text{ cm}^{-1}$ or 0.17 eV according to the quantum chemical calculations, but only $\sim 937 \text{ cm}^{-1}$ or 0.12 eV according to the solution measurements, and in LHC II it is only 828 cm^{-1} or 0.10 eV. Obviously, as already pointed out for the solution studies, also the LHC II protein environment has different effects on different carotenoids (122). Zea has a similar overall molecular structure as Vio, except that it lacks the epoxy groups at either end and that the terminal β -ionone rings are less twisted.

Our measurements on the LHC II samples do not directly reveal the position of Lut^{•+} absorption, but according to the energetic order from the solution measurements and taking into account the red shift caused by protein binding, one can estimate the location of the Lut^{•+} absorption to be at ~960 nm, and the one of β -Car^{•+} to be around 1000 nm. Previous studies on spinach photosystem II membranes found the β -Car^{•+} λ_{max} at 996 nm (123).

4.6.1 Location and Mechanism of qE.

Our TA measurements on LHC II-Vio and LHC II-Zea samples indicate that simple replacement of Vio by Zea in LHC II is not sufficient for chlorophyll fluorescence quenching. Furthermore, I found in the R2P2CI measurements the position of the Zea cation in LHC II at 983 nm which is about 20 nm blue shifted compared to the carotenoid cation which was previously identified during qE (15).

Zea, and in smaller amount, Lut affect the rate of qE induction and the net amount of quenching. Overexpressing of PsbS in *Arabidopsis thaliana* mutants leads to an increase of the qE level compared to WT (146, 147). Steady state absorption experiments performed under qE state on leaf and intact thylakoid membranes indicate that zeaxanthin undergoes a dramatic spectroscopic change during qE, i.e a rise of a 535 nm band in the difference spectrum was ascribed to a red shift of the Zea (117), whereas leaf, deficient in Zea have a maximum positioned around 525 nm (147), which may be related to the 535 nm absorption change but induced by other xanthophylls such as lutein or neoxanthin. The amplitude of the absorption change was enhanced in PsbS overexpressing plants (147). Moreover, binding Zea to PsbS *in vitro* gave rise to a strong red shift in the absorption spectrum, evidence that the 535 nm absorption change is correlated with qE (114).

Another hint for the connection between Zea, PsbS and ΔA_{535} is given by the experiments performed by Ma *et al.* where after selective excitation of Chl, TA kinetics have been measured on thylakoid membranes of different *Arabidopsis* mutants under low light conditions and under maximal qE (148). The experiments, during maximal qE, reveal a decay component with 11 ps correlated with the presence of Zea and PsbS attributed to the $S_1 \rightarrow S_N$ transition as an effect of EET Chl \rightarrow Car. However, the TA kinetics during maximal qE exhibits a lower amplitude compared with the unquenched state, thus most likely due to a bleach and not an ESA. Taking into account the formation of a red shifted Zea during qE, and the fact that the TA signal shows a lower amplitude during the quenching state, it is more likely that TA kinetic differences observed are due to the bleach of the red-shifted Zea, present only under quenching conditions.

As pointed out in the introduction, it is proposed that upon qE induction the PsbS monomers associated with the LHC antenna are responsible for *in vivo* energy dissipation (118-120). Thus, if Zea indeed binds to the same site as Vio in LHC II, one Zea OH group would be buried, but the other one would be exposed to the hydrophobic membrane environment (Fig. 4.13). If one still wants to retain the model which proposes Zea bound to LHC II as the quenching site, one possible scenario to complete this model is a PsbS-LHC II complex, which may provide a highly polar environment that strongly affects the photophysical properties of Zea during qE induction. As a result, Chl excitation energy can be quenched.

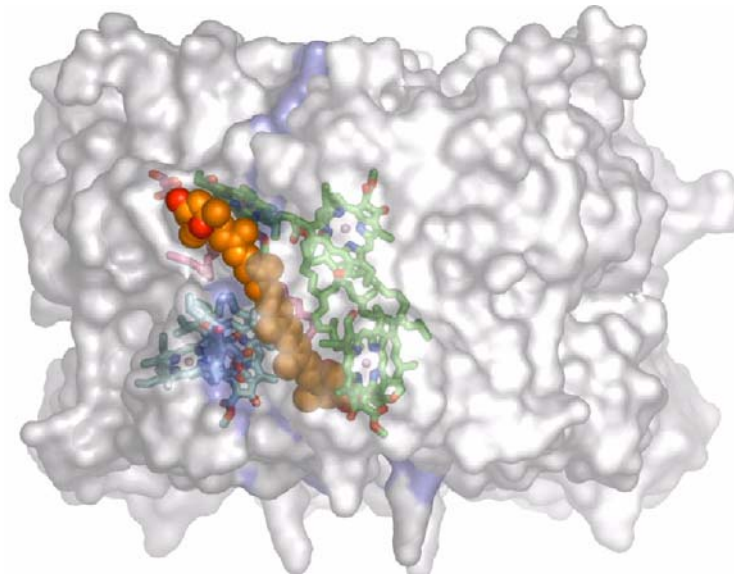


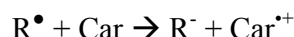
Fig. 4.13. Location of violaxanthin at the interface between two monomers of the trimeric LHC II protein.

As a next step, I plan to perform R2P2CI experiments on LHC II in the presence of PsbS to study whether a LHC II/PsbS complex leads to a $Zea^{\bullet+}$ signal at the same wavelength (1000 nm) as the one found during qE. This might confirm my proposed qE mechanism, and would finally identify the location of qE in the photosynthetic apparatus of green plants.

5 Carotenoid Radical Cation Properties

5.1 Introduction

Carotenoids (Car) fulfill important functions in light harvesting and photo-protection and are well-known as antioxidants. As photo-protective pigments, they scavenge dangerous singlet oxygen molecules and quench both singlet and triplet states of electronically excited chlorophylls (Chls) (4, 149-152). The fundamental molecular processes underlying these functions are energy and electron transfer between Cars and Chls (19, 153). In addition, Cars are recognized to play important roles as potent scavengers of free radicals preventing human diseases, such as atherosclerosis and cataracts, that are believed to be initiated by free radicals (154). The mechanism of the reaction is given by:



While β -carotene (β -Car) is a very important protective agent in almost all living organisms, the most important function of zeaxanthin and lutein (Lut) is protection of the retina against photo-oxidation. The retina is the only organ in the body which is continually exposed to high levels of focused radiation and which is in a highly oxygenated environment. This combination of light and oxygen, together with the presence of photosensitizers, provides the basis for oxygen free radical and singlet oxygen generation. Lutein and zeaxanthin play particularly efficient roles in scavenging these free radicals and in dissipating excess energy off the retina via generation of carotenoid radical cations (Car^{•+}) (155). Therefore, detailed knowledge of the optical and kinetic properties of the Car^{•+} and, in particular, of their excited electronic states is essential to achieve a detailed understanding of these processes.

One of the central functions of Cars, extensively studied yet poorly understood at the molecular level, is the quenching of Chl singlet excited states in photosynthetic systems under high-light conditions, when the harvested energy exceeds the turnover capacity of the reaction center (4, 6, 103). It has been observed that photosynthetic systems can adapt to high levels of light by switching to specific states (6), which safely dissipate excess energy as heat. In green plants, for example, this process is known as non-photochemical quenching (NPQ). Recently, the so-called energy-dependent quenching component qE of NPQ has been in the focus of photosynthesis research (15, 88, 122, 156-161). At present, neither the exact location of qE nor the detailed molecular mechanism are known and are thus a matter of ongoing debate (15, 107, 122, 160, 161). Based on recent quantum chemical calculations and elaborate time-resolved spectroscopic experiments, an NPQ mechanism has been proposed, in which Car^{•+} formation is the terminal quenching step via electron transfer from Car to Chl (15, 112). Along this line of research, Car^{•+} have recently been observed in several photosynthetic pigment protein complexes, including bacterial light-harvesting complexes (LHC) LH2 (127, 162), and isolated plant LHCs supporting the above described mechanism of qE (88, 157, 161).

Nevertheless, only little is known about the optical properties of the Car^{•+}, the energetic positions of their excited states and their interaction with neighboring photosynthetic pigments. Hence, a detailed knowledge of the excited state properties of Car^{•+} would not only present a step forward in understanding natural photosynthetic processes but also in studying and designing artificial photosynthetic systems (163-165). In artificial systems the key step is efficient photo-induced electron transfer eventually producing a final charge-separated state. Cars are excellent candidates for the design of such artificial systems due to their low ionization potential, which makes them excellent electron donors (123, 166).

In this chapter I present experimental investigations of the excited state properties of Lut and β -Car radical cations by means of time-resolved transient absorption (TA) spectroscopy. As a first step static absorption spectra are recorded and their dependence on the solvent properties is discussed. Most importantly, the pump-probe experiments reveal the existence of a new low-lying excited state in Car^{•+}, which is corroborated by quantum chemical calculations. Based on these findings, a simple mechanism for quenching of Chl excited states is proposed, which has important implications for NPQ in photosynthetic organisms.

5.2 Materials and Methods

Sample Preparation. Lutein and β -carotene were purchased from Sigma and stored at -20°C . Chloroform, acetonitrile and CS_2 were also purchased from Sigma. To obtain the desired cation concentration and to avoid formation of carotenoid dications equal amounts of 0.5 M FeCl_3 were added to 1 M Car. For the time resolved experiments, the typical sample OD was 0.6/mm at 935 nm. Sample stability was confirmed by measuring the absorption spectra before and after the time resolved measurements. The samples were prepared under an argon atmosphere to prevent reaction with oxygen. Nevertheless, a decrease of 10% of the cation band between the spectrum before and after the ultrafast measurements was observed.

Time-resolved and Steady-state Absorption Spectroscopy. Absorption spectra of the Car^{•+} were recorded at room temperature using a Jena-Specord S100 photodiode array spectrometer for measurements up to 1020 nm, and a Jasco V 670 spectrometer to cover the spectral range above 1000 nm.

The chemically generated carotenoid radical cations were excited by pulses generated using a noncollinear optical parametric amplifier (NOPA) with the output tuned to 935 nm for which the maximum excitation energy was kept at 30 nJ. For the 4 pulse experiment, the amplified pulses were divided into four parts: three pump pulses and one probe pulse. The first excitation pulses were generated using the NOPA. The maximum excitation energy was kept at 60 nJ and de central wavelength at 490 nm. For the second pulse used for the R2P2CI experiment the direct output from the amplifier with a pulse energy of 200 nJ was used. While for the third pump pulse, the second harmonic generation (SHG) of the CPA (388 nm) with a pulse energy of 30 nJ was chosen. For the probe pulses a white light continuum was generated by focusing amplified 775 nm light into a 5 mm sapphire window. To select the spectral region of interest in the near-IR, a RG 830 filter was used. Femtosecond time delays between pump and probe were controlled by a translation stage covering delay times up to 1.5 ns. To minimize accumulation of photoproducts, the sample was translated continuously both horizontally and vertically in a direction normal to the bisector of the pump and probe beams at ~ 10 cm/s.

5.3 Results and Discussion

5.3.1 Optical Properties of Lutein and β -Carotene Radical Cations.

Generation and detection of Car^{•+} can be achieved by several optical methods both in solution and directly in the protein environment. Typically, photo-ionization techniques exploit one-photon excitation into higher auto-ionizing Car excited states (167-169), however, Car^{•+} generation employing two-photon ionization has recently been reported (88). Two photons of lower energy have the great advantage that experiments can be performed in the natural biological environment without large perturbation of the natural situation. Nevertheless, all these methods only lead to short-lived populations of Car^{•+} species, which decay within microseconds to milliseconds due to charge recombination. In contrast, chemical oxidation is an attractive and simple method to generate long-lived Car^{•+} molecules (16, 125), which are stable for hours and decay essentially only by reaction with O₂. Pump-probe spectroscopy can then be easily applied to study excited state dynamics. The oxidizing agent used in this work is ferric chloride (FeCl₃), which reacts with the neutral Car and leads to the formation of the Car^{•+}.



The formation of Car^{•+} was initiated by addition of an FeCl₃ solution to the Car solution and was monitored by changes in the absorption spectrum of the Car and its radical cation (Fig. 5.1).

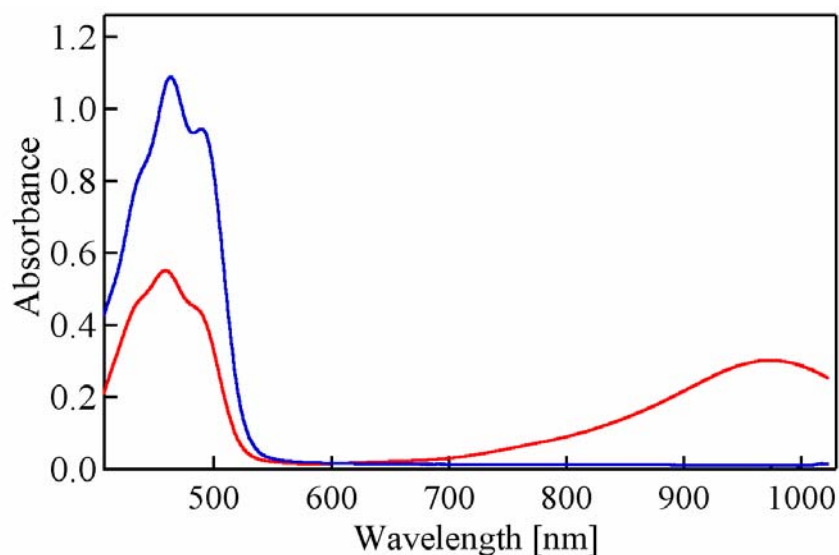


Fig. 5.1. Optical absorption of the neutral β -carotene (blue line) and β -carotene radical cation (red line) recorded upon addition of 0.5 M equivalent of FeCl₃ in chloroform.

When equal amounts of 0.5 M FeCl₃ were added to a 1 M β -Car donor solution, the concentration of the neutral compound decreased by a factor of two which is seen as a decrease of the intensity of the S₀→S₂ transition of the neutral Car at $\lambda_{\text{max}} = 463$ nm. At the same time, an absorption signal emerged at $\lambda_{\text{max}} = 975$ nm which is attributed to the formation of Car^{•+}.

Following this protocol, room temperature absorption spectra of β -Car^{•+} were measured in solvents with decreasing polarity, as defined by the dielectric constant ϵ , and with increasing polarizability α (acetonitrile ($\epsilon=37.5$, $\alpha=4.48$ Å³), chloroform ($\epsilon=4.8$, $\alpha=8.2$ Å³) and CS₂ ($\epsilon=2.6$, $\alpha=8.74$ Å³)) and are displayed in the inset of Figure 5.2.

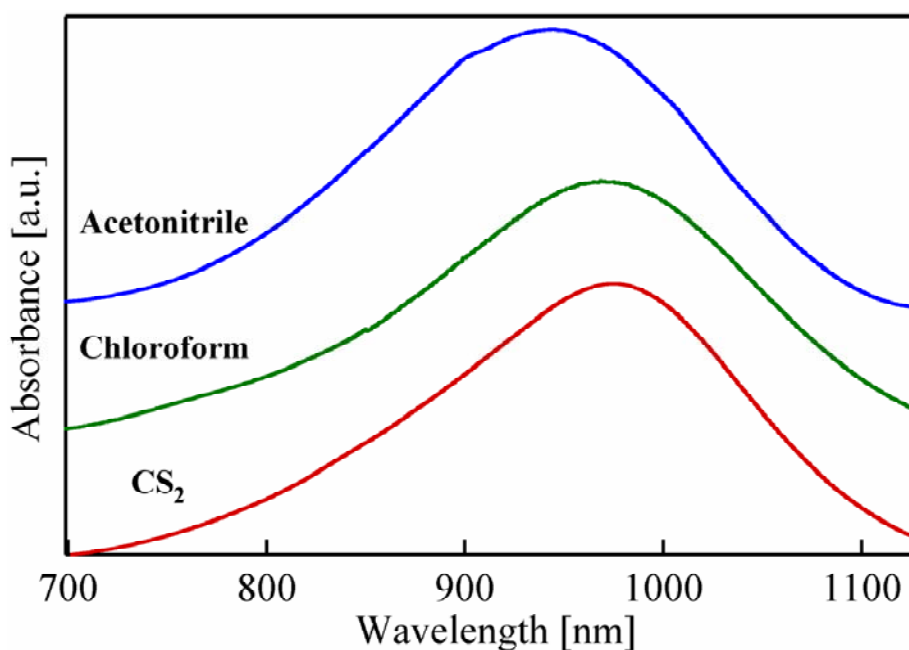


Fig. 5.2. Optical absorption of β -carotene radical cation in different solutions: acetonitrile, chloroform and CS₂.

The spectra were taken immediately after adding the FeCl₃ solution. To facilitate the comparison, the Car^{•+} spectra have been normalized to the same absorbance value at the wavelength of maximum absorption. It is apparent that the absorption band of the β -Car^{•+} exhibits a significant spectral shift: its λ_{max} value shifts to lower energy, i.e. longer excitation wavelengths, with decreasing polarity and increasing polarizability of the solvent. In detail, the band shifts by about 35 nm from acetonitrile to CS₂, reflecting the carotenoid-solvent interaction (Fig. 5.2). The β -Car^{•+} bands have maxima located at 940 nm in acetonitrile, 970 nm in chloroform, and 975 nm in CS₂. Previous measurements revealed that the β -Car^{•+} has its absorption maximum at 920 nm in ethanol (88), at 935 nm in acetonitrile (125), at 970 nm in dichloromethane (16) and at about 1000 nm in PS II (145). Although it is in principle difficult to distinguish between the influence of the polarity and polarizability of the solvent, it appears that the polarizability of the solvent is the relevant quantity determining the spectral shift. The trend of the observed shifts can be described better by using the trend of

the polarizabilities than by the dielectric constants. Also in previous studies, the modulation of the spectral shift of the Car^{•+} absorption band has been assigned to the polarizability of the solvent (170).

Comparison of the maximum absorption wavelengths of Lut^{•+} and β -Car^{•+} in chloroform reveals a shift of the absorption band towards lower energies from Lut^{•+} (927 nm) to β -Car^{•+} (970 nm) (Fig. 5.3).

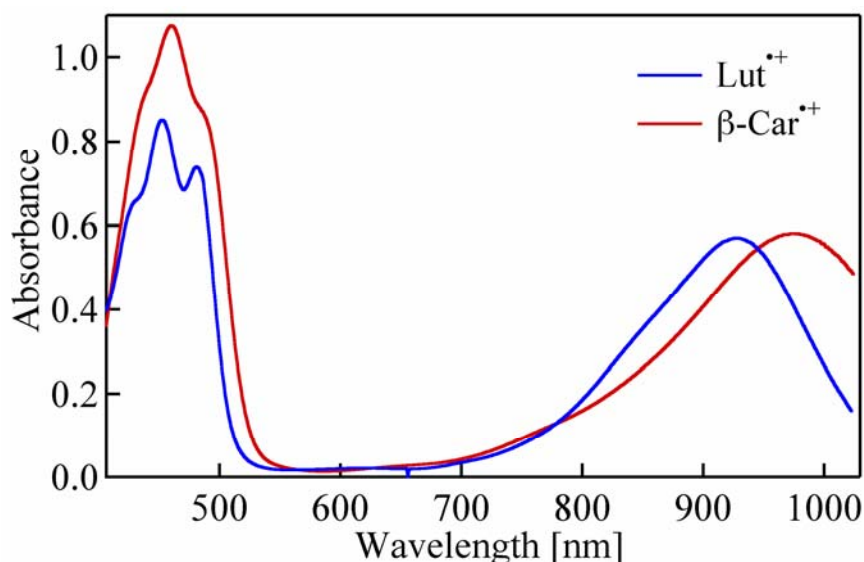


Fig. 5.3. Optical absorption of lutein (blue line) and β -carotene (red line) radical cations recorded upon addition of 0.5 M equivalent of FeCl₃ in chloroform.

This shift is well-known to occur due to the difference in conjugation length of the carotenoids, and is thus a direct consequence of the shorter conjugated chain length of Lut compared with β -Car, which is in nice agreement with previous reports (88, 171).

In summary, the wavelength of the Car^{•+} absorption band in the near-IR region is most notably influenced by the polarizability of the solvent and the number of conjugated double bonds of the Car. When the conjugation length of a Car is known, it may serve as a sensor for the polarizability of the environment.

5.3.2 Excited State Dynamics of Carotenoid Radical Cations.

To investigate the properties and in particular the lifetimes of the low-lying excited states of the radical cations of Lut and β -Car, TA spectra were measured using a high intensity pump pulse centered at 935 nm, and a broadband white-light probe pulse which spans two spectral regions (400-700 nm and 800-1100 nm). TA spectra of Lut^{•+} and β -Car^{•+} were recorded in chloroform upon excitation into the strongly one-photon allowed state absorbing around 950 nm. In previous works, this state is commonly referred to as D₂ excited state (16, 123, 140, 172), in analogy to the S₂ state of neutral Cars. The results will, however, reveal later that

for Lut^{•+} and β -Car^{•+} this state corresponds to the third lowest excited state of the Car^{•+} and will thus be denoted as D₃ in the following.

There are three distinct regions observed in the time-resolved TA spectra (Fig. 5.4): the ground state bleach around 950 nm stemming from the depopulation of the ground state by the initial pump pulse, and two excited-state absorption (ESA) bands, one in the visible region around 570 nm and one above 1000 nm.

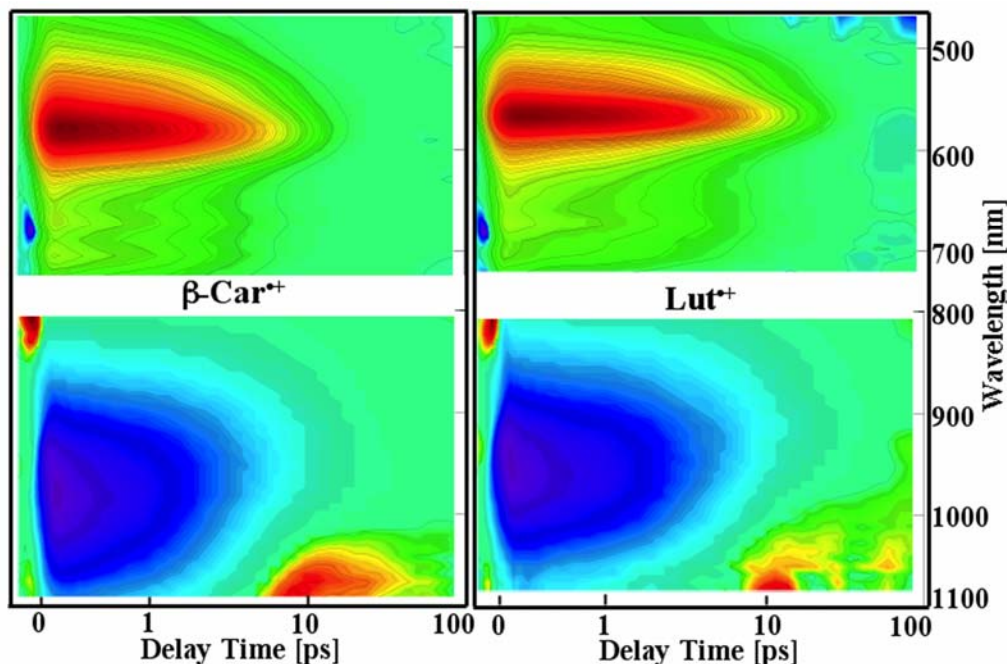


Fig. 5.4. 2D plot of the transient absorption data of lutein and β -carotene radical cations upon excitation at 935 nm.

In analogy to the steady state spectra shown in Figure 5.3, where the absorption bands of Car^{•+} shift to longer wavelengths with increasing number of conjugated double bonds, the main positive absorption band in the time-resolved spectra shown in Figure 5.4 also shifts to lower energies from 566 nm for Lut^{•+} to 582 nm for β -Car^{•+}. Similarly, the weaker ESA in the near-IR region also shows a red-shift of 16 nm from Lut^{•+} (1040 nm) to β -Car^{•+} (1056 nm). Previous analogous experiments on neutral Cars have revealed similar red-shifts for the dominating ESA bands corresponding to the S₁→S_N transition with increasing conjugation length of xanthophyll Cars (173, 174).

To explore in more detail the photo-initiated processes, i.e. the lifetime and decay pathways of the initial excited state population, the temporal evolution of the absorption spectrum was analyzed at the maximum of the ESA bands and at the minimum of the ground state bleach (Fig. 5.5).

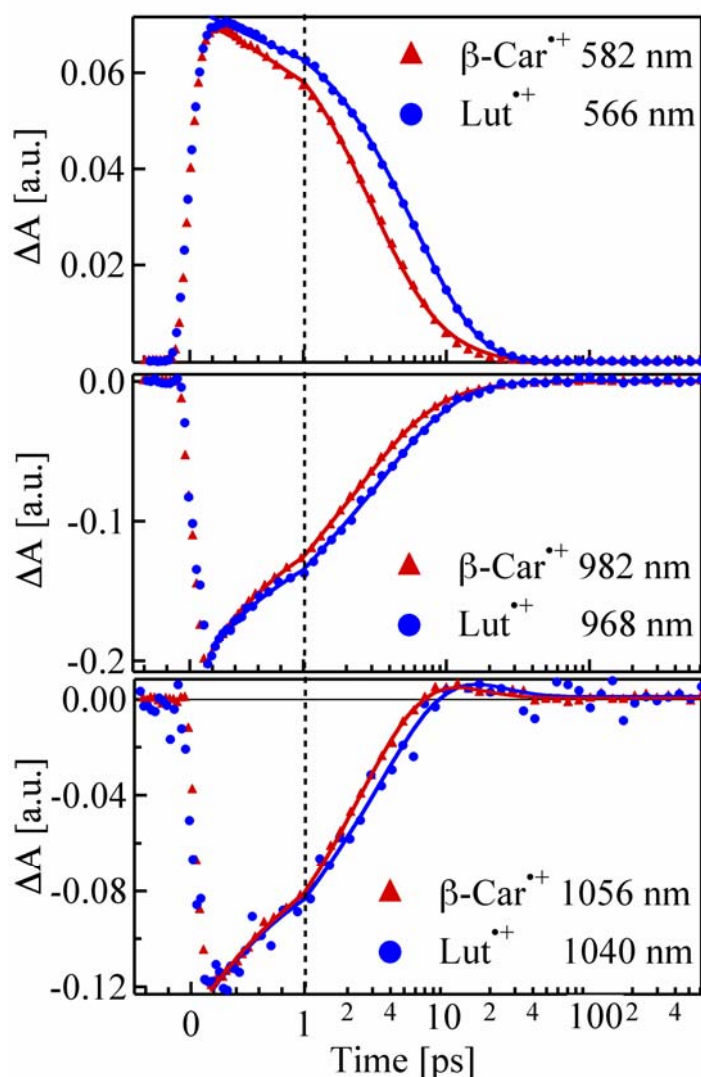


Fig. 5.5. Transient absorption kinetic traces of lutein (circles) and β -carotene (triangles) radical cations probed at the $D_2 \rightarrow D_M$ ESA maxima (top panel), at the ground state bleach minima (middle panel), and at the $D_1 \rightarrow D_N$ ESA maxima (bottom panel) after excitation to 935 nm.

The corresponding kinetic traces measured at 568 nm ($\text{Lut}^{\bullet+}$) and 582 nm ($\beta\text{-Car}^{\bullet+}$) are displayed in Figure 5.5 (top). They contain large positive signals which appear within the first 200 fs and decay exponentially in two steps. The lifetime of $\beta\text{-Car}^{\bullet+}$ is shorter than the one of $\text{Lut}^{\bullet+}$, which might be related to the number of conjugated double bonds. The second kinetic traces shown in Figure 5.5 (middle) were selected at the minima of the ground state bleach signals, i.e. at 968 nm for $\text{Lut}^{\bullet+}$ and 992 nm for $\beta\text{-Car}^{\bullet+}$ and both are dominated by large negative signals. The ground state recovery of $\beta\text{-Car}^{\bullet+}$ proceeds slightly faster than the one of $\text{Lut}^{\bullet+}$. For the last set of kinetic traces recorded 1040 nm ($\text{Lut}^{\bullet+}$) and 1056 nm

(β -Car^{•+}) (Fig. 5.5, bottom), a rapidly formed negative signal is observed, which decays within the first few picoseconds followed by a weak positive transient signal with a maximum at about 10 ps after excitation. Also in this spectral region, the excited state dynamics of β -Car^{•+} seems to proceed slightly faster than for Lut^{•+}.

The time-resolved TA spectra have been analyzed with a global exponential fit procedure. This allows me to relate the observed kinetics to individual excited state populations with distinct lifetimes and spectral features. Figure 4 shows the resulting amplitude spectra of the global exponential fit of the TA spectra of β -Car^{•+} and Lut^{•+}.

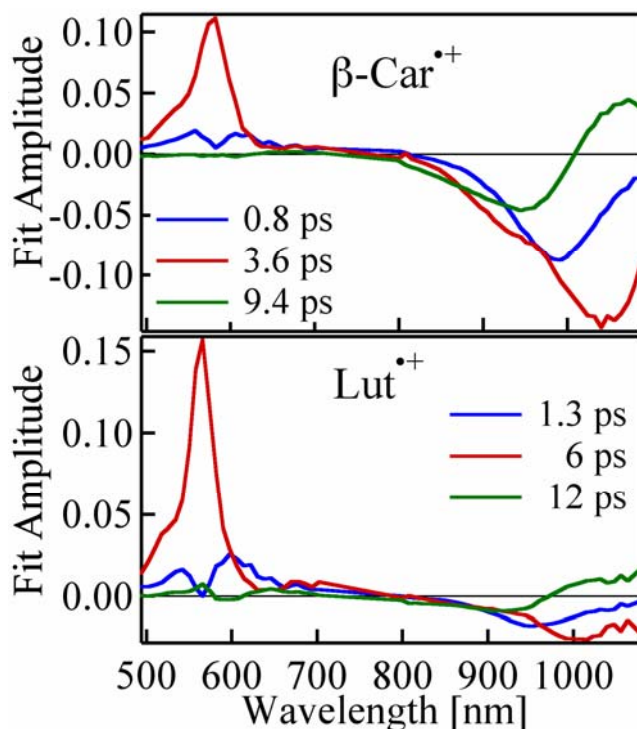


Fig. 5.6. Amplitude spectra represented by the global fit amplitude of β -carotene (top panel) and lutein (bottom panel) radical cations upon 935 nm excitation.

For both Car^{•+}, three components were necessary to obtain satisfactory fits. According to the fit, the experimentally observed excited state dynamics of the investigated Car^{•+} can be described with the following three kinetic components: 1) A fast component τ_1 with a time constant of 0.8 ps for β -Car^{•+} and 1.3 ps for Lut^{•+}, which has spectral features of Car^{•+} ground state bleach corresponding to negative absorption centred around 950 nm and which exhibits a positive amplitude due to ESA between 500 and 700 nm. These spectral shapes and lifetimes can be interpreted as an ultrafast radiationless transition from the initially populated excited state into an energetically lower lying excited state. 2) The second component τ_2 has the largest amplitude and possesses time constants of 3.6 ps for β -Car^{•+} and 6 ps for Lut^{•+}. The corresponding amplitude spectra show a strong ESA at 582 nm for β -Car^{•+} and 566 nm for Lut^{•+} together with a broad negative profile which spans the spectral range above 800 nm, red-shifted compared to the first component by about 50 nm. The negative amplitude of this

component can be interpreted as on the one hand ground state recovery, which will give negative contributions to the amplitude around 950 nm, and on the other as a growing ESA signal of some other new excited state above 1000 nm. Together these two contributions result in the broad negative band of the second component displayed in Figure 5.6. 3) The third kinetic component τ_3 has time constants of 9.4 and 12 ps for β -Car^{•+} and Lut^{•+}, respectively. The corresponding amplitude spectra are overall similar, although the amplitude of the Lut^{•+} spectrum is significantly smaller than the one of β -Car^{•+}. However, both amplitude spectra consist of a negative signal around 950 nm, a sign change and a positive band above 1000 nm. This shape is typical for ground state recovery stemming from the decay of the new additional excited state previously populated with time constant τ_2 .

In summary, the global fit analysis reveals three excited states to be involved in the observed excited state dynamics of β -Car^{•+} and Lut^{•+}. The initially excited state D_3 decays rapidly with a time-constant of about one picosecond into a lower lying state D_2 . The latter state possesses two possibilities to decay within about 5 ps: via transition to the ground state D_0 and or to a second low-lying excited state D_1 . Finally the D_1 state returns to the ground state with a time constant of about 10 ps. From the analysis of the experimental data it is clear that the investigated two Car^{•+} possess two excited states with different spectral properties and lifetimes below the well-known state absorbing in the near-IR region.

5.3.3 Nature of the Low Lying Excited States of Carotenoid Radical Cations.

Previous early calculations gave no evidence of the existence of two low-lying excited states below the well-known allowed excited state (172, 175). Only one forbidden D_1 and the well-known allowed state (D_2 at that time) were found. Based on a simple MO theory (172), these D_1 and D_2 states result from configuration mixing and are, respectively, the sum and difference of two singly-excited configurations corresponding to the nearly isoenergetic promotions of an electron from HOMO-1 to HOMO and from HOMO to HOMO+1. In the case of molecular cations the resulting states should give rise to a large intensity of the $D_0 \rightarrow D_2$ transition and the weakness of the $D_0 \rightarrow D_1$ transition due to summing up and cancellation of two components in the transition dipole moments. Theoretical studies on a series of polyene radical cations from butadiene to decapentaene (175), revealed the complex structure of D_1 and D_2 and predicted a next excited state above D_2 to be of ground state symmetry. Moreover, the trend observed in the calculations (175), indicates that this excited state could go lower in energy, below D_2 in radical cations of significantly longer polyenes, and in this respect this excited state can be an analogue of the low lying S_1 state in neutral polyene and carotenoids, which is invisible in single-photon absorption spectra. Indeed, the experiments presented here and the new quantum chemical calculations (176), clearly demonstrate the existence of two excited states below the strong allowed state in the Lut^{•+} and β -Car^{•+}. These quantum chemical calculations performed on the excited states of cation radicals of Lut and β -Car show that the three energetically lowest states of the Car^{•+} possess $\pi\pi^*$ character and have 2B_g (D_1, D_3) and 2A_u (D_2) pseudo-symmetry in C_{2h} (176). Since the electronic ground state also has 2A_u pseudo-symmetry, the D_2 state is one-photon forbidden, while D_1 has a small oscillator strength and D_3 is strongly allowed with a very large oscillator strength with excitation energies of 1.5 and 1.61 eV (176). Both β -Car^{•+} and Lut^{•+} possess two lower lying excited $\pi\pi^*$ states D_1 (2B_g) and D_2 (2A_u) at 0.90 and 0.95 eV and at 1.44 and

1.51 eV, respectively (176). In the case of β -Car^{•+}, the D₁ state has a small oscillator strength of 0.05 while the D₂ state is practically symmetry forbidden.

In comparison with the excitation energies of neutral Cars, the excited states of Car^{•+} are shifted to substantially lower energies resulting in much smaller excitation energies. The strong decrease of the excitation energy upon ionization results on one hand from the positive charge of the cations leading to a reduced HOMO-LUMO gap. On the other hand, removing one electron from the HOMO orbital of the neutral Car to generate the cation allows for a new additional excitation of an electron from the former HOMO-1 into the now singly-occupied former HOMO. This electronic transition exhibits a small excitation energy and since it mixes with all ²B_g symmetric states of the Car^{•+} and thus lowers their total energy, their excitation energies are particularly decreased.

Since the D₁ and D₂ states possess different spatial symmetry ²B_g and ²A_u, respectively, it is clear that the two experimentally observed ESA bands for D₂ and D₁ must stem from transitions to different excited states denoted here D_N and D_M (Fig. 5.7). Combining the experimental and theoretical data (176), for the excited states of the Car^{•+} one arrives finally at a kinetic model for the observed excited state dynamics upon excitation of the D₃ electronic state, which is displayed in Figure 5.7. It can be expected that this model is similar for all organic compounds with long chains of conjugated C=C bonds and in particular for all Cars, since the π -electrons determine their spectral features.

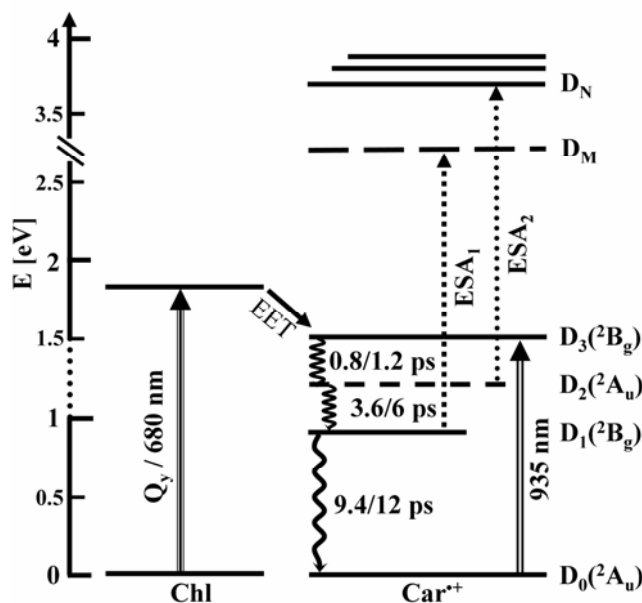


Fig. 5.7. Energy level diagram depicting relaxation processes that occur after photoexcitation of lutein/ β -carotene radical cations. Double arrow represents excitation of the D₃ state, dotted arrows corresponds to excited state transitions of D₁→D_M (ESA₁) and D₂→D_N (ESA₂), while wavy arrows denote intramolecular relaxation processes. The processes described in this study are labeled by their corresponding time constant. Excitation of chlorophylls into the first excited state (Q_y transition) leads to efficient excitation energy transfer (EET) to D₃ excited state. See the text for details.

5.3.4 Chlorophyll Excited State Quenching by Carotenoid Radical Cations - Implications for NPQ.

Recalling the previously proposed NPQ mechanism via electron transfer from a Car to Chl, the electron transfer and the formation of the Car^{•+} were suggested as final quenching step. In view of the findings presented here for the excited state properties of Car^{•+}, in particular their excitation energies and oscillator strengths, new possibilities for Chl fluorescence quenching during NPQ by Cars arise.

Through the formation of the cation, the excitation energies of the neutral Car drop drastically, and most importantly, the strongly allowed D₃ state of the Car^{•+} is clearly lower in energy than the Q_y state of Chl (Fig. 5.7). Thus the Car^{•+} itself can in principle act as terminal quencher of excess excitation energy (EET) via Förster energy transfer Q_y(Chl)→D₃(Car^{•+}). Moreover, this EET can be expected to be highly efficient due to the large transition dipole moment of the D₀→D₃ transition of the Cars^{•+}. Once arrived on the Car^{•+}, the excess excitation energy is rapidly dissipated according to the internal conversion pathway D₃→D₂→D₁→D₀ as identified in a combined experimental and theoretical study (176), (Fig. 5.7).

Thus, this appealingly simple mechanism is an obvious extension of the previously proposed scenario and can be summarized as follows. The first excitation is used to generate the Car^{•+} under NPQ conditions according to Holt *et al.* (15). The Car^{•+} has been shown to exist for about 150 ps. During its lifetime, however, the cation itself can efficiently act as quencher accepting excitation energy from neighboring excited Chls and dissipate it as heat within 10 ps. If the Car^{•+} is isolated or the excitation level is low, the effect is negligible but when the Car^{•+} is tightly coupled to the other pigment molecules, it acts as an energy sink and quenches excess excitation energy of the entire coupled unit. In light harvesting complexes the pigments are in fact tightly packed and strongly coupled, which ensures not only efficient light absorption per unit volume but also increases the ease of photo-protection.

So far, the proposed extension of the electron transfer mechanism is motivated by the findings for isolated Car^{•+}. It would be obvious and appealing to extend these results directly to light harvesting complexes, i.e. in the natural environment, however experimental verification was still required for this. Thus, I performed a pump probe experiment to study the excited state lifetime of Chls of light harvesting complexes in the presence of Car^{•+}. I performed a four pulses experiment in which, firstly carotenid radical cations were generated by means of R2P2CI (see Chapter 4) and, 40 ps after generation a pump-probe experiment is performed on plant LHC minors (Fig. 5.8). The results indicate a substantial drop of the Chl excited state lifetime when Car^{•+} are generated in light harvesting complexes of plants by resonant two-photon two-color ionization.

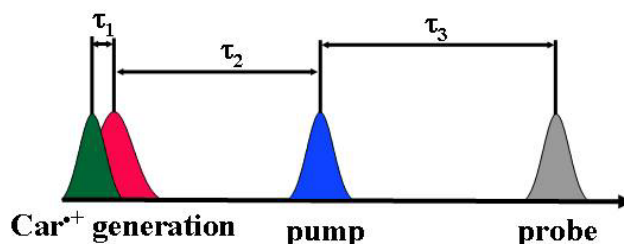


Fig. 5.8. Experimental approach for chlorophyll excited state quenching by carotenoid radical cations. First two pulses of 490 and 775 nm, separated by $\tau_1=50$ fs, leads to generation of carotenoid radical cations. The pump-probe experiment is performed upon chlorophyll excitation of 388 nm at $\tau_2=40$ ps, and probing the chlorophyll excited state dynamics by varying τ_3 .

The generation of carotenoid cation via R2P2CI accordingly to chapter 5 and (88) is shown in Figure 5.9. in detail.

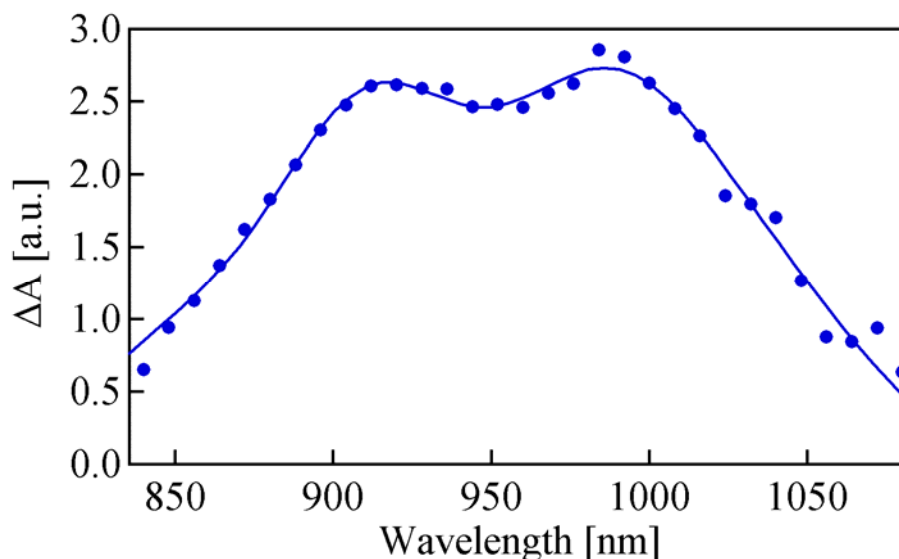


Fig. 5.9. Difference transient absorption spectra between R2P2CI and PP revealing all Car^{•+} in LHC minors, detected 40 ps upon generation. The solid line corresponds to Gaussian fits of the data points.

This represents the R2P2CI - PP difference spectra of LHC minors samples which correspond to sums of all different carotenoid cations spectroscopically generated in the R2P2CI experiment (violaxanthin, neoxanthin, and lutein). According to (88, 171), the peak around 910 nm will thus correspond to violaxanthin and neoxanthin, while the peak at 980 nm to lutein.

The quenching of the Chl excitation by carotenoid radical cations is clearly seen in Figure 5.10, which shows the kinetic trace probed at 900 nm (Chl *a* ESA) in the presence (triangles) or absence (squares) of carotenoid radical cations.

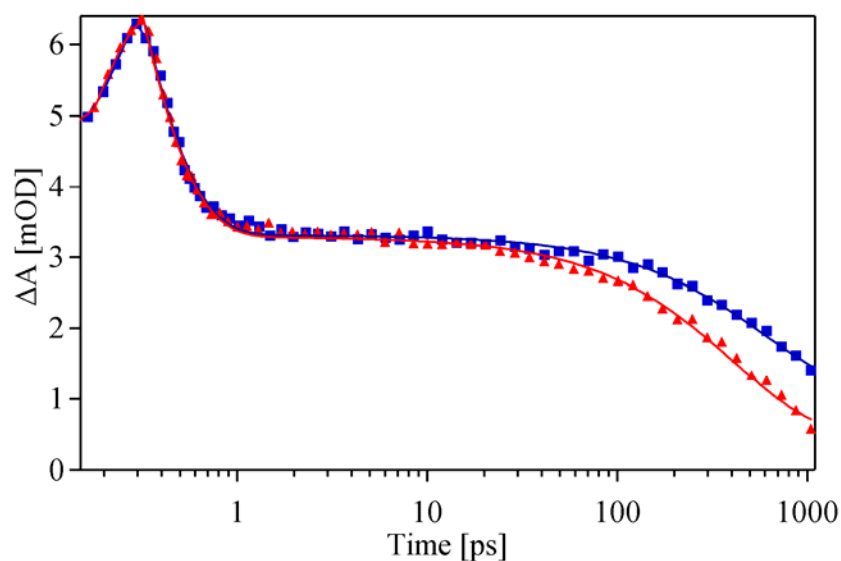


Fig 5.10. TA kinetic traces for LHC minors in the presence (triangles) or absence (squares) of carotenoid radical cations, detected at 900 nm upon excitation into Chl *soret* band at 388 nm. The solid lines correspond to the fit curve obtained by a global fitting routine.

The kinetic traces in Figure 5.10 show a fast rise and decay of a transient ESA for the delay times up to 300 fs, which is similar for both samples. This fast component can be attributed to carotenoid ESA ($S_2 \rightarrow S_N$ transition) due to energy transfer from the chlorophyll B_y excited state to the carotenoid S_2 excited state. The attribution is supported by its fast decay, which is characteristic for the carotenoid S_2 excited state (i.e. about 200 fs in light harvesting complexes). For longer delay times only chlorophyll ESA can be observed, since at this delay time, all excitation energy is already transferred to the chlorophylls.

In summary, by photo-induced generation of carotenoid radical cations in plant LHC minors a clearly decrease of the Chl excitation energy in the presence of Car^{•+} is observed.

General Conclusions. In this experimental investigation employing femtosecond TA spectroscopy, the excited states of the radical cations of Lut and β -Car and their properties have been investigated. The absorption wavelengths of the electronic excitations are demonstrated to depend on the polarizability of the solvent and on the number of conjugated double bonds of the Cars. Most importantly, this results undoubtedly reveal the existence of two low-lying excited states below the well-known excited state absorbing in the near-IR region. In analogy to neutral Cars possessing a strongly allowed S_2 state, this state has been denoted as D_2 state in Car^{•+}, but based on this study it is proposed to refer to it as D_3 in the future. The three energetically lowest states of the Car^{•+} possess $\pi\pi^*$ character and have 2B_g (D_1, D_3) and 2A_u (D_2) pseudo-symmetry in C_{2h} . Since the electronic ground state has also 2A_u pseudo-symmetry, the D_2 state is one-photon forbidden, while D_1 has a small oscillator strength and D_3 is strongly allowed with a very large oscillator strength. In comparison with the excitation energies of neutral Cars, the excited states of Car^{•+} are shifted to substantially lower energies resulting in much smaller excitation energies. The lifetimes of the excited states of the Car^{•+} are short and exhibit values of 1.3, 6 and 12 ps for the D_3, D_2 and D_1 states of Lut^{•+} and 0.8, 3.6 and 9.4 ps for the corresponding states of β -Car^{•+}. Similar to neutral Cars, the excited state lifetimes decrease with increasing number of the conjugated double bonds. These findings have important consequences for the ability to quench excited states of Chls via Förster energy transfer and thus for the role of Car^{•+} in NPQ. In view of this findings, Car^{•+} are most likely not generated via electron transfer from Car to Chl as final quenching product during NPQ, but instead are formed as active quenching site, since they can efficiently accept excitation energy from Chl due to the low excitation energy and large oscillator strength of their D_3 state. In addition Car^{•+} can rapidly dissipate the excitation energy within 15 ps.

6 Excited State Dynamics of Astaxanthin Radical Cation

6.1 Introduction

Among the xanthophylls, the astaxanthin molecule contains the longest conjugated, double-bond polyene chain, with both hydroxy and carbonyl functional groups present on the 6-membered rings at each end. This unique molecular structure gives it pronounced antioxidant capacity. The astaxanthin molecule is similar to the more familiar carotenoid molecule, β -carotene, but the small differences in structure such as the presence of two additional functional groups (keto and hydroxy) at each end (Fig. 6.1), confer large differences on the chemical and biological properties of the two molecules. The importance of the carotenoid structure in determining the antioxidant activity has been demonstrated in many studies. Contributions of various carotenoids to radical scavenging have been compared (177-181), and β -carotene was generally found to be less effective than those carotenoids that possess keto groups at the 4 and 4' positions in the β -ionone ring, such as cantaxanthin and astaxanthin.

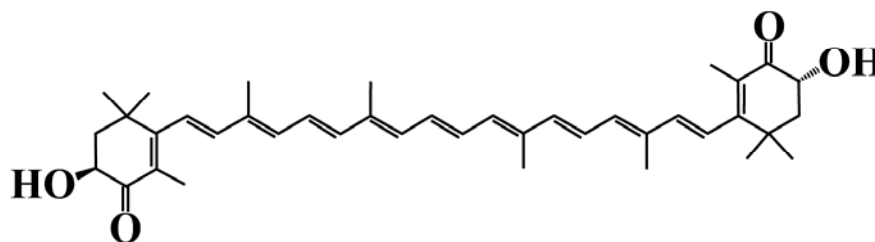


Fig. 6.1. Molecular structure of astaxanthin.

Carotenoids quench singlet as well as triplet states of electronically excited chlorophylls (4, 149-152). In addition, they effectively quench free radical species in liposomes (182), lipoproteins (183), membranes (184), cells (185), and animal models (186-189).

The absorption properties of astaxanthin and carotenoids are determined primarily by the extent of π -electron conjugation along their C_{40} carbon-carbon bond skeleton (190). They are further fine-tuned by the presence of functional groups, configurational and conformational twisting, the polarity and polarizability of the environment (191). The strong, visible light absorption by carotenoids is known to be due to the $S_0 \rightarrow S_2$ transition (191, 192). In contrast, the $S_0 \rightarrow S_1$ transition however is symmetry forbidden and typically extremely weak (193, 194). Despite numerous detailed spectroscopic investigations of many different carotenoid-containing pigment-protein complexes, the factors controlling the spectral features of protein-bound carotenoids are not well understood (19, 195, 196). For example, the absorption spectrum of astaxanthin is bathochromically shifted by about 150 nm in α -crustacyanin (195). The visible absorption spectrum of free astaxanthin has a $\lambda_{\max} = 472$ nm (in hexane) or 492 nm (in pyridine), while the visible absorption spectra of bound astaxanthin has a $\lambda_{\max} = 580$ -590 nm in the β -crustacyanins (i.e. a shift of 100 nm) or $\lambda_{\max} = 632$ nm in α -crustacyanin (197).

A further, even stronger shift of the absorption spectrum of astaxanthin is observed upon oxidation (141, 176). In chloroform the absorption maximum shifts from 480 nm in its neutral state to 870 nm upon oxidation. Moreover, the first excited state of the astaxanthin radical cation gains more oscillator strength.

In the previous chapter "Carotenoid Radical Cation Properties" I described experiments performed on β -carotene and lutein radical cations which revealed the existence of an additional excited state between the well-known excited states D_1 and D_3 (previously known as D_2) absorbing in the near-IR region (176). In this chapter I will present a comprehensive approach combining femtosecond time-resolved pump-probe and steady state absorption spectroscopy allowing me to unravel the excited state dynamics of the astaxanthin radical cation in solution. In the first step transient absorption measurements of neutral astaxanthin in chloroform are presented. Subsequently, the optical properties of the astaxanthin radical cation generated by resonant two-photon two-color ionization (see Chapter 4) and combined chemical oxidation, together with their dependency on solvent properties are discussed. Finally, a pump-probe absorption experiments are used to elucidate the excited state dynamics of the astaxanthin radical cation.

6.2 Materials and Methods

Sample Preparation. Astaxanthin was purchased from Sigma and stored at -20°C . Chloroform, acetonitrile and CS_2 were also purchased from Sigma and used without further purification. To obtain the desired cation concentration and to avoid formation of carotenoid dications 0.5 M FeCl_3 was added to 1 M astaxanthin. For the time resolved experiments, the typical sample OD was $0.6/\text{mm}$ at 890 nm . Sample stability was confirmed by measuring the absorption spectra before and after the time resolved measurements.

Steady State Absorption. Absorption spectra of the $\text{Car}^{\bullet+}$ were recorded at room temperature using a Jena-Specord S100 photodiode array spectrometer for measurements up to 1020 nm , and a Jasco V 670 spectrometer to cover the spectral range above 1000 nm .

Time Resolved Absorption Spectroscopy. Chemically generated astaxanthin radical cations were excited by pulses generated using a noncollinear optical parametric amplifier (NOPA) with the output tuned to 500 nm for the neutral astaxanthin and to 890 nm for its radical cation, while the maximum excitation energy was kept below 30 nJ to avoid photo-degradation. For the probe pulses a white light continuum was generated by focusing amplified 775 nm light into a 5 mm sapphire window. To select the spectral region of interest in the near-IR, a RG 830 filter was used. Femtosecond time delays between pump and probe were controlled by a translation stage covering delay times up to 1.5 ns . To minimize accumulation of photoproducts, the sample was translated continuously both horizontally and vertically in a direction normal to the bisector of the pump and probe beams at $\sim 10\text{ cm/s}$.

6.3 Results

6.3.1 Excited State Dynamics of Astaxanthin in Chloroform.

Figure 6.2 (right) shows the broad, featureless absorption spectrum of astaxanthin in chloroform. This absorption band with maximum at 470 nm is associated with the strongly allowed $S_0 \rightarrow S_2$ transition. Its broad spectral shape is a consequence of the loss of vibrational structure, unlike the other xanthophylls for which the absorption spectrum is well resolved (Fig. 6.2 left, 173).

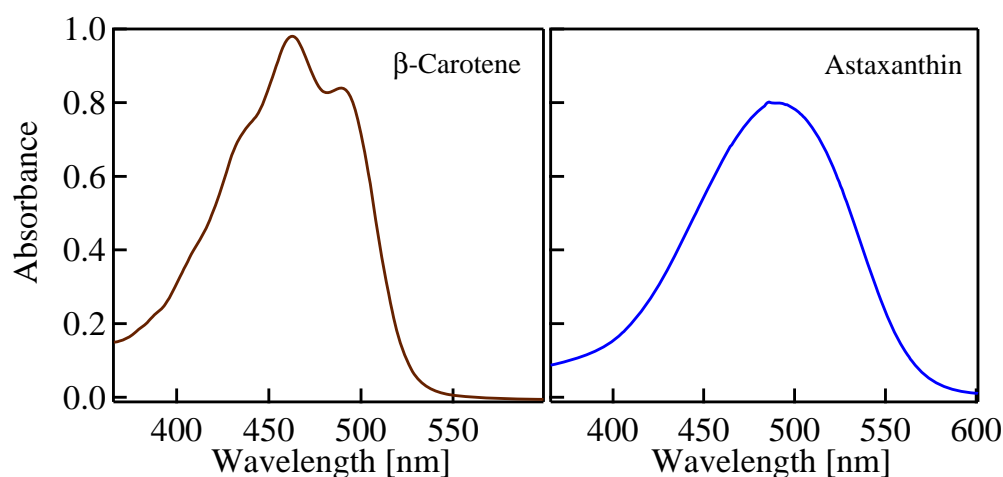


Fig. 6.2. Absorption spectrum of astaxanthin in chloroform.

Astaxanthin was excited with a pump pulse centred at 500 nm and the excited state dynamics was monitored by a broad white light probe pulse spanning the spectral range between 450 nm and 700 nm (Fig. 6.3).

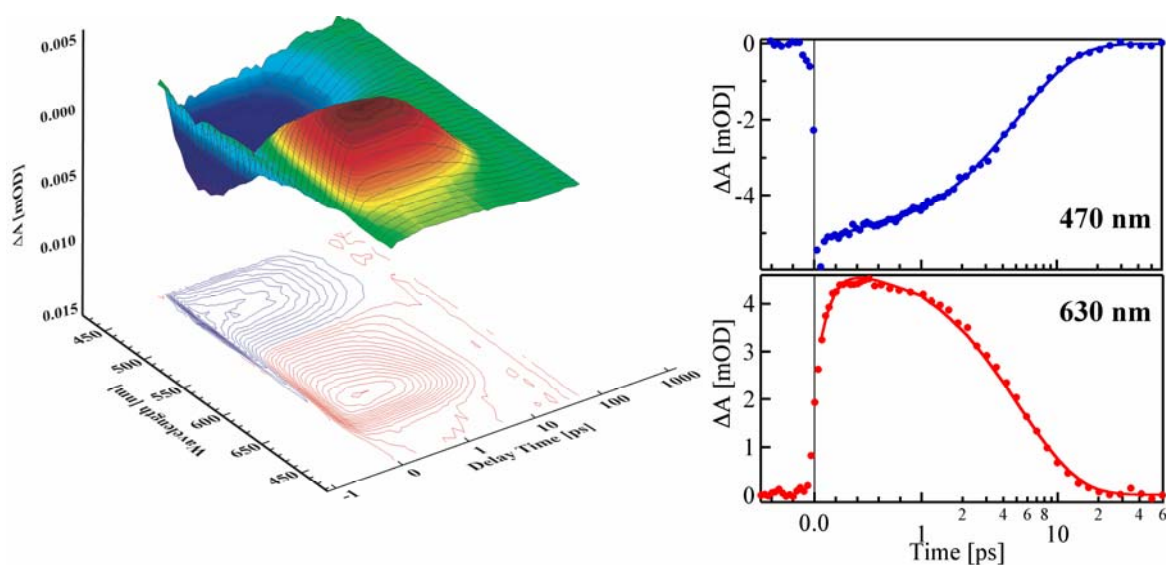


Fig. 6.3. Transient absorption spectra of astaxanthin in chloroform. 3D plot (left) and kinetic traces selected at the ground state bleach minimum (right top), and excited state absorption maximum (right bottom).

The transient spectra shows a broad ground state bleach in the 450-550 nm spectral region that corresponds to the disappearance of the $S_0 \rightarrow S_2$ absorption band upon excitation. Subsequently, a build up of an excited state absorption signal in the 550-700 nm region corresponding to the $S_1 \rightarrow S_N$ transition is observed (Fig. 6.3 left). The kinetic trace recorded at 470 nm displays the instantaneous bleach and the subsequent recovery of the ground state absorption that occurs upon excitation. The kinetic trace at 630 nm contains the rise and decay of the $S_1 \rightarrow S_N$ transient absorption, the delayed increase indicates the $S_2 \rightarrow S_1$ internal conversion.

The time resolved spectra were analyzed with a global fitting program which enables the observed kinetics to be related to the individual excited state populations with distinct lifetimes and spectral features. The result of the global fit analysis of the data is shown in Figure 6.4.

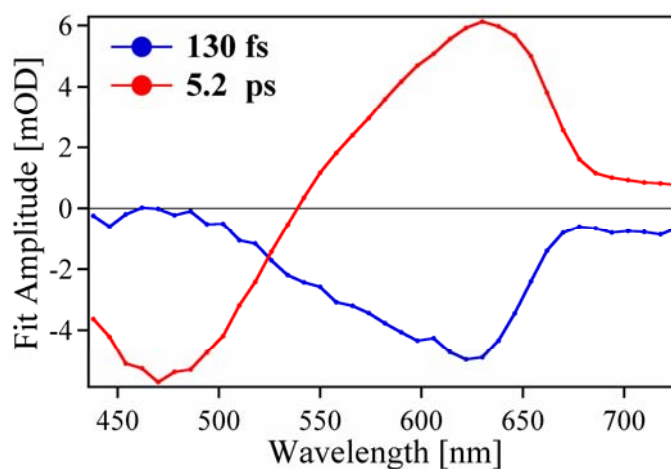


Fig. 6.4. Amplitude spectra represented by the global fit amplitude of astaxanthin upon 500 nm excitation.

Two components, with lifetimes of 130 fs and 5.2 ps, were sufficient to describe the time resolved data satisfactorily (Fig. 6.4). The first component, with a lifetime of 130 fs, contains stimulated emission from the pumped S_2 excited state and the build-up of the S_1 population. The second component represents exclusively the decay of the S_1 excited state, indicated by the positive signal above 550 nm, and the recovery of the ground state bleach, observed as a negative signal below 550 nm. The excited state dynamics of astaxanthin is well represented with a three energy-level diagram depicted in Figure 6.5 and can be summarized as follows: Upon excitation, the transiently populated S_2 excited state decays within 130 fs into the lower S_1 excited state which decays in 5.2 ps by internal conversion to the ground state.

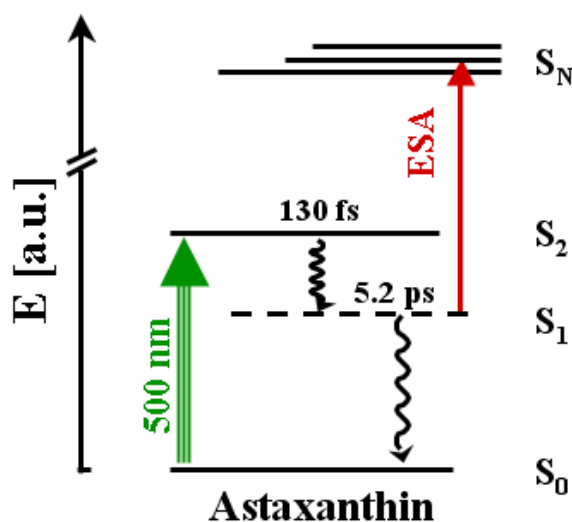


Fig. 6.5. Energy level diagram depicting relaxation processes that occur after photoexcitation of astaxanthin.

6.3.2 Optical Properties of the Astaxanthin Radical Cation.

Following the same procedure as described in Chapter 5, astaxanthin radical cations were produced by chemical oxidation, that is carotenoid radical cations were generated by addition of a 0.5 M FeCl_3 solution to a 1 M carotenoid solution. Figure 6.6 shows room temperature absorption spectra of astaxanthin radical cations measured in solvents with increasing polarity (acetone, chloroform, dichloromethane, and CS_2).

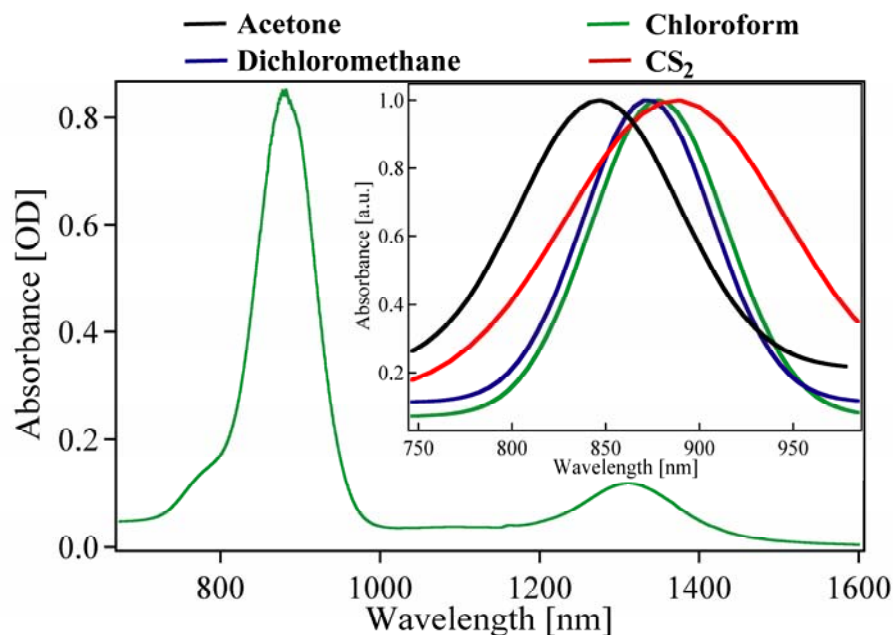


Fig. 6.6. Absorption spectra of the astaxanthin radical cation in different solvents: acetone, chloroform, dichloromethane and CS_2 .

The strong absorption of the radical cation with its maximum between 800 and 950 nm is due to the $D_0 \rightarrow D_3$ transition. A bathochromic shift of this transition is observed. The D_3 absorption shifted from 846.6 nm in acetone to 887.5 nm in CS_2 , a bathochromic shift corresponding to 545 cm^{-1} . The exact peak positions the D_3 bands for the different solvents are summarized in Table 6.1.

	$D_0 \rightarrow D_3$ maximum [nm]	
	Chemical Oxidation	R2P2CI
Acetone	846.6	852.1
Chloroform	872.5	875.6
Dichloromethane	878.1	870
CS_2	887.5	958.6

Table 6.1. Absorption maxima of the D_3 bands obtained by chemical oxidation or resonant two-photon two-color ionization (R2P2CI).

Another possibility to generate carotenoid radical cations is the two-photon two-color ionization technique described in chapter 5. Here, the first pump pulse is centered at 500 nm which excites astaxanthin to the S_2 state, while the second pulse (resonant with the $S_2 \rightarrow S_N$ transition) induces further excitation of the transiently populated S_2 state into higher electronically unbound excited states which decay by ionization forming the astaxanthin radical cation. Figure 6.7 shows transient absorption spectra of astaxanthin radical cations generated as mentioned above in solvents of increasing polarity (acetone, dichloromethane, chloroform and CS_2).

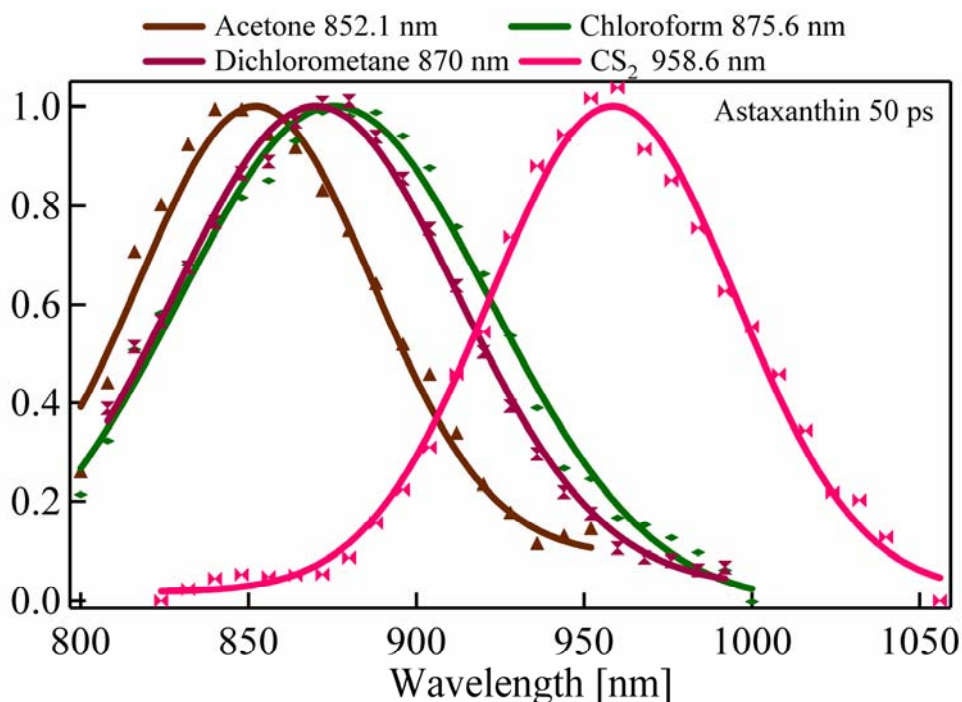


Fig. 6.7. Transient absorption spectra of astaxanthin radical cation recorded 55 ps after generation in acetone, dichloromethane, chloroform and CS_2 .

The spectra are taken at a delay time of 50 ps after the generation of the radical cations. For easy comparison, the cation spectra were normalized to the same maximum absorbance. Compared to the chemical oxidation spectra (Fig. 6.6), the astaxanthin radical cation shows a stronger solvent dependent spectral change in the R2P2CI measurements (Fig. 6.7). The λ_{max} shifts to lower energy upon decreasing polarity from acetone to CS_2 by about 106 nm for R2P2CI and only 41 nm by chemical oxidation. The absorption shifts of astaxanthin radical cations obtained by chemical oxidation and by R2P2CI are compared in Table 6.1.

6.3.3 Excited State Dynamics of the Astaxanthin Radical Cation.

To investigate the excited state dynamics of the astaxanthin radical cation time-resolved transient absorption measurements upon excitation of the $D_0 \rightarrow D_3$ transition at 890 nm is performed. Kinetic traces were measured over a broad spectral region for both visible as well as near-IR regions at a probing window from 400 to 1100 nm. The 2D plot of the transient absorption data for astaxanthin radical cation is shown in Figure 6.8, where two measurements are combined to probe the full spectral range.

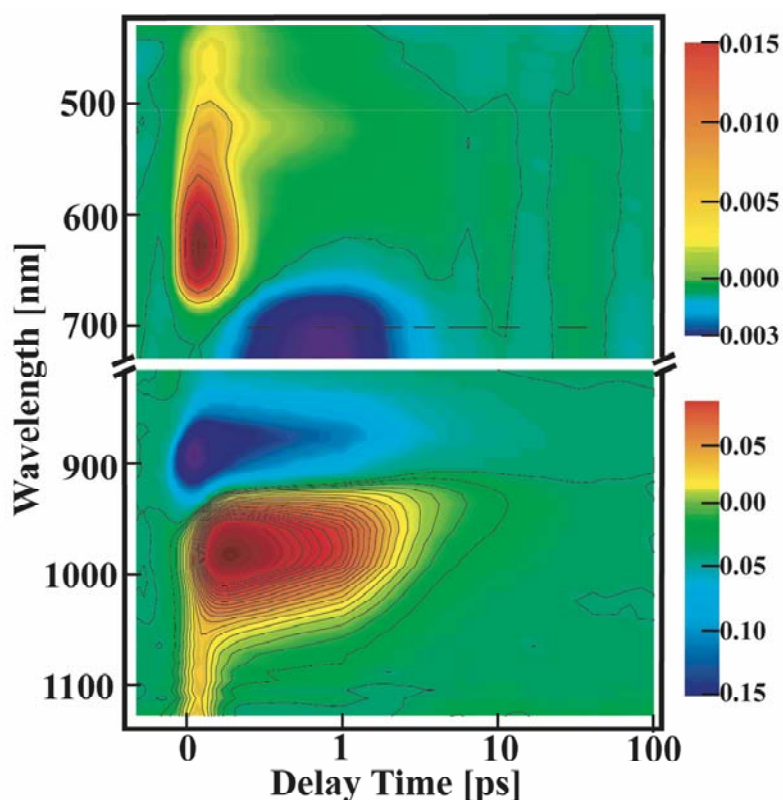


Fig. 6.8. 2D plot of transient absorption data for astaxanthin radical cation upon excitation at 890 nm.

There are several distinct regions with different temporal behavior observed in the time-resolved TA spectrum (Fig. 6.8). In the visible spectral region (upper panel), a weak ESA is observed around 510 nm (ESA_1) with picoseconds lifetime and an intense ESA around 630 nm (ESA_2) which has a short life-time of few hundreds of femtoseconds. Furthermore, a small negative contribution is also observed above 700 nm which continues in the nearIR spectral region (lower panel). Here, two major spectral features are resolved: the ground state bleach around 870 nm (GSB) and a strong ESA around 1000 nm, which has two components with different lifetimes: the long-lived ESA_3 on the short wavelength side, and the short-lived

ESA₄ on the long wavelength side. The nearIR spectral region also contains a broad but only short-lived ESA above 1050 nm (ESA₅).

For a more detailed picture of the photo-initiated processes, sections of the above mentioned ESA's and GSB are displayed in Figure 6.9.

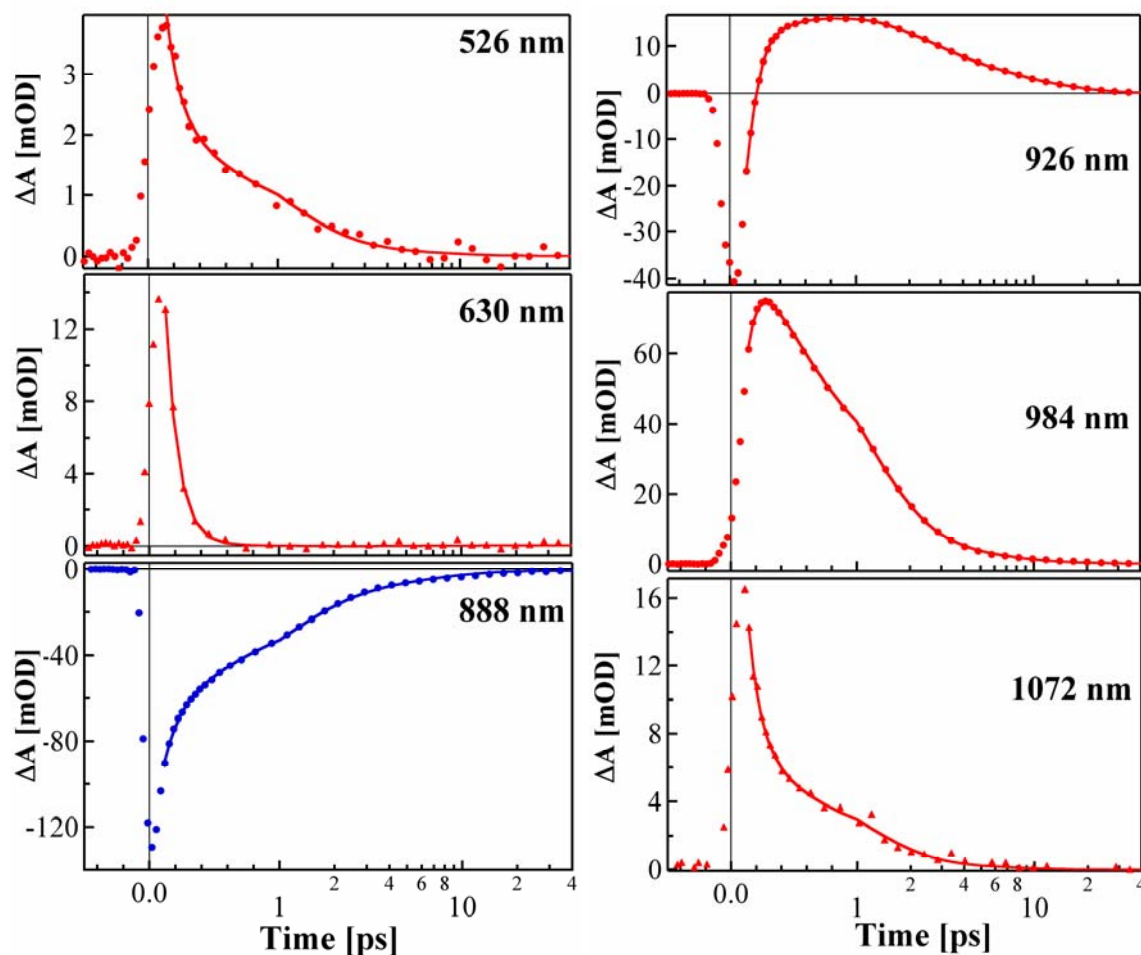


Fig. 6.9. Transient absorption kinetic traces of astaxanthin radical cation probed at the excited state absorption (ESA) maxima ESA₁, ESA₂, ESA₃, ESA₅ and at the ground state bleach (GSB) minimum after excitation at 890 nm.

The kinetic trace at 526 nm recorded at the maximum of ESA₁ contains a positive signal which appears within 100 fs and decays biexponentially. The fastest decay component is related to the more intense and broad ESA₂ shown in the 630 nm kinetic trace, while the longer component belongs exclusively to ESA₁. The ground state bleach recorded at 888 nm contains a negative signal which decays also biexponentially. Subsequently, the 984 nm transient shows the temporal evolution of ESA₃ comprising a positive signal which rises in the first 200 fs and decays within a few ps. Lastly, the 1072 nm kinetic trace illustrates the

exponential decay of ESA_5 , the fast component, and that of ESA_4 , the slower and weaker component.

To attribute the observed kinetics to individual excited state populations which have distinct lifetimes and spectral features, the time-resolved spectra have been analyzed with a global exponential fit procedure. Figure 6.10 shows the resulting amplitude of the astaxanthin radical cation.

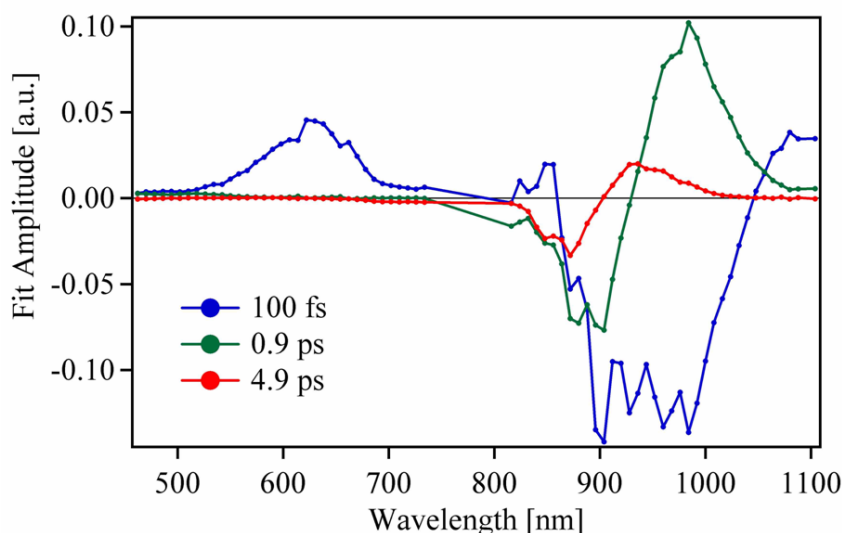


Fig. 6.10. Amplitude spectra represented by the global fit amplitude of astaxanthin radical cation upon 890 nm excitation.

Three components were necessary to satisfactorily fit the data. Based on the fit and according to the kinetic model discussed in the previous chapter, the experimentally observed excited state dynamics of the astaxanthin radical cation can be described by three kinetic components: i) A fast component τ_1 with a time constant of 100 fs which contains two positive amplitudes, one centred at 630 nm corresponding to ESA_2 and one above 1050 nm corresponding to ESA_4 . These two ESA contributions are transitions from the pumped excited state D_3 to higher excited states. The negative amplitude of the first component has the spectral features of the astaxanthin radical cation ground state bleach with negative absorption centred around 900 nm, while the negative amplitude around 980 nm represents an ultrafast radiationless transition from the initially populated excited state into the energetically lower lying excited state D_2 . ii) The second component τ_2 has the largest positive amplitude and possesses a time constant of 0.9 ps. The corresponding amplitude spectra show both a weak ESA at 510 nm (ESA_1) and a strong ESA at 980 nm (ESA_4). The negative amplitude of this component is slightly blue-shifted compared to the negative amplitude of the first component. iii) The third kinetic component τ_3 has a time constant 4.9 ps and possess a positive amplitude at 920 nm and a negative one at 870 nm. This shape is typical for ground state recovery stemming from the decay of the new additional excited state previously populated with time constant τ_2 .

In summary, the global fit analysis revealed three excited states which are involved in the observed excited state dynamics of the astaxanthin radical cation. The initial excited state D_3

decays rapidly with a time-constant of about 100 fs into a lower lying excited state D_2 . The latter state decays within about 0.9 ps to a second low-lying excited state D_1 . Finally the D_1 state returns to the ground state with a time constant of about 4.9 ps. From the analysis of the experimental data it is clear that the astaxanthin radical cation, similar to both the β -carotene and lutein radical cations, possesses two excited states with different spectral properties and lifetimes below the well-known state absorbing in the near-IR region.

6.4 Discussion

The absorption spectrum of carotenoids is caused by the strongly allowed $S_0 \rightarrow S_2$ transition and usually exhibits a characteristic three-peak structure corresponding to the lowest three vibrational levels of the S_2 state. The room temperature absorption spectrum of astaxanthin however (Fig. 6.2.), shows a broad and structureless form, and the three-peak structure becomes visible only at a lower temperatures (198). The resolution of vibrational peaks in the absorption spectrum is an important spectroscopic measure as it reflects certain structural properties of a carotenoid molecule. The vibrational structure is well resolved for linear carotenoids such as lycopene or spheroidene, while a clear loss of resolution of vibrational bands is observed for carotenoids having conjugation extended to various end groups. A typical example is β -carotene, for which the conjugation extends to the terminal β -ionylidene rings. The conjugated double bonds located on the β -ionylidene ring are in the *s-cis* orientation with respect to the main conjugated backbone. The loss of vibrational resolution is attributed to the repulsion between methyl groups on the β -ionylidene ring and hydrogen atoms on the conjugated backbone that forces the conjugated double bond of the β -ionylidene ring out of plane. Accordingly, the spectral inhomogeneity of astaxanthin is due to conjugation extended into the terminal β -ionylidene ring and the presence of keto and hydroxyl groups, which leads to a broader distribution of conformers (199).

Intramolecular relaxation of the photoexcited S_1 and S_2 states of carotenoids proceeds primarily via nonradiative pathways. The results are in good agreement with the dynamics obtained from single wavelength fitting and from global analysis of astaxanthin in methanol and in acetonitrile (199). In these cases, two kinetic components corresponding to time constants of 130 fs and 5.2 ps were sufficient to account for the kinetic behavior. The profile of the 5.2 ps component is consistent with $S_1 \rightarrow S_N$ absorption, while the negative band with minimum at 470 nm is due to ground state bleaching and stimulated emission from the S_2 excited state. This band rises with the resolution of the experiment and decays with two time constants; a 130 fs component due to the $S_2 \rightarrow S_0$ stimulated emission (reflecting the $S_2 \rightarrow S_1$ relaxation) and a component of 5.2 ps representing the recovery of the ground state absorption ($S_1 \rightarrow S_0$ decay). The lifetime of 5.2 ps obtained for the S_1 excited state in chloroform differs however with the lifetime of 1.8 ps found for astaxanthin bound to α -crustacyanin (199). The difference can be explained by planarization of astaxanthin which leads to a longer effective π -electron conjugated chain, a lower S_1 energy, and consequently a shorter S_1 lifetime in the protein compared to that in solution. Only three energy-levels (S_2 , S_1 and S_0) were sufficient to describe the data. No involvement of the so-called S^* state is observed, which usually exhibits a blue shoulder at the $S_1 \rightarrow S_N$ band.

The astaxanthin radical cation spectrum for both D_3 and D_1 excited states is very sensitive to solvent polarity. The changes in the absorption band are the result of solute-solvent interactions that alter the energy difference between the solvated ground and excited states of astaxanthin radical cation. $Axt^{+\cdot}$ is hypsochromic showing a negative solvatochromism, where the ground state of the dye is more dipolar than its corresponding excited state.

The measurements performed in chapter 5 for β -Car $^{+\cdot}$ (Fig. 5.2), show the same modulation of the spectral shift of the Car $^{+\cdot}$ absorption band. Moreover, the same trend for the $D_0 \rightarrow D_3$ band is observed (Table 6.1).

The formation of $\beta\text{-Car}^{\bullet+}$ by R2P2CI occurs on a femtosecond time-scale by direct electron ejection into the solvent. The observed difference between R2P2CI and chemical oxidation, as discussed in chapter 4, has also been explained by the presence of an ejected electron, which provides a strong environmental change, affecting the optical properties of the carotenoid radical cation. This is further enforced by the R2P2CI measurements of astaxanthin in toluene, a solvent with a high organic redox couple value ($E^0=2.6$ V). R2P2CI does not result in the formation of radical cations in toluene, i.e. the electron is not ejected since the redox potential of toluene is much too high.

The global fit analysis reveals the involvement of three excited states in the observed excited state dynamics of the astaxanthin radical cation. According to chapter 5 and to Amarie *et al.* (176), the initially excited state is D_3 , which decays rapidly with a time-constant of about 100 fs into a lower lying state D_2 . The latter state possesses two possibilities to decay within about 0.9 ps: via transition to the ground state D_0 and or to a second low-lying excited state D_1 . Finally the D_1 state returns to the ground state with a time constant of about 4.9 ps (Figure 6.11).

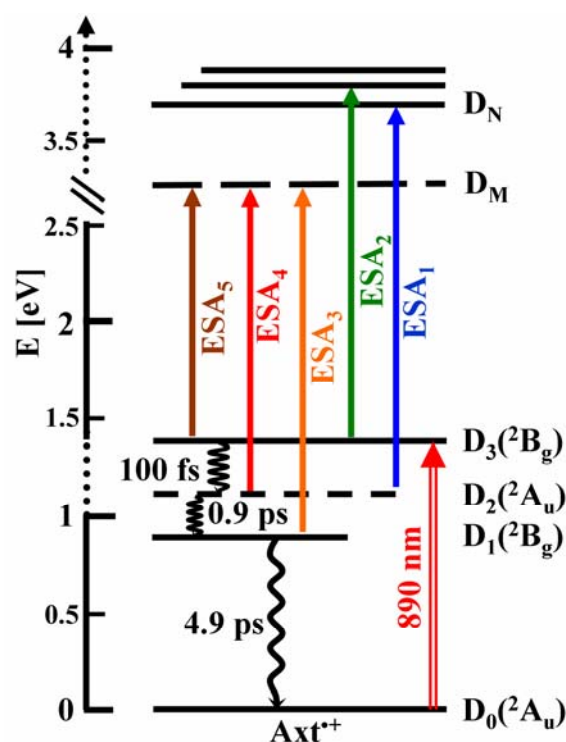


Fig. 6.11. Energy level diagram depicting relaxation processes that occur after photoexcitation of astaxanthin radical cations. The red double arrow represents excitation of the D_3 state, colored arrows correspond to excited state transitions of $D_2 \rightarrow D_N$ (ESA_1), $D_3 \rightarrow D_N$ (ESA_2), $D_1 \rightarrow D_M$ (ESA_3), $D_2 \rightarrow D_M$ (ESA_4) and $D_3 \rightarrow D_M$ (ESA_5), while wavy arrows denote intramolecular relaxation processes. The processes described in this study are labeled by their corresponding time constant (see the text for details).

From the analysis of the experimental data it is clear that the investigated astaxanthin radical cation possesses two excited states with different spectral properties and lifetimes below the well-known state absorbing in the near-IR region.

7 Summary and Outlook

In the present work, the photo-protection mechanisms in plants and purple bacteria were investigated experimentally at the molecular level. For this purpose, several spectroscopic methods were combined and applied to elucidate the function of carotenoids, pigments of the photosynthetic apparatus, in photo-protection. The experiments were focused on the mechanisms involved in quenching of singlet and triplet states of the electronically excited (bacterio)chlorophylls. This photosynthetic reaction events occur on an ultrafast time-scale (10^{-12} s). Measuring such short-lived events, and understanding the underlying principles, demand some of the most precise experiments and exact measurement technologies currently available. This implies certain requirements for the light source used: a suitable wavelength within the absorption band of the sample, sufficient power, and, most importantly, a pulse duration short compared to the studied reaction. Nowadays, we can achieve all this requirements using femtosecond-spectroscopic systems, which produce laser pulses shorter than 100 femtoseconds (fs), ($1 \text{ fs} = 10^{-15} \text{ s}$). Transient absorption spectroscopy provides important information on molecular dynamics interrogating electronic transitions. The technique is based on photochemical generation of transient species with femtoseconds pump pulses and measuring transient absorption changes of the sample using a second, time delayed probe pulse which in this case is a spectrally broad white-light pulse.

Using femtosecond transient absorption techniques, such as pump-probe (PP) or resonant two-photon two-color ionization (R2P2CI), a series of photosynthetic antenna systems were investigated: the light-harvesting complex 1 (LH1) from the photosynthetic purple bacteria, the light-harvesting complex II (LHC II) and the chlorophyll-bound-proteins CP24, CP26 and CP29 of higher plants. Furthermore, a series of carotenoids and their corresponding radical cations have been investigated in solution. These experiments explore the effect of solvent polarity on the spectroscopic behavior of carotenoids, especially the energetic position and dynamics of their excited states and their interaction with neighboring photosynthetic pigments.

Unlike plant light-harvesting systems, the bacterial LH1 of *R. rubrum* forms a macromolecular complex with a very high degree of symmetry and contains just two pigments: one carotenoid molecule and one BChl dimer, being thus a perfect model to start with transient absorption measurements. The photosynthetic unit of purple bacteria consists of a reaction center (RC) surrounded by a light-harvesting complex. The purple bacteria *R. rubrum* employed in this study shows a heterotrimer reaction center containing the membrane bound subunits, L, M and H. In previous studies, it has been suggested that the RC is completely enclosed by the LH1 complex which consists of a ring-like array of 16 subunits formed from the non-identical α and β polypeptides, with each $\alpha\beta$ subunit binding a pair of BChls and one spirilloxanthin (Spx) (carotenoid molecule with 13 double conjugated C=C bonds). However it is not yet clear if the LH1 ring is circularly symmetric, but if a significant distortion from LH1 circular symmetry is present, this should affect the relative distances between the BChl and Spx molecules, thus affecting also the rates of energy transfer between them. This consideration provided a major motivation to re-examine the ultrafast pathways of Spx-BChl energy transfer in chromatophores obtained from wild-type (WT) *R. rubrum* and those of mutants lacking either the complete RC (mutant SPUHK1) or the L and M subunits (mutant SK Δ LM). Measurements of the excitation energy transfer pathways for these two mutants were compared with the data from the now well characterized intact, WT system. The study shows that deletion of the H subunit inhibits the formation of the RC, i.e. no spectral signature of the reaction center components have been observed.

Excitation of Spx at 550 nm in the SPUHK1 and SK Δ LM samples initiates a spectral evolution similar to that of the WT sample while probing the carotenoid spectral range. The excitation to the Spx S_2 excited state is followed by the simultaneous population of the lower singlet excited states S_1 and S^* , which then decay with lifetimes of 1.4 and 5 ps, respectively, for both mutants, and 1.4 and 4 ps for the wild-type, suggesting that the Spx lowest excited state dynamics in these complexes do not differ significantly. However, a longer excited state lifetime of BChl for SPUHK1 in comparison to WT was observed, consistent with a photochemical quenching channel by the RC. The trapping of the excitation energy by the RC has been estimated to be 46 ps. For long delay times the WT but not the mutants, exhibits a negative signal, due to photobleaching of the RC special pair and an electrochromic blue-shift of the monomeric BChl *a*. The $T_1 \rightarrow T_N$ excited state absorption of Spx at 575 nm reveals the process of $^3\text{BChl} \rightarrow ^3\text{Spx}$ energy transfer, which has a time constant of 1.2 ns. Remarkably, this is the first direct observation of the triplet-to-triplet energy transfer measured on an ultrafast time-scale in a photosynthetic antenna. The similarity of the excited state decay processes of all strains indicates that the pigment geometry of the LH1 complex in modified membranes is unaffected by the absence of an RC.

Non-photochemical quenching (NPQ) is a fundamental mechanism in photosynthesis which protects plants against excess excitation energy and is of crucial importance for their survival and fitness. Feedback deexcitation mechanism (qE), the energy dependent component of NPQ, involves deexcitation of the singlet excited state of chlorophyll in the light-harvesting antenna of photosystem II, thereby minimizing the deleterious effects of high light via thermal dissipation of excess excitation energy. While the physiological importance of qE

has been recognized for many years, a description of its physical mechanisms remains elusive.

A recent model for qE suggests that the replacement of violaxanthin (carotenoid with 9 conjugated C=C double bonds) by zeaxanthin (11 C=C) in its LHC II binding pocket can in principle result in qE via the so-called "gear-shift" mechanism. As a requirement, the violaxanthin first excited state (S_1) has to be higher in energy than the first excited state (Q_y) of Chl *a*, and the S_1 state of zeaxanthin has to be lower. To confirm the proposed model, I performed ultrafast pump-probe measurements on native LHC II and on LHC II in which violaxanthin has been biochemically converted to zeaxanthin. The experimental approach employs excitation of LHC II chlorophylls into the first excited state when violaxanthin or zeaxanthin is present. The lifetime of Chl *a* excited state was probed by measuring the kinetics of the ESA signal. In this thesis, it is undoubtedly shown that the replacement of violaxanthin by zeaxanthin in the light-harvesting complex II (LHC II) has no influence on the Chl excited state lifetime. Moreover, the same experimental approach applied on reconstituted light-harvesting minor complexes, referred to as CP29, CP26, and CP24, which in the native system occupy an intermediate position between the peripheral LHC II and the reaction center, support the conclusion that the presence of zeaxanthin does not lead to Chl quenching. The absence of the excitation energy transfer from the lowest Chl excited state to the lowest zeaxanthin excited state can be explained in terms of weak coupling of these two excited states, due to the small transition dipole moment of the carotenoid S_1 excited state.

In another model for NPQ, zeaxanthin is thought to play an indirect role in quenching the excitation energy: a quenching complex forms between Chl *a* and zeaxanthin during the induction time of qE, and zeaxanthin acts as terminal quencher via electron transfer, leading to carotenoid radical cation formation. This hypothesis was first predicted by theory, showing that for a suitable geometry of the Chl-Zea heterodimer quenching by charge transfer is possible; this corresponds to non-radiative decay into an appropriate energetically low-lying charge transfer excited state. The corresponding experiment was performed on intact spinach thylakoid membranes and the near-IR region was probed after excitation at 664 nm under quenched and unquenched conditions. The spectral differences observed between the quenched and unquenched states were ascribed to the formation of zeaxanthin radical cations. The experiments presented in this thesis are performed on isolated light-harvesting complexes (LHC II, CP24, CP26 and CP29), where the quenched/unquenched state was simulated by presence or absence of zeaxanthin in the light-harvesting complex. The formation of zeaxanthin radical cations were monitored by plotting the transient absorption difference spectrum of the complex enriched in zeaxanthin and the one without zeaxanthin. The transient absorption spectra within the same light-harvesting complex are similar over the entire investigated spectral range, displaying only minor differences, which are not significant within the experimental errors. Besides CP26, for which a bigger amount of zeaxanthin was replaced and a small radical cation signal could be detected, all other difference spectra do not show absorption spectra expected for a zeaxanthin radical cation. This is in contrast with recent studies in which zeaxanthin radical cation signature has been used to infer qE quenching suggesting that all minor LHCs (CP24, CP26 and CP29) provide sites for charge transfer quenching. Nevertheless, the signal observed for the minor LHCs is about 50 times smaller and 20 nm red-shifted than the one observed in intact thylakoids, which hints to a zeaxanthin radical formed at the interface of the light-harvesting complexes.

Hence, it still remains to be shown where exactly and in which pigment-protein complex of the photosynthetic apparatus qE actually occurs. This is a further crucial step for the understanding of the qE protection mechanism in higher plants. Therefore, in this thesis multiple light pulses were used to investigate the ultrafast dynamics of carotenoid radical cation formation in light-harvesting complexes revealing the spectroscopic signature of zeaxanthin radical cations in zeaxanthin enriched complexes. The generation of carotenoid radical cations was achieved by means of resonant two-photon two-color ionization (R2P2CI) spectroscopy.

The ultrafast dynamics of carotenoid radical cation formation was investigated both in solutions of the pure compounds and in LHC II isolated from plant thylakoids. This three-pulse technique involves contributions from two high-intensity pulses initiating a resonant two-photon two-color ionization process and a low-intensity broad-band probe pulse. The R2P2CI measurements reveal the spectroscopic properties of $\text{Car}^{\bullet+}$ and the spectral characteristics of zeaxanthin and violaxanthin radical cations in LHC II. The $\text{Car}^{\bullet+}$ bands in ethanol have maxima located at 830 nm (violaxanthin), 880 nm (lutein), 900 nm (zeaxanthin), and 920 nm (β -carotene). The positions of these maxima depend strongly on the solvent, the number of conjugated C=C bonds, and the molecular structure. Furthermore, R2P2CI measurements on LHC II samples with or without zeaxanthin reveal the violaxanthin radical cation ($\text{Vio}^{\bullet+}$) band at 909 nm and the $\text{Zea}^{\bullet+}$ band at 983 nm, which is about 20 nm blue shifted compared to the carotenoid cation which was previously identified during qE in intact thylakoids. Moreover, the transient absorption measurements show that the zeaxanthin enriched LHC II is not a quenched state. Previous biochemical studies proposed that upon qE induction PsbS, a protein subunit of photosystem II for which a central role in qE has been reported, monomerizes and associates with the LHC antenna. Thus, if zeaxanthin indeed binds to the same site as violaxanthin in LHC II, one zeaxanthin OH group would be buried, but the other one would be exposed to the hydrophobic membrane environment. If one still wants to retain the model which proposes zeaxanthin bound to LHC II as the quenching site, one possible scenario to complete this model is a PsbS/LHC II complex, which may provide a highly polar environment that strongly affects the photophysical properties of zeaxanthin during qE induction. As a result, Chl excitation energy can be quenched. How carotenoid radical cations can quench the Chl excitation energy is also discussed here and a possible quenching mechanism it is proposed.

It has been shown that carotenoids are the crucial pigments involved in photo-protection but they are also involved in scavenging harmful free radicals in all living organisms. The underlying chemical processes are charge transfer and free radical reactions, both of them leading to carotenoid radical cation formation. Despite their fundamental importance in non-photochemical quenching in green plants, only little is known about the optical properties of the $\text{Car}^{\bullet+}$, the energetic positions of their excited states and their interaction with neighboring photosynthetic pigments. Hence, a detailed knowledge of the excited state properties of $\text{Car}^{\bullet+}$ is a step forward not only in understanding natural photosynthetic processes but also in studying and designing artificial photosynthetic systems. In artificial systems the key step is an efficient photo-induced electron transfer eventually producing a final charge-separated state. Carotenoids are excellent candidates for the design of such artificial systems due to their low ionization potential, which makes them excellent electron donors.

In principle, generation and detection of $\text{Car}^{\bullet+}$ can be achieved by several optical methods both in solution and directly in the protein environment. The two-photon two-color technique has been discussed, which has the great advantage that experiments can be performed in the natural biological environment without large perturbation of the natural situation. Nevertheless, this method only leads to short-lived populations of $\text{Car}^{\bullet+}$ species, which decay within microseconds due to charge recombination. In contrast, chemical oxidation is an attractive and simple method to generate long-lived $\text{Car}^{\bullet+}$ molecules, which are stable for hours and decay essentially only by reacting with O_2 . Pump-probe spectroscopy can then be easily applied to study excited state dynamics. The oxidizing agent used in this work is ferric chloride (FeCl_3), which reacts with the neutral carotenoid and leads to the formation of the $\text{Car}^{\bullet+}$.

The results show that the wavelength of the $\text{Car}^{\bullet+}$ absorption band is most notably influenced by the polarizability of the solvent and the number of conjugated double bonds of the carotenoid. This finding can be used in practice to probe the microenvironmental polarity of carotenoids. When the conjugation length of a carotenoid is known, it may serve as a sensor for the polarizability of the environment. Moreover, in chapter 5, experimental investigations employing femtosecond time-resolved pump-probe spectroscopy proves the existence of a second low-lying $\pi\pi^*$ excited state energetically below the strongly allowed excited state responsible for the intense absorption of $\text{Car}^{\bullet+}$ in the near-IR region. Since this state was so far termed D_2 in the literature, we suggest denoting it as D_3 state in the future. The finding of a low lying excited state has also implications for non-photochemical quenching in green plants, since direct quenching of chlorophyll excited states by Förster energy transfer to $\text{Car}^{\bullet+}$ is possible and efficient. And indeed, in a 4 pulse experiment it could be shown a decreased of the Chl excited state lifetime when $\text{Car}^{\bullet+}$ are induced by R2P2CI in light-harvesting complexes of plants.

Throughout all carotenoids, astaxanthin, with 11 conjugated C=C bonds is a ten times more powerful antioxidant than any other carotenoid. The astaxanthin molecule is similar to the more familiar carotenoid β -carotene, but the small differences in structure such as the presence of two additional functional groups (keto and hydroxy) at each end, confer large differences in the chemical and biological properties of the two molecules. Unlike β -carotene, astaxanthin shows a broad band which is a consequence of the loss of vibrational structure. Photoexcitation of astaxanthin is followed by intramolecular relaxation of the S_2 and S_1 excited states, which proceeds via nonradiative pathways. The results presented in this thesis are in good agreement with previous dynamics obtained from single wavelength fitting and from global analysis of astaxanthin in methanol and acetonitrile. In this thesis, I used a global fit procedure to analyze the time-resolved data of astaxanthin in chloroform. Two kinetic components corresponding to time constants of 130 fs (decay of the S_2 excited state) and 5.2 ps (decay of the S_1 excited state) were sufficient to account for the kinetic behavior.

On the other hand, the absorption spectrum of the astaxanthin radical cation in chloroform differs considerably from its neutral form, giving a strong band at 880 nm ($D_0 \rightarrow D_3$ transition) and a weak band at 1320 nm ($D_0 \rightarrow D_1$ transition). Moreover, the D_3 excited state is very sensitive to the solvent polarity. The changes in the absorption band are the result of solute-solvent interactions that alter the energy difference between the solvated ground and excited states of astaxanthin radical cation. The formation of astaxanthin radical cation $\text{Axt}^{\bullet+}$

upon R2P2CI occurs on a femtosecond time-scale by direct electron ejection into the solvent. The observed differences in the absorption spectra between R2P2CI and chemical oxidation are explained by the presence of the ejected electron, which provides a strong environmental change, affecting the optical properties of the carotenoid radical cation.

The global fit analysis reveals the involvement of three excited states in the observed excited state dynamics of astaxanthin radical cation. The initially excited state is D_3 , which decays rapidly with a time-constant of about 100 fs into the lower lying D_2 state. The latter state decays within about 0.9 ps: via transition to the ground state D_0 and or to a second low-lying excited state D_1 . Finally the D_1 state returns to the ground state with a time constant of about 4.9 ps. In contrast to the neutral astaxanthin, its radical cation shows two low-lying excited states energetically below the strongly allowed excited state responsible for the intense absorption in the near-IR region.

This work allows now to improve the basic methods and to perform them on several related systems. As an example, the two-photon two-color technique developed here can be applied to sustain experimentally the proposed kinetic model of carotenoid radical formation in LH2 complexes, model based on quantum chemical calculations. Thus, after pumping of the carotenoid S_2 state and a certain delay time, the S_1 state can be depleted by a second laser pulse at the excited state absorption of the carotenoid, and the radical cation signature can be probed. If the mechanism is correct, the radical cation signal will be diminished when the S_1 state is depleted.

References

1. Nield, J.; Orlova, E. V.; Morris, E. P.; Gowen, B.; Van Heel, M. and Barber, J. 3D Map of the Plant Photosystem II Supercomplex Obtained by Cryoelectron Microscopy and Single Particle Analysis (2000) *Nat. Struct. Biol.* 7, 44-47.
2. Kulheim, C.; Agren, J. and Jansson, S. Rapid Regulation of Light Harvesting and Plant Fitness in the Field (2002) *Science* 297, 91-93.
3. Barber, J. and Andersson, B. Too Much of a Good Thing - Light Can Be Bad for Photosynthesis (1992) *Trends Biochem. Sci.* 17, 61-66.
4. Niyogi, K. K. Photo-protection Revisited: Genetic and Molecular Approaches (1999) *Annu. Rev. Plant Physiol. Plant Molec. Biol.* 50, 333-359.
5. Horton, P. and Hague, A. Studies on the Induction of Chlorophyll Fluorescence in Isolated Barley Protoplasts 4. Resolution of Non-photochemical Quenching (1988) *Biochim. Biophys. Acta* 932, 107-115.
6. Muller, P.; Li, X. P. and Niyogi, K. K. Non-photochemical Quenching. A Response to Excess Light Energy (2001) *Plant Physiol.* 125, 1558-1566.
7. Landrum, J. T. and Bone, R. A. Lutein, Zeaxanthin, and the Macular Pigment (2001) *Archives of Biochemistry and Biophysics* 385, 28-40.
8. Nishino, H. Cancer Prevention by Natural Carotenoids (1997) *J. Cell. Biochem.*, 86-91.
9. Walla, P. J. Linden, P. A.; Hsu, C. P.; Scholes, G. D. And Fleming, G. R. Femtosecond Dynamics of the Forbidden Carotenoid S₁ State in Light-Harvesting Complexes of Purple Bacteria Observed after Two-photon Excitation (2000) *PNAS* 97, 10808-10813.
10. Walla, P. J. Linden, P. A.; Ohta, K.; and Fleming, G. R. Excited-state Kinetics of the Carotenoid S₁ State in Lhc II and Two-Photon Excitation Spectra of Lutein and β -Carotene in Solution: Efficient Car S₁ to Chl Electronic Energy Transfer Via Hot S₁ States (2002) *J. Phys. Chem. A* 106, 1909-1916.
11. Hsu, C. P. Walla, P. J.; Head-Gordon, M.; Fleming, G. R. The Role of the S₁ state of Carotenoids in Photosynthetic Energy Transfer: The Light Harvesting Complex II of Purple Bacteria (2001) *J. Phys. Chem. B.* 105, 11016-11025.

12. Wentworth, M.; Ruban, A. V. and Horton, P. Chlorophyll Fluorescence Quenching in Isolated Light Harvesting Complexes Induced by Zeaxanthin (2000) *FEBS Lett.* 471, 71-74.
13. Holt, N. E.; Fleming, G. R. and Niyogi, K. K. Toward an Understanding of the Mechanism of Non-photochemical Quenching in Green Plants (2004) *Biochemistry* 43, 8281-8289.
14. Holt, N. E.; Kennis, J. T. M.; Dall'osto, L.; Bassi, R. and Fleming, G. R. Carotenoid to Chlorophyll Energy Transfer in Light Harvesting Complex II from Arabidopsis Thaliana Probed by Femtosecond Fluorescence Upconversion (2003) *Chem. Phys. Lett.* 379, 305-313.
15. Holt, N. E.; Zigmantas, D.; Valkunas, L.; Li, X. P.; Niyogi, K. K. and Fleming, G. R. Carotenoid Cation Formation and the Regulation of Photosynthetic Light Harvesting (2005) *Science* 307, 433-436.
16. Jeevarajan, J. A.; Wei, C. C.; Jeevarajan, A. S. and Kispert, L. D. Optical Absorption Spectra of Dications of Carotenoids (1996) *J. Phys. Chem.* 100, 5637-5641.
17. Dreuw, A.; Fleming, G. R. and Head-Gordon, M. Charge-transfer State as a Possible Signature of a Zeaxanthin-Chlorophyll Dimer in the Non-photochemical Quenching Process in Green Plants (2003) *J. Phys. Chem. B* 107, 6500-6503.
18. Barber, J.; Rhee, K. H.; Morris, E.; Hankamer, B.; Nield, J.; Boekema, E. and Kühlbrandt, W. Towards the Elucidation of the Structure of Photosystem II at High Resolution (1998) *Biophys. J.* 74, A328-A328.
19. Polivka, T. and Sundstrom, V. Ultrafast Dynamics of Carotenoid Excited States from Solution to Natural and Artificial Systems (2004) *Chem. Rev.* 104, 2021-2071.
20. Bittner, T.; Irrgang, K. D.; Renger, G. and Wasielewski, M. R. Ultrafast Excitation-Energy Transfer and Exciton-Exciton Annihilation Processes in Isolated Light-Harvesting Complexes of Photosystem-II (LHC-II) from Spinach (1994) *J. Phys. Chem.* 98, 11821-11826.
21. Connelly, J. P.; Muller, M. G.; Hucke, M.; Gatzen, G.; Mullineaux, C. W.; Ruban, A. V.; Horton, P. and Holzwarth, A. R. Ultrafast Spectroscopy of Trimeric Light-Harvesting Complex II from Higher Plants (1997) *J. Phys. Chem. B* 101, 1902-1909.
22. Gradinaru, C. C.; Pascal, A. A.; Van Mourik, F.; Robert, B.; Horton, P.; Van Grondelle, R. and Van Amerongen, H. Ultrafast Evolution of the Excited States in the

- Chlorophyll a/b Complex CP29 from Green Plants Studied by Energy-Selective Pump-Probe Spectroscopy (1998) *Biochemistry* 37, 1143-1149.
23. Kleima, F. J.; Gradinaru, C. C.; Calkoen, F.; Van Stokkum, I. H. M.; Van Grondelle, R. and Van Amerongen, H. Energy Transfer in LHC II Monomers at 77 K Studied by Sub-Picosecond Transient Absorption Spectroscopy (1997) *Biochemistry* 36, 15262-15268.
 24. Linnanto, J.; Martiskainen, J.; Lehtovuori, V.; Ihalainen, J.; Kananavicius, R.; Barbato, R. and Korppi-Tommola, J. Excitation Energy Transfer in the LHC-II Trimer: A Model Based on the New 2.72 Å Structure (2006) *Photosynthesis Research* 87, 267-279.
 25. Barzda, V.; Gulbinas, V.; Kananavicius, R.; Cervinskis, V.; Van Amerongen, H.; Van Grondelle, R. and Valkunas, L. Singlet-Singlet Annihilation Kinetics in Aggregates and Trimers of LHC II (2001) *Biophys. J.* 80, 2409-2421.
 26. Zucchelli, G.; Dainese, P.; Jennings, R. C.; Breton, J.; Garlaschi, F. M. and Bassi, R. Gaussian Decomposition of Absorption and Linear Dichroism Spectra of Outer Antenna Complexes of Photosystem-II (1994) *Biochemistry* 33, 8982-8990.
 27. Green, B. R. and Kühlbrandt, W. Sequence Conservation of Light-Harvesting and Stress-response Proteins in Relation to the 3-Dimensional Molecular-structure of Lhc II (1995) *Photosynthesis Research* 44, 139-148.
 28. Sandona, D.; Croce, R.; Pagano, A.; Crimi, M. and Bassi, R. Higher Plants Light Harvesting Proteins. Structure and Function as Revealed by Mutation Analysis of Either Protein or Chromophore Moieties (1998) *Biochim. Biophys. Acta-Bioenergetics* 1365, 207-214.
 29. Pesaresi, P.; Sandona, D.; Giuffra, E. and Bassi, R. A Single Point Mutation (E166q) Prevents Dicyclohexylcarbodiimide Binding to the Photosystem II Subunit CP29 (1997) *FEBS Lett.* 402, 151-156.
 30. Ruban, A. V.; Walters, R. G. and Horton, P. The Molecular Mechanism of the Control of Excitation-Energy Dissipation in Chloroplast Membranes - Inhibition of Δ pH-dependent Quenching of Chlorophyll Fluorescence by Dicyclohexylcarbodiimide (1992) *FEBS Lett.* 309, 175-179.
 31. Karrasch, S. B., P. A.; Ghosh, R. The 8.5 Å Projection Map of the Light-Harvesting Complex I from *Rhodospirillum Rubrum* Reveals a Ring Composed of 16 Subunits. (1995) *EMBO J.* 14, 631-638.

32. McDermott, G.; Prince, S. M.; Freer, A. A.; Hawthornthwaitelawless, A. M.; Papiz, M. Z.; Cogdell, R. J. and Isaacs, N. W. Crystal-Structure of an Integral Membrane Light-Harvesting Complex from Photosynthetic Bacteria (1995) *Nature* 374, 517-521.
33. Gai, F.; Hasson, K. C.; McDonald, J. C. and Anfinrud, P. A. Chemical Dynamics in Proteins: The Photoisomerization of Retinal in Bacteriorhodopsin (1998) *Science* 279, 1886-1891.
34. Van Amerongen, H. and Van Grondelle, R. Transient Absorption Spectroscopy in Study of Processes and Dynamics in Biology (1995) *Methods Enzymol* 246, 201-226.
35. Zewail, A. H. Femtochemistry: Atomic-Scale Dynamics of the Chemical Bond (2000) *J. Phys. Chem. A* 104, 5660-5694.
36. Squier, J.; Salin, F.; Mourou, G. and Harter, D. 100-Fs Pulse Generation and Amplification in Ti-Al₂O₃ (1991) *Opt. Lett.* 16, 324-326.
37. Huber, R.; Satzger, H.; Zinth, W. and Wachtveitl, J. Noncollinear Optical Parametric Amplifiers with Output Parameters Improved by the Application of a White Light Continuum Generated in CaF₂ (2001) *Opt. Commun.* 194, 443-448.
38. Cheriaux, G.; Rousseau, P.; Salin, F. Chambaret, J. P.; Walker, B. and Dimauro L. F. Aberration-free Stretcher Design for Ultrashort-pulse Amplification (1996) *Opt Lett* 21, 1996.
39. Moulton, P. Spectroscopic and Laser Characteristics of Ti-Al₂O₃ *J. Opt. Soc. Am. B* 3, 125-133
40. Alfano, R. R. (1989) *The Supercontinuum Laser Source* (Springer-Verlag, Berlin).
41. Fork, R. L.; Shank, C. V.; Hirlimann, C.; Yen, R. and Tomlinson, W. J. Femtosecond White-light Continuum Pulses (1983) *Opt. Lett.* 8, 1-3.
42. Yang, G. Z. and Shen, Y. R. Spectral Broadening of Ultrashort Pulses in a Nonlinear Medium (1984) *Opt. Lett.* 9, 510-512.
43. Corkum, P. B.; Rolland, C. and Srinivasanrao, T. Supercontinuum Generation in Gases (1986) *Phys. Rev. Lett.* 57, 2268-2271.
44. Ilkov, F. A.; Ilkova, L. S. and Chin, S. L. Supercontinuum Generation Versus Optical-Breakdown in CO₂ Gas (1993) *Opt. Lett.* 18, 681-683.

45. Ranka, J. K.; Schirmer, R. W. and Gaeta, A. L. Observation of Pulse Splitting in Nonlinear Dispersive Media (1996) *Phys. Rev. Lett.* 77, 3783-3786.
46. Smith, W. L.; Liu, P. and Bloembergen, N. Superbroadening in H₂O and D₂O by Self-focused Picosecond Pulses from a YAlG:Nd Laser (1977) *Phys. Rev. A* 15, 2396-2403.
47. Feng, Q.; Moloney, J. V.; Newell, A. C.; Wright, E. M.; Cook, K.; Kennedy, P. K.; Hammer, D. X.; Rockwell, B. A. and Thompson, C. R. Theory and Simulation on the Threshold of Water Breakdown Induced by Focused Ultrashort Laser Pulses (1997) *Ieee J. Quant. Electr.* 33, 127-137.
48. Kennedy, P. K. A First-Order Model for Computation of Laser-Induced Breakdown Thresholds in Ocular and Aqueous-Media .1. Theory (1995) *Ieee J. Quant. Electr.* 31, 2241-2249.
49. Brodeur, A. and Chin, S. L. Ultrafast White-Light Continuum Generation and Self-Focusing in Transparent Condensed Media (1999) *J. Opt. Soc. Am. B Opt. Phys.* 16, 637-650.
50. Lecroy Catalog Lecroy Research Systems; Chestnut Ridge Road NY, USA (1996) 10977-6499.
51. Van Stokkum, I. H. M.; Larsen, D. S. and Van Grondelle, R. Global and Target Analysis of Time-resolved Spectra (2004) *Biochim. Biophys. Acta-Bioenergetics* 1657, 82-104.
52. Van Grondelle, R.; Dekker, J. P.; Gillbro, T. and Sundstrom, V. Energy-Transfer and Trapping in Photosynthesis (1994) *Biochim. Biophys. Acta-Bioenergetics* 1187, 1-65.
53. Ghosh, R.; Hoenger, A.; Hardmeyer, A.; Mihailescu, D.; Bachofen, R.; Engel, A. and Rosenbusch, J. P. 2-Dimensional Crystallization of the Light-Harvesting Complex from *Rhodospirillum Rubrum* (1993) *J. Molec. Biol.* 231, 501-504.
54. Hu, X. C.; Damjanovic, A.; Ritz, T. and Schulten, K. Architecture and Mechanism of the Light-Harvesting Apparatus of Purple Bacteria (1998) *PNAS* 95, 5935-5941.
55. Jungas, C.; Ranck, J. L.; Rigaud, J. L.; Joliot, P. and Vermeglio, A. Supramolecular Organization of the Photosynthetic Apparatus of *Rhodobacter Sphaeroides* (1999) *EMBO J.* 18, 534-542.

56. Karrasch, S.; Bullough, P. A. and Ghosh, R. The 8.5-Angstrom Projection Map of the Light-Harvesting Complex-I from *Rhodospirillum Rubrum* Reveals a Ring Composed of 16 Subunits (1995) *EMBO J.* 14, 631-638.
57. Miller, K. R. 3-Dimensional Structure of a Photosynthetic Membrane (1982) *Nature* 300, 53-55.
58. Stahlberg, H.; Dubochet, J.; Vogel, H. and Ghosh, R. Are the Light-Harvesting I Complexes from *Rhodospirillum Rubrum* Arranged around the Reaction Centre in a Square Geometry? (1998) *J. Molec. Biol.* 282, 819-831.
59. Stark, W.; Kühlbrandt, W.; Wildhaber, I.; Wehrli, E. and Muhlethaler, K. The Structure of the Photoreceptor Unit of *Rhodospseudomonas Viridis* (1984) *EMBO J.* 3, 777-783.
60. Walz, T. and Ghosh, R. Two-Dimensional Crystallization of the Light-Harvesting I Reaction Centre Photounit from *Rhodospirillum Rubrum* (1997) *J. Molec. Biol.* 265, 107-111.
61. Law, C. J.; Roszak, A. W.; Southall, J.; Gardiner, A. T.; Isaacs, N. W. and Cogdell, R. J. The Structure and Function of Bacterial Light-Harvesting Complexes (Review) (2004) *Molec. Membrane Biol.* 21, 183-191.
62. Amarie, S.; Lupo, D. Lenz, M. O.; Saegesser, R.; Ghosh, R. and Wachtveitl, J. Excitation Energy Pathways in the Photosynthetic Units of Reaction Center LM and H Subunit Deletion Mutants of *Rhodospirillum rubrum* submitted to *Biochemistry*.
63. Picorel, R. B., G.; Gingras, G. Antenna Holochrome B880 of *Rhodospirillum Rubrum* S1. Pigment, Phospholipid, and Polypeptide Composition (1983) *Biochemistry* 22, 2491-2497.
64. Cogdell, R. J.; Lindsay, J. G.; Valentine, J. and Durant, I. A Further Characterization of the B890 Light-Harvesting Pigment Protein Complex from *Rhodospirillum Rubrum* Strain-S1 (1982) *FEBS Lett.* 150, 151-154.
65. Jamieson, S. J.; Wang, P. Y.; Qian, P.; Kirkland, J. Y.; Conroy, M. J.; Hunter, C. N. and Bullough, P. A. Projection Structure of the Photosynthetic Reaction Centre-Antenna Complex of *Rhodospirillum Rubrum* at 8.5 Å Resolution (2002) *EMBO J.* 21, 3927-3935.
66. Fotiadis, D.; Qian, P.; Philippsen, A.; Bullough, P. A.; Engel, A. and Hunter, C. N. Structural Analysis of the Reaction Center Light-Harvesting Complex I Photosynthetic

- Core Complex of *Rhodospirillum Rubrum* Using Atomic Force Microscopy (2004) *J. Biol. Chem.* 279, 2063-2068.
67. Schulten, K. (1999) *Simplicity and Complexity in Proteins and Nucleic Acids* (Dahlem University Press).
68. Scheuring, S.; Francia, F.; Busselez, J.; Melandri, B. A.; Rigaud, J. L. and Levy, D. Structural Role of Pufx in the Dimerization of the Photosynthetic Core Complex of *Rhodobacter Sphaeroides* (2004) *J. Biol. Chem.* 279, 3620-3626.
69. Ketelaars, M.; Hofmann, C.; Kohler, J.; Howard, T. D.; Cogdell, R. J.; Schmidt, J. and Aartsma, T. J. Spectroscopy on Individual Light-Harvesting 1 Complexes of *Rhodospseudomonas Acidophila* (2002) *Biophys. J.* 83, 1701-1715.
70. Farchaus, J. W.; Wachtveitl, J.; Mathis, P. and Oesterhelt, D. Tyrosine-162 of the Photosynthetic Reaction Center L-Subunit Plays a Critical Role in the Cytochrome-C(2) Mediated Rereduction of the Photooxidized Bacteriochlorophyll Dimer in *Rhodobacter Sphaeroides* 1. Site-Directed Mutagenesis and Initial Characterization (1993) *Biochemistry* 32, 10885-10893.
71. Wachtveitl, J.; Farchaus, J. W.; Mathis, P. and Oesterhelt, D. Tyrosine-162 of the Photosynthetic Reaction Center L-Subunit Plays a Critical Role in the Cytochrome-C(2) Mediated Rereduction of the Photooxidized Bacteriochlorophyll Dimer in *Rhodobacter Sphaeroides* 2. Quantitative Kinetic-Analysis (1993) *Biochemistry* 32, 10894-10904.
72. Belanger, G.; Berard, J.; Corriveau, P. and Gingras, G. The Structural Genes-Coding for the L-Subunit and M-Subunit of *Rhodospirillum Rubrum* Photoreaction Center (1988) *J. Biol. Chem.* 263, 7632-7638.
73. Gerken, U.; Lupo, D.; Tietz, C.; Wrachtrup, J. and Ghosh, R. Circular Symmetry of the Light-Harvesting 1 Complex from *Rhodospirillum Rubrum* Is Not Perturbed by Interaction with the Reaction Center (2003) *Biochemistry* 42, 10354-10360.
74. Roszak, A. W.; Howard, T. D.; Southall, J.; Gardiner, A. T.; Law, C. J.; Isaacs, N. W. and Cogdell, R. J. Crystal Structure of the RC-LH1 Core Complex from *Rhodospseudomonas Palustris* (2003) *Science* 302, 1969-1972.
75. Scheuring, S.; Sturgis, J. N.; Prima, V.; Bernadac, A.; Levy, D. and Rigaud, J. L. Watching the Photosynthetic Apparatus in Native Membranes (2004) *PNAS* 101, 11293-11297.

76. Lupo, D. and Ghosh, R. The Reaction Center H Subunit Is Not Required for High Levels of Light-Harvesting Complex 1 in *Rhodospirillum Rubrum* Mutants (2004) *J. Bacteriol.* 186, 5585-5595.
77. Saegesser, R. Identifikation und Charakterisierung des Photosynthese Genclusters aus *Rhodospirillum rubrum* (1992) PhD Thesis (University of Zurich, Zurich).
78. Gradinaru, C. C.; Kennis, J. T. M.; Papagiannakis, E.; Van Stokkum, I. H. M.; Cogdell, R. J.; Fleming, G. R.; Niederman, R. A. and Van Grondelle, R. An Unusual Pathway of Excitation Energy Deactivation in Carotenoids: Singlet-to-triplet Conversion on an Ultrafast Timescale in a Photosynthetic Antenna (2001) *PNAS* 98, 2364-2369.
79. Okamoto, H.; Ogura, M.; Nakabayashi, T. and Tasumi, M. Sub-picosecond Excited-State Dynamics of a Carotenoid (Spirilloxanthin) in the Light-Harvesting Systems of *Chromatium Vinosum*. Relaxation Process from the Optically Allowed S₂ State (1998) *Chem. Phys.* 236, 309-318.
80. Papagiannakis, E.; Kennis, J. T. M.; Van Stokkum, I. H. M.; Cogdell, R. J. and Van Grondelle, R. An Alternative Carotenoid-to-Bacteriochlorophyll Energy Transfer Pathway in Photosynthetic Light Harvesting (2002) *PNAS* 99, 6017-6022.
81. Papagiannakis, E. D., S. K.; Gall, A.; Stokkum, I. H. M.; Robert, B.; Van Grondelle, R.; Frank, H. A.; Kennis, J. T. M. Light Harvesting by Carotenoids Incorporated into the B850 Light-Harvesting Complex from *Rhodobacter Sphaeroides* R-26.1: Excited-State Relaxation, Ultrafast Triplet Formation, and Energy Transfer to Bacteriochlorophyll (2003) *J. Phys. Chem. B* 107, 5642-5649.
82. Wohlleben, W.; Buckup, T.; Herek, J. L.; Cogdell, R. J.; Motzkus, M. Multichannel Carotenoid Deactivation in Photosynthetic Light Harvesting as Identified by an Evolutionary Target Analysis (2003) *Biophys. J.* 85, 442-450.
83. Wohlleben, W.; Buckup, T.; Herek, J. L. And Motzkus, M. Coherent Control for Spectroscopy and Manipulation of Biological Dynamics (2005) *ChemPhysChem* 6, 850-857.
84. Ricci, M.; Bradforth, S. E.; Jimenez, R.; and Fleming, G.R. Internal Conversion and Energy Transfer Dynamics of Spheroidene in Solution and in the LH1 and LH2 Light-Harvesting Complexes (1996) *Chem. Phys. Lett.* 259, 381-390.
85. Ghosh, R.; Hardmeyer, A.; Thoenen, I. and Bachofen, R. Optimization of the Sstrom Culture-medium for Large-scale Batch Cultivation of *Rhodospirillum Rubrum* under Semiaerobic Conditions with Maximal Yield of Photosynthetic Membranes (1994) *Appl. Environment. Microbiol.* 60, 1698-1700.

86. Cheng, Y. J. S.; Brantner, C. A.; Tsapin, A. and Collins, M. L. P. Role of the H Protein in Assembly of the Photochemical Reaction Center and Intracytoplasmic Membrane in *Rhodospirillum Rubrum* (2000) *J. Bacteriol.* 182, 1200-1207.
87. Wilhelm, T.; Piel, J. and Riedle, E. Sub-20-fs Pulses Tunable across the Visible from a Blue-pumped Single-pass Noncollinear Parametric Converter (1997) *Opt. Lett.* 22, 1494-1496.
88. Amarie, S.; Standfuss, J.; Barros, T.; Kühlbrandt, W.; Dreuw, A. and Wachtveitl, J. Carotenoid Radical Cations as a Probe for the Molecular Mechanism of Non-photochemical Quenching in Oxygenic Photosynthesis (2007) *J. Phys. Chem. B* 111, 3481-3487.
89. Cerullo, G.; Lanzani, G.; Zavelani-Rossi, M. and De Silvestri, S. Early Events of Energy Relaxation in All-trans- β -Carotene Following Sub-10 fs Optical-pulse Excitation (2001) *Phys. Rev. B* 63, 2411041- 2411044.
90. Shreve, A. P.; Trautman, J. K.; Owens, T. G. and Albrecht, A. C. Determination of the S_2 Lifetime of β -Carotene (1991) *Chem. Phys. Lett.* 178, 89-96.
91. Yoshizawa, M.; Aoki, H. and Hashimoto, H. Vibrational Relaxation of the $^2A_g^-$ Excited State in All-trans- β -carotene Obtained by Femtosecond Time-resolved Raman Spectroscopy (2001) *Phys. Rev. B* 63 180-301.
92. Zhang, J. P.; Skibsted, L. H.; Fujii, R. and Koyama, Y. Transient Absorption from the $^1B_u^+$ State of All-trans- β -carotene Newly Identified in the near-Infrared Region (2001) *Photochem. Photobiol.* 73, 219-222.
93. Novoderezhkin, V. and Fetisova, Z. Exciton Delocalization in the B808–866 Antenna of the Green Bacterium *Chloroflexus Aurantiacus* as Revealed by Ultrafast Pump-Probe Spectroscopy (1999) *Biophys. J* 77, 424-430.
94. Novoderezhkin, V. I., and Razjivin, A. P. Excitonic Interactions in the Light-Harvesting Antenna of Photosynthetic Purple Bacteria and Their Influence on Picosecond Absorbance Difference Spectra (1993) *FEBS Lett.* 330, 5–7.
95. Monger, T. G.; Cogdell, R. J. and Parson, W. Triplet States of Bacteriochlorophyll and Carotenoids in Chromatophores of Photosynthetic Bacteria (1976) *Biochim. Biophys. Acta - Bioenergetics* 449, 136-153.
96. Valkunas, L.; Akesson, E.; Pullerits, T. and Sundstrom, V. Energy Migration in the Light-Harvesting Antenna of the Photosynthetic Bacterium *Rhodospirillum Rubrum*

- Studied by Time-Resolved Excitation Annihilation at 77 K (1996) *Biophys. J.* 70, 2373-2379.
97. Visser, H. M.; Somsen, O.J.; van Mourik, F.; Lin, S.; van Stokkum, I.H. and van Grondelle, R. Direct Observation of Sub-Picosecond Equilibration of Excitation Energy in the Light-Harvesting Antenna of *Rhodospirillum Rubrum* (1995) *Biophys. J.* 69, 1083-1099.
 98. van Grondelle, R. Excitation Energy Transfer, Trapping and Annihilation in Photosynthetic Systems (1985) *Biochim. Biophys. Acta* 811, 147-195.
 99. Monshouwer, R.; Abrahamsson, M.; van Mourik, F. and van Grondelle, R. Superradiance and Exciton Delocalization in Bacterial Photosynthetic Light-Harvesting Systems (1997) *J. Phys. Chem. B* 101, 7241-7248.
 100. Gradinaru, C. C.; Kennis, J. T. M.; Papagiannakis, E.; van Stokkum, I. H. M.; Cogdell, R. J.; Fleming, G. R.; Niederman, R. A.; van Grondelle, R. An Unusual Pathway of Excitation Energy Deactivation in Carotenoids: Singlet-to-triplet Conversion on an Ultrafast Timescale in a Photosynthetic Antenna (2001) *PNAS* 98, 2364-2369.
 101. Gaertner, P.; Port, H.; Branschaedel, M. and Ghosh, R. Fs-Study on Energy Relaxation in Light-Harvesting (Lh1) Complexes from *Rhodospirillum Rubrum* with Carotenoids of Different Conjugation Length (2004) *J. Lumin.* 108, 111-116.
 102. Feng, J.; Wang, Q.; Wu, Y. S.; Ai, X. C.; Zhang, X. J.; Huang, Y. G.; Zhang, X. K. and Zhang, J. P. Triplet Excitation Transfer between Carotenoids in the LH2 Complex from Photosynthetic Bacterium *Rhodopseudomonas Palustris* (2004) *Photosynth. Res.* 82, 83-94.
 103. Horton, P.; Ruban, A. V. and Walters, R. G. Regulation of Light Harvesting in Green Plants (1996) *Annu. Rev. Plant Physiol. Plant Molec. Biol.* 47, 655-684.
 104. Li, X. P.; Bjorkman, O.; Shih, C.; Grossman, A. R.; Rosenquist, M.; Jansson, S. and Niyogi, K. K. A Pigment-Binding Protein Essential for Regulation of Photosynthetic Light Harvesting (2000) *Nature* 403, 391-395.
 105. Li, X. P.; Gilmore, A. M.; Caffarri, S.; Bassi, R.; Golan, T.; Kramer, D. and Niyogi, K. K. Regulation of Photosynthetic Light Harvesting Involves Intrathylakoid Lumen pH Sensing by the PsbS Protein (2004) *J. Biol. Chem.* 279, 22866-22874.

106. Frank, H. A.; Cua, A.; Chynwat, V.; Young, A.; Gosztola, D. and Wasielewski, M. R. Photophysics of the Carotenoids Associated with the Xanthophyll Cycle in Photosynthesis (1994) *Photosynth. Re.* 41, 389-395.
107. Pascal, A. A.; Liu, Z. F.; Broess, K.; van Oort, B.; van Amerongen, H.; Wang, C.; Horton, P.; Robert, B.; Chang, W. R. and Ruban, A. Molecular Basis of Photo-protection and Control of Photosynthetic Light-Harvesting (2005) *Nature* 436, 134-137.
108. Demmigadams, B. Carotenoids and Photo-protection in Plants - A Role for the Xanthophyll Zeaxanthin (1990) *Biochem Biophys Acta* 1020, 1-24.
109. Berera, R.; Herrero, C.; van Stokkum, L. H. M.; Vengris, M.; Kodis, G.; Palacios, R. E.; van Amerongen, H.; van Grondelle, R.; Gust, D.; Moore, T. A.; Moore, A. L. and Kennis, J. T. M. A Simple Artificial Light-Harvesting Dyad as a Model for Excess Energy Dissipation in Oxygenic Photosynthesis (2006) *PNAS* 103, 5343-5348.
110. Horton, P.; Ruban, A. V.; Rees, D.; Pascal, A. A.; Noctor, G. and Young, A. J. Control of the Light-Harvesting Function of Chloroplast Membranes by Aggregation of the LHC II Chlorophyll Protein Complex (1991) *FEBS Lett.* 292, 1-4.
111. Dreuw, A.; Fleming, G. R. and Head-Gordon, M. Chlorophyll Fluorescence Quenching by Xanthophylls (2003) *Physical Chemistry Chemical Physics* 5, 3247-3256.
112. Dreuw, A.; Fleming, G. R. and Head-Gordon, M. Role of Electron-transfer Quenching of Chlorophyll Fluorescence by Carotenoids in Non-photochemical Quenching of Green Plants (2005) *Biochem. Soc. Trans.* 33, 858-862.
113. Gilmore, A. M.; Hazlett, T. L. and Govindjee. Xanthophyll Cycle-Dependent Quenching of Photosystem-II Chlorophyll *a* Fluorescence - Formation of a Quenching Complex with a Short Fluorescence Lifetime (1995) *PNAS* 92, 2273-2277.
114. Aspinall-O'dea, M.; Wentworth, M.; Pascal, A.; Robert, B.; Ruban, A. and Horton, P. *In vitro* Reconstitution of the Activated Zeaxanthin State Associated with Energy Dissipation in Plants (2002) *PNAS* 99, 16331-16335.
115. Bilger, W. and Bjorkman, O. Relationships among Violaxanthin Deepoxidation, Thylakoid Membrane Conformation, and Non-photochemical Chlorophyll Fluorescence Quenching in Leaves of Cotton (*Gossypium-Hirsutum L*) (1994) *Planta* 193, 238-246.

116. Ruban, A. V.; Young, A. J. and Horton, P. Induction of Non-photochemical Energy-dissipation and Absorbency Changes in Leaves - Evidence for Changes in the State of the Light-Harvesting System of Photosystem-II *in vivo* (1993) *Plant Physiol.* 102, 741-750.
117. Ruban, A. V.; Pascal, A. A.; Robert, B. and Horton, P. Activation of Zeaxanthin Is an Obligatory Event in the Regulation of Photosynthetic Light Harvesting (2002) *J. Biol. Chem.* 277, 7785-7789.
118. Bergantino, E.; Segalla, A.; Brunetta, A.; Teardo, E.; Rigoni, F.; Giacometti, G. M. and Szabo, I. Light and pH-dependent Structural Changes in the PsbS Subunit of Photosystem II (2003) *PNAS* 100, 15265-15270.
119. Jansson, S. A Guide to the LHC Genes and Their Relatives in Arabidopsis (1999) *Trends Plant Science* 4, 236-240.
120. Li, X. P.; Phippard, A.; Pasari, J. and Niyogi, K. K. Structure-function Analysis of Photosystem II Subunit S (PsbS) *in vivo* (2002) *Function. Plant Biol.* 29, 1131-1139.
121. Liu, Z. F.; Yan, H. C.; Wang, K. B.; Kuang, T. Y.; Zhang, J. P.; Gui, L. L.; An, X. M. and Chang, W. R. Crystal Structure of Spinach Major Light-Harvesting Complex at 2.72 Å Resolution (2004) *Nature* 428, 287-292.
122. Standfuss, J.; van Scheltinga, A. C. T.; Lamborghini, M. and Kühlbrandt, W. Mechanisms of Photo-protection and Non-photochemical Quenching in Pea Light-Harvesting Complex at 2.5 Å Resolution (2005) *EMBO J.* 24, 919-928.
123. Tracewell, C. A. and Brudvig, G. W. Two Redox-active β -Carotene Molecules in Photosystem II (2003) *Biochem.* 42, 9127-9136.
124. Schenck, C. C.; Diner, B.; Mathis, P. and Satoh, K. Flash-induced Carotenoid Radical Cation Formation in Photosystem-II (1982) *Biochim Biophys. Acta* 680, 216-227.
125. Polyakov, N. E.; Leshina, T. V.; Salakhutdinov, N. F. and Kispert, L. D. Host-guest Complexes of Carotenoids with β -Glycyrrhizic Acid (2006) *J. Phys. Chem. B* 110, 6991-6998.
126. Schlucker, S.; Szeghalmi, A.; Schmitt, M.; Popp, J. and Kiefer, W. Density Functional and Vibrational Spectroscopic Analysis of β -Carotene (2003) *J. Raman Spectrosc.* 34, 413-419.

127. Polivka, T.; Pullerits, T.; Frank, H. A.; Cogdell, R. J. and Sundstrom, V. Ultrafast Formation of a Carotenoid Radical in LH2 Antenna Complexes of Purple Bacteria (2004) *J. Phys. Chem. B* 108, 15398-15407.
128. Muller-Moule, P.; Conklin, P. L. and Niyogi, K. K. Ascorbate Deficiency Can Limit Violaxanthin De-epoxidase Activity *in vivo* (2002) *Plant Physiol.* 128, 970-977.
129. Burke, J. J.; Ditto, C. L. and Arntzen, C. J. Involvement of Light-Harvesting Complex in Cation Regulation of Excitation Energy Distribution in Chloroplasts (1978) *Archiv. Biochem. Biophys.* 187, 252-263.
130. Gilmore, A. M.; Shinkarev, V. P.; Hazlett, T. L. and Govindjee. Quantitative Analysis of the Effects of Intrathylakoid pH and Xanthophyll Cycle Pigments on Chlorophyll *a* Fluorescence Lifetime Distributions and Intensity in Thylakoids (1998) *Biochemistry* 37, 13582-13593.
131. Porra, R. J.; Thompson, W. A. and Kriedemann, P. E. Determination of Accurate Extinction Coefficients and Simultaneous-equations for Assaying Chlorophyll *a* and Chlorophyll *b* Extracted with 4 Different Solvents - Verification of the Concentration of Chlorophyll Standards by Atomic Absorption Spectroscopy (1989) *Biochim. Biophys. Acta* 975, 384-394.
132. Gilmore, A. M. and Yamamoto, H. Y. Resolution of Lutein and Zeaxanthin Using a Non-encapped, Lightly Carbon-Loaded C-18 High-Performance Liquid-Chromatographic Column (1991) *J. Chromatograph.* 543, 137-145.
133. Palsson, L. O.; Spangfort, M. D.; Gulbinas, V. and Gillbro, T. Ultrafast Chlorophyll *b* Chlorophyll *a* Excitation-energy Transfer in the Isolated Light-Harvesting Complex, LHC II, of Green Plants - Implications for the Organization of Chlorophylls (1994) *FEBS Lett.* 339, 134-138.
134. Savikhin, S.; van Amerongen, H.; Kwa, S. L. S.; van Grondelle, R. and Struve, W. R. Low-temperature Energy Transfer in LHC II Trimers from the Chl *a/b* Light-Harvesting Antenna of Photosystem II (1994) *Biophys. J.* 66, 1597-1603.
135. Mullineaux, C. W.; Pascal, A. A.; Horton, P. and Holzwarth, A. R. Excitation-energy Quenching in Aggregates of the LHC II Chlorophyll-Protein Complex - a Time-resolved Fluorescence Study (1993) *Biochim. Biophys. Acta* 1141, 23-28.
136. Frank, H. A.; Bautista, J. A.; Josue, J. S. and Young, A. J. Mechanism of Non-photochemical Quenching in Green Plants: Energies of the Lowest Excited Singlet States of Violaxanthin and Zeaxanthin (2000) *Biochemistry* 39, 2831-2837.

137. Polivka, T.; Herek, J. L.; Zigmantas, D.; Akerlund, H. E. and Sundstrom, V. Direct Observation of the (Forbidden) S₁ State in Carotenoids (1999) *PNAS* 96, 4914-4917.
138. Polivka, T.; Zigmantas, D.; Sundstrom, V.; Formaggio, E.; Cinque, G. and Bassi, R. Carotenoid S₁ State in a Recombinant Light-Harvesting Complex of Photosystem II (2002) *Biochemistry* 41, 439-450.
139. Dreuw, A. Influence of Geometry Relaxation on the Energies of the S₁ and S₂ States of Violaxanthin, Zeaxanthin, and Lutein (2006) *J. Phys. Chem. A* 110, 4592-4599.
140. Papagiannakis, E.; Vengris, M.; Larsen, D. S.; van Stokkum, I. H. M.; Hiller, R. G. and van Grondelle, R. Use of Ultrafast Dispersed Pump-Dump-Probe and Pump-Repump-Probe Spectroscopies to Explore the Light-Induced Dynamics of Peridinin in Solution (2006) *J. Phys. Chem. B* 110, 512-521.
141. Galinato, M. G.; Niedzwiedzki, D.; Deal, C.; Birge, R. R. and Frank, H. A. Cation Radicals of Xanthophylls (2007) *Photosynth. Res.* 94, 67-78.
142. Niedzwiedzki, D.; Rusling, J. F. and Frank, H. A. Voltammetric Redox Potentials of Carotenoids Associated with the Xanthophyll Cycle in Photosynthesis (2005) *Chem. Phys. Lett.* 416, 308-312.
143. Pan, J.; Benko, G.; Xu, Y. H.; Pascher, T.; Sun, L. C.; Sundstrom, V. and Polivka, T. Photoinduced Electron Transfer between a Carotenoid and TiO₂ Nanoparticle (2002) *J. Am. Chem. Soc.* 124, 13949-13957.
144. Wohlleben, W.; Buckup, T.; Herek, J. L. and Motzkus, M. Coherent Control for Spectroscopy and Manipulation of Biological Dynamics (2005) *ChemPhysChem* 6, 850-857.
145. Bautista, J. A.; Tracewell, C. A.; Schلودer, E.; Cunningham, F. X.; Brudvig, G. W. and Diner, B. A. Construction and Characterization of Genetically Modified *Synechocystis Sp.* Pcc 6803 Photosystem II Core Complexes Containing Carotenoids with Shorter π -conjugation than β -Carotene (2005) *J. Biol. Chem.* 280, 38839-38850.
146. Kiss, A. Z.; Ruban, A. V. and Horton P. The PsbS Protein Controls the Organization of the Photosystem II Antenna in Higher Plant Thylakoid Membranes (2008) *J. Biol. Chem.* 283, 3972-3978.
147. Crouchman, S.; Ruban, A. and Horton, P. PsbS Enhances Non-photochemical Fluorescence Quenching in the Absence of Zeaxanthin (2006) *FEBS Lett.* 580, 2053-2058.

148. Ma, Y. Z.; Holt, N. E.; Li, X. P.; Niyogi, K. K. and Fleming, G. R. Evidence for Direct Carotenoid Involvement in the Regulation of Photosynthetic Light Harvesting (2003) *PNAS* 100, 4377-4382.
149. Foote, C. S. Mechanisms of Photosensitized Oxidation - There Are Several Different Types of Photosensitized Oxidation Which May Be Important in Biological Systems (1968) *Science* 162, 963-970.
150. Foote, C. S.; Chang, Y. C. and Denny, R. W. Chemistry of Singlet Oxygen. X. Carotenoid Quenching Parallels Biological Protection (1970) *J. Am. Chem. Soc.* 92, 5216-5218.
151. Griffiths, M.; Sistrom, W. R.; Cohenbazire, G. and Stanier, R. Y. Function of Carotenoids in Photosynthesis (1955) *Nature* 176, 1211-1214.
152. Renger, G. and Wolff, C. Further Evidence for Dissipative Energy Migration Via Triplet-states in Photosynthesis - Protective Mechanism of Carotenoids in *Rhodospseudomonas Spheroides* Chromatophores (1977) *Biochim. Biophys. Acta* 460, 47-57.
153. Frank, H. A. and Cogdell, R. J. Carotenoids in Photosynthesis (1996) *Photochem. Photobiol.* 63, 257-264.
154. Edge, R.; Mcgarvey, D. J. and Truscott, T. G. The Carotenoids as Anti-oxidants - a Review (1997) *J. Photochem. Photobiol., B* 41, 189-200.
155. Seddon, J. M.; Ajani, U. A.; Sperduto, R. D.; Hiller, R.; Blair, N.; Burton, T. C.; Farber, M. D.; Gragoudas, E. S.; Haller, J.; Miller, D. T.; Yannuzzi, L. A. and Willett, W. Dietary Carotenoids, Vitamin A, Vitamin C, and Vitamin E, and Advanced Age-related Macular Degeneration (1994) *JAMA, J. Am. Med. Assoc.* 272, 1413-1420.
156. Pérez-Bueno, M. L.; Johnson, M. P.; Zia, A.; Ruban, A. V. and Horton P. The Lhcb Protein and Xanthophyll Composition of the Light-Harvesting Antenna Controls the Δ pH-dependency of Non-photochemical Quenching in *Arabidopsis Thaliana* (2008) *FEBS. Lett.* 582, 1477-1482.
157. Avenson, T. J.; Ahn, T. K.; Zigmantas, D.; Niyogi, K. K.; Li, Z.; Ballottari, M.; Bassi, R. and Fleming, G. R. Zeaxanthin Radical Cation Formation in Minor Light-Harvesting Complexes of Higher Plant Antenna (2007) *J. Biol. Chem.*, 3550-3558.
158. Bode, S.; Quentmeier, C. C.; Liao, P. N.; Barros, T. and Walla, P. J. Xanthophyll Cycle Dependence of the Energy Transfer between Carotenoid Dark States and Chlorophylls

- in NPQ Mutants of Living Plants and in LHC II (2008) *Chem. Phys. Lett.* 450, 379-385.
159. Dreuw, A. and Wormit, M. Simple Replacement of Violaxanthin by Zeaxanthin in LHC II Does Not Cause Chlorophyll Fluorescence Quenching (2008) *J. Inorg. Biochem.* 102, 458-465.
160. Ruban, A. V.; Berera, R.; Iliaia, C.; Van Stokkum, I. H. M.; Kennis, J. T. M.; Pascal, A. A.; van Amerongen, H.; Robert, B.; Horton, P. and van Grondelle, R. Identification of a Mechanism of Photoprotective Energy Dissipation in Higher Plants (2007) *Nature* 450, 575-578.
161. Ahn, T. K.; Avenson, T. J.; Ballottari, M.; Cheng, Y. C.; Niyogi, K. K.; Bassi, R. and Fleming, G. R. Architecture of a Charge Transfer State Regulating Light Harvesting in a Plant Antenna Protein (2008) *Science* 320, 794-797.
162. Polivka, T.; Zigmantas, D.; Herek, J. L.; He, Z.; Pascher, T.; Pullerits, T.; Cogdell, R. J.; Frank, H. A. and Sundstrom, V. The Carotenoid S₁ State in LH2 Complexes from Purple Bacteria Rhodospirillum rubrum and Rhodospirillum rubrum: S₁ Energies, Dynamics, and Carotenoid Radical Formation (2002) *J. Phys. Chem. B* 106, 11016-11025.
163. Fungo, F.; Otero, L.; Durantini, E.; Thompson, W. J.; Silber, J. J.; Moore, T. A.; Moore, A. L.; Gust, D. and Sereno, L. Correlation of Fluorescence Quenching in Carotenoporphyryl Dyads with the Energy of Intramolecular Charge Transfer States. Effect of the Number of Conjugated Double Bonds of the Carotenoid Moiety (2003) *Phys. Chem. Chem. Phys.* 5, 469-475.
164. Moore, T. A.; Gust, D.; Mathis, P.; Mialocq, J. C.; Chachaty, C.; Bensasson, R. V.; Land, E. J.; Doizi, D.; Liddell, P. A.; Lehman, W. R.; Nemeth, G. A. and Moore, A. L. Photodriven Charge Separation in a Carotenoporphyryl Quinone Triad (1984) *Nature* 307, 630-632.
165. Savolainen, J.; Dijkhuizen, N.; Fanciulli, R.; Liddell, P. A.; Gust, D.; Moore, T. A.; Moore, A. L.; Hauer, J.; Buckup, T.; Motzkus, M. and Herek, J. L. Ultrafast Energy Transfer Dynamics of a Bioinspired Dyad Molecule (2008) *J. Phys. Chem. B* 112, 2678-2685.
166. Frank, H. A. and Brudvig, G. W. Redox Functions of Carotenoids in Photosynthesis (2004) *Biochemistry* 43, 8607-8615.

167. Fujii, R.; Koyama, Y.; Mortensen, A. and Skibsted, L. H. Generation of the Radical Cation of β -Carotene in Chloroform Via the Triplet State as Revealed by Time Resolved Absorption Spectroscopy (2000) *Chem. Phys. Lett.* 326, 33-38.
168. Gurzadyan, G. G. and Steenken, S. Photoionization of β -Carotene Via Electron Transfer from Excited States to Chlorinated Hydrocarbon Solvents. A Picosecond Transient Absorption Study (2002) *Phys. Chem. Chem. Phys.* 4, 2983-2988.
169. Zhang, J. P.; Fujii, R.; Koyama, Y.; Rondonuwu, F. S.; Watanabe, Y.; Mortensen, A. and Skibsted, L. H. The $^1B_u^-$ Type Singlet State of β -Carotene as a Precursor of the Radical Cation Found in Chloroform Solution by Sub-Picosecond Time Resolved Absorption Spectroscopy (2001) *Chem. Phys. Lett.* 348, 235-241.
170. Andersson, P. O.; Gillbro, T.; Ferguson, L. and Cogdell, R. J. Absorption Spectral Shifts of Carotenoids Related to Medium Polarizability (1991) *Photochem. Photobiol.* 54, 353-360.
171. Galinato, M. G.; Niedzwiedzki, D.; Deal, C.; Birge, R. R. and Frank, H. A. Cation Radicals of Xanthophylls (2007) *Photosynth. Res.* 94, 67-78.
172. Bally, T.; Nitsche, S.; Roth, K. and Haselbach, E. Excited States of Polyene Radical Cations - Limitations of Koopmans Theorem (1984) *J. Am. Chem. Soc.* 106, 3927-3933.
173. Niedzwiedzki, D. M.; Sullivan, J. O.; Polivka, T.; Birge, R. R. and Frank, H. A. Femtosecond Time Resolved Transient Absorption Spectroscopy of Xanthophylls (2006) *J. Phys. Chem. B* 110, 22872-22885.
174. Backup, T.; Savolainen, J.; Wohlleben, W.; Herek, J. L.; Hashimoto, H.; Correia, R. R. B. and Motzkus, M. Pump-probe and Pump-Deplete-Probe Spectroscopies on Carotenoids with N=9-15 Conjugated Bonds (2006) *J. Chem. Phys.* 125, 194505.1-194505.7.
175. Kawashima, Y.; Nakayama, K.; Nakano, H. and Hirao, K. Theoretical Study of the $\pi \rightarrow \pi^*$ Excited States of Linear Polyene Radical Cations and Dications (1997) *Chem. Phys. Lett.* 267, 82-90.
176. Amarie, S.; Starcke, J. H.; Dreuw, A. and Wachtveitl, J. Identification of an Additional Low-Lying Excited State of Carotenoid Radical Cations. (2008) *J. Phys. Chem. B* 112, 14011-14017.

177. Lawlor, S. M. and Obrien, N. M. Astaxanthin - Antioxidant Effects in Chicken Embryo Fibroblasts (1995) *Nutrition Res.* 15, 1695-1704.
178. Lawlor, S. M. and Obrien, N. M. Modulation of Oxidative Stress by β -Carotene in Chicken Embryo Fibroblasts (1995) *British J. Nutrition* 73, 841-850.
179. Miki, W. Biological Functions and Activities of Animal Carotenoids (1991) *Pure App. Chem.* 63, 141-146.
180. Palozza, P. and Krinsky, N. I. Astaxanthin and Canthaxanthin Are Potent Antioxidants in a Membrane Model (1992) *Archiv. Biochem. Biophys.* 297, 291-295.
181. Terao, J. Antioxidant Activity of β -Carotene Related Carotenoids in Solution (1989) *Lipids* 24, 659-661.
182. Krinsky, N. I. and Deneke, S. M. Interaction of Oxygen and Oxy-radicals with Carotenoids (1982) *J. Nat. Cancer Inst.* 69, 205-210.
183. Jialal, I.; Norkus, E. P.; Cristol, L. and Grundy, S. M. β -Carotene Inhibits the Oxidative Modification of Low-Density-Lipoprotein (1991) *Biochimica Et Biophysica Acta* 1086, 134-138.
184. Palozza, P.; Moualla, S. and Krinsky, N. I. Effects of β -Carotene and α -Tocopherol on Radical-initiated Peroxidation of Microsomes (1992) *Free Radical Biol. Med.* 13, 127-136.
185. Luxnewirth, O. and Millar, T. J. Lipid Soluble Antioxidants Preserve Rabbit Corneal Cell Function (1990) *Current Eye Res.* 9, 103-109.
186. Kunert, K. J. and Tappel, A. L. The Effect of Vitamin C on *in vivo* Lipid-peroxidation in Guinea-pigs as Measured by Pentane and Ethane Production (1983) *Lipids* 18, 271-274.
187. Leibovitz, B.; Hu, M. L. and Tappel, A. L. Dietary Supplements of Vitamin E, β -Carotene, Coenzyme-Q10 and Selenium Protect Tissues against Lipid Peroxidation in Rat Tissue Slices (1990) *J. Nutrition* 120, 97-104.
188. Mayne, S. T. and Parker, R. S. Antioxidant Activity of Dietary Canthaxanthin (1989) *Nutrition Cancer Internat. J.* 12, 225-236.

189. Zamora, R.; Hidalgo, F. J. and Tappel, A. L. Comparative Antioxidant Effectiveness of Dietary β -Carotene, Vitamin E, Selenium and Coenzyme-Q10 in Rat Erythrocytes and Plasma (1991) *J. Nutrition* 121, 50-56.
190. Isler, O. (1971) *Carotenoids* (Ed. Birkhauser, Basel).
191. Frank, H. A. (1999) *The Photochemistry of Carotenoids* (Kluwer, Dordrecht, The Netherlands).
192. Christensen, R. L.; Barney, E. A.; Broene, R. D.; Galinato, M. G. I. and Frank, H. A. Linear Polyenes: Models for the Spectroscopy and Photophysics of Carotenoids (2004) *Archiv. Biochem. Biophys.* 430, 30-36.
193. Hudson, B. and Kohler, B. Linear Polyene Electronic Structure and Spectroscopy (1974) *Ann. Rev. Phys. Chem.* 25, 437-460.
194. Hudson, B. S. and Kohler, B. E. Polyene Spectroscopy - Lowest Energy Excited Singlet-state of Diphenyloctatetraene and Other Linear Polyenes (1973) *J. Chem. Phys.* 59, 4984-5002.
195. Chayen, N. E.; Cianci, M.; Grossmann, J. G.; Habash, J.; Helliwell, J. R.; Nneji, G. A.; Raftery, J.; Rizkallah, P. J. and Zagalsky, P. F. Unravelling the Structural Chemistry of the Colouration Mechanism in Lobster Shell (2003) *Acta Crystallograph. D-Biological Crystallography* 59, 2072-2082.
196. Zagalsky, P. F. β -Crustacyanin, the Blue-Purple Carotenoprotein of Lobster Carapace: Consideration of the Bathochromic Shift of the Protein Bound Astaxanthin (2003) *Acta Crystallograph. D-Biological Crystallography* 59, 1529-1531.
197. Buchwald, M. and Jencks, W. P. Properties of Crustacyanins and Yellow Lobster Shell Pigment (1968) *Biochemistry* 7, 844-859.
198. Krawczyk, S. and Britton, G. A Study of Protein-Carotenoid Interactions in the Astaxanthin-Protein Crustacyanin by Absorption and Stark Spectroscopy; Evidence for the Presence of Three Spectrally Distinct Species (2001) *Biochim. Biophys. Acta-Protein Structure and Molecular Enzymology* 1544, 301-310.
199. Ilagan, R. P.; Christensen, R. L.; Chapp, T. W.; Gibson, G. N.; Pascher, T.; Polivka, T. and Frank, H. A. Femtosecond Time-Resolved Absorption Spectroscopy of Astaxanthin in Solution and in α -Crustacyanin (2005) *J. Phys. Chem. A* 109, 3120-3127.

Acknowledgements

A journey is easier when you travel together. This thesis is the result of four years of work whereby I have been accompanied and supported by many people. I have now the opportunity to express my gratitude to all of them.

The first person I would like to thank is my direct supervisor Prof. Josef Wachtveitl, which gave me the freedom and support that was required to complete this work.

I gratefully thank to PD Dr. Andreas Dreuw for his detailed and constructive comments, and for his important support throughout this work.

During this work I have collaborated with the groups of Prof Werner Kühlbrandt and Prof. Robin Ghosh who have providing me the samples, without which I could not do my work, and where helping me with useful discussions. Here I want to thank Jörg Standfuss, Tiago Barros and Laura Wilk for the project on LHC II as well to Domenico Lupo and Caroline Autenrieth for helping me with the LH1 project.

I would also like to thank my colleagues: Martin, Karsten, Thomas, Lisa, Victor, Mirka, Ute, Heike, Nina, Kibrom, Lars and Radhan, helping me with different aspects of this thesis.

Many thanks to Jan Hendrik Starcke and Michael Wormit from the group of Andreas Dreuw for their quantum chemical calculations support involved in this work.

My thanks go also to Claudia v. Sulecki Madic our secretary for her friendly assistance in the university administrative issues.

Above all, this thesis is dedicated to the people I love at most: Oana, Luca and my parents.

Publications

Amarie, S.; Wilk, L.; Barros, T.; Kühlbrandt, W.; Dreuw, A. and Wachtveitl, J. Properties of Zeaxanthin and its Radical Cation Bound to the Minor Light-Harvesting Complexes CP24, CP26 and CP29. (2009) *BBA-Bioenergetics*, accepted for publication.

Wormit, M.; Harbach, P. H. P.; Mewes, J. M.; **Amarie, S.;** Wachtveitl J.; and Dreuw A. Excitation Energy and Electron Transfer in Light Harvesting Complexes - A Theoretical Perspective. (2009) *BBA-Bioenergetics*, accepted for publication.

Amarie, S.; Förster, U. and Wachtveitl J. Excited State Dynamics of Astaxanthin Radical Cation. *Chemical Physics* (special issue), in preparation.

Verhoeven, M-K.; Lenz, M. O.; **Amarie, S.;** Klare, J. P.; Tittor, J.; Oesterhelt, D.; Engelhard, M. and Wachtveitl, J. Primary Reaction Dynamics of Sensory Rhodopsin II Mutant D75N and the Influence of Azide., in preparation

Amarie, S.; Lupo, D. Lenz, M. O.; Saegesser, R.; Ghosh, R. and Wachtveitl, J. Excitation Energy Pathways in the Photosynthetic Units of Reaction Center LM and H Subunit Deletion Mutants of *Rhodospirillum rubrum*. (2008) submitted.

Amarie, S.; Starcke, J. H.; Dreuw, A. and Wachtveitl, J. Identification of an Additional Low-Lying Excited State of Carotenoid Radical Cations. (2008) *J. Phys. Chem. B* 112, 14011–14017.

Amarie, S.; Wilk, L.; Barros, T.; Kühlbrandt, W.; Dreuw, A. and Wachtveitl, J. Two Photon Two Color Generation of Zeaxanthin Radical Cation in CP29 Light Harvesting Complex. (2008) in: *Ultrafast Phenomena XVI*, (E. Riedle, R. Schoenlein eds.), Springer, Berlin / Heidelberg / New York.

Gildenhoff, N.; **Amarie, S.;** Beer, A.; Gundermann, K.; Büchel, C. and Wachtveitl, J. Light Harvesting, Energy Transfer and Photoprotection in the Fucoxanthin-Chlorophyll Proteins of *Cyclotella meneghiniana*. (2008) in: *Ultrafast Phenomena XVI*, (E. Riedle, R. Schoenlein eds.), Springer, Berlin / Heidelberg / New York.

Amarie, S.; Standfuss, J.; Barros, T.; Kühlbrandt, W.; Dreuw, A. and Wachtveitl, J. Carotenoid Radical Cations as a Probe for the Molecular Mechanism of Non-photochemical Quenching in Oxygenic Photosynthesis. (2007) *J. Phys. Chem. B* 111, 3481-3487.

Verhoeven, M-K.; **Amarie, S.;** Lenz, M. O.; Klare, J. P.; Engelhard, M. and Wachtveitl, J., Primary Reaction of Sensory Rhodopsin II Mutant D75N. (2007) in: *Ultrafast Phenomena XV*, Springer, Berlin / Heidelberg / New York

Amarie, S.; Barros, T.; Standfuss, J.; Dreuw, A.; Kühlbrandt, W. and Wachtveitl, J. Molecular Basis of Nonphotochemical Quenching; The Role of the Major Light Harvesting Complex II. (2007) in: *Ultrafast Phenomena XV*, Springer, Berlin / Heidelberg / New York

Lebenslauf

Name: Sergiu Amarie
Geburtsdatum: 02. 09.1977
Geburtsort: Dorohoi/Rumänien
Familienstand: verheiratet, 1 Kind
Nationalität: rumänisch



Studium

10/04 – Doktorand am Institut für Physikalische und Theoretische Chemie
Universität Frankfurt.
Thema: Kurzzeitspektroskopische Untersuchungen der
Fotoschutzmechanismen an Lichtsammelkomplexen.
Prof. J. Wachtveitl

01/01 – 06/04 Fritz Haber Institut der Max-Planck Gesellschaft, Berlin
Schwerpunkt: Oberflächenphysik
Prof. H. Conrad

01/00 - 06/00 Diplomarbeit an Institut für Technologische Physik, Iasi Rumänien
Titel der Diplomarbeit: Zerstörungsfreie Untersuchung der
mehrschichtigen Materialien mittels Ultraschallwellen.
Prof. R. Grinberg

10/95 – 06/00 Al. I. Cuta Universität, Iasi Rumänien
Studiengang: Physik
Studienabschluss: Diplom Ing. Phys.